Synthesis and Characterization of Antigen-Containing Bioconjugates Used to Probe and Modulate Autoimmunity

By

Martin Antonio Leon

Submitted to the graduate degree program in Chemistry and the Graduate Faculty of the University of Kansas in partial fulfillment of the requirements for the degree of Doctor of Philosophy.

_____

Chairperson Dr. Cory Berkland

_____

Dr. Jon Tunge

_____

Dr. Michael Rubin

_____

Dr. James D. Blakemore

_____

Dr. Michael Hageman

Date Defended: September 18th, 2018

The Dissertation Committee for Martin Antonio Leon certifies that this is the approved version of the following dissertation:

Synthesis and Characterization of Antigen-Containing Bioconjugates Used to Probe and Modulate Autoimmunity

_____

Chairperson Dr. Cory Berkland

Date Approved: September 18th, 2018

Abstract

Autoimmune diseases afflict a significant part of the world population and current treatments only treat symptoms or delay the progression of the disease. In the first chapter of this dissertation, an introduction into autoimmunity and current clinically available non-antigen-specific treatments was presented, along with an overview of the rise of antigen-specific immunotherapies (ASIT) as an improved strategy for the treatment of autoimmune diseases. Furthermore, a detailed background into the chemistry utilized in this work to construct novel antigen-specific probes as potential therapies for autoimmune disorders was also offered. A novel class of bioconjugates known as antigen-drug conjugates (AgDCs) have been developed in our group. AgDCs utilize a similar directing strategy as antibody-drug conjugates (ADCs), which use a protein or peptide autoantigen (vehicle) to direct a conjugated drug (payload) to antigen-specific immune cells. Thus, AgDCs are a novel ASIT that may be used to treat autoimmune disorders. Chapter 2 is focused on the synthesis of various chemical biology tools, and the synthetic optimization of 'clicking' a modified-mimotope or a synthetic epitope to a potent drug via copper-catalyzed cycloaddition (CuAAC). This work also explored another potential novel therapeutic known as Soluble Antigen Arrays (SAgAs) developed in our group. SAgAs are constructed by using a hydrophilic linear polymer, hyaluronic acid (HA), grafted with multiple repeating autoantigen. SAgA technology introduced tolerance and suppressed disease in several studies in the mouse model of Multiple Sclerosis. SAgAs were also designed for flexibility in accommodating other autoantigens and for facilitating screening of antigen valency effects. Two new type of SAgAs were constructed and characterized using different Type 1 Diabetes autoantigens, namely p79 (chapter 3) and human insulin (chapter 4). Both $cSAgA_{p79}$ and $SAgA_{Ins}$ were tested *in vitro* to determine if the SAgAs are able to modulate immunological systems.

Acknowledgements

This would work not be possible without my advisor, Cory Berkland, who was supportive, patient, and offered guidance. I would also like to thank the department of Chemistry at KU for giving me the opportunity to continue my education. I would like to thank the faculty members who participated in my dissertation and oral exam committees: Jon Tunge, Michael Rubin, James D. Blakemore, Michael Hageman, Paul Hanson, and Laird Forrest. I appreciate the opportunity and financial support provided by the NIH Dynamic Aspects of Chemical Biology Training Grant. I would like thank Paul Hanson, Audrey Lamb, and Tom Prisinzano for their guidance, intellectual leadership, and their input towards my professional development. I also appreciate the support and guidance graciously provided to me by Michael Clift and his group. Finally, I would like to thank my collaborators: Remi J. Creusot (Columbia University) and John C. Cambier (UC Denver).

My dissertation would not be possible without contributions from other scientists. In Chapter 3, Rebuma Firdessa-Fite (Columbia University) was my collaborator for the $cSAgA_{p79}$ *in vitro* work and provided feedback. Joshua Sestak provided hydrolyzable $SAgA_{p79}$ material for biophysical analysis and *in vitro* testing. In Chapter 4, Scott M. Wemlinger (UC Denver) was my collaborator for the $SAgA_{Ins}$ *ex vivo* work. I would like to thank both Chad J. Pickens and Jimmy Song for helping to lay the group's synthetic foundation and for reading my document, respectively. I would also like to thank Stephanie Johnson for her contributions. I would like to thank my undergraduate assistants, Nicole Montoya, Renee Ellengood, and finally, Justin Ruffalo.

I would like to thank my mother, father, sister, and brother for their emotional support these past five years. While my father passed away before my dissertation defense, he remains a major driving force in my life. Finally, I would like to thank my wife Aroob Abdelhamid-Leon for her support.

Table of Contents

CHAPTER 1:

AUTOIMMUNE DISEASES, ANTIGEN-SPECIFIC IMMUNOTHERAPIES, AND COPPER-CATALYZED CYCLOADDITION (CUAAC) FOR BIOCONJUGATION

CHAPTER 1: AUTOIMMUNE DISEASES, ANTIGEN-SPECIFIC IMMUNOTHERAPIES, AND COPPER-CATALYZED AZIDE-ALKYNE CYCLOADDITION (CUAAC) FOR BIOCONJUGATION

1.1. Introduction to autoimmune disorders

Over 80 identified autoimmune diseases are a result of an aberrant immune response targeting various organs, tissues, and cells.[1] Over 5 % of the world's population is afflicted by an autoimmune disorder and extensive efforts have gone into the development of therapies, but none have been successful in curing any of the diseases. Autoimmune disorders are believed to be caused by the loss of tolerance to self-antigen (autoantigen) and they typically develop through these three major phases: initiation, propagation, and resolution. Either genetic predisposition and/or environmental triggers in an individual often lead to initiation of autoimmunity. During the propagation phase, inflammation and tissue damage occur because of cytokine (soluble messengers that create tolerogenic or inflammatory responses dependent on their microenvironment) production, epitope spreading, and an increase in the accumulation of effector T cells. In addition, a decrease in Treg cells or an increase of dysfunctional Treg would also occur during the propagation phase, thus disrupting the Teff/Treg balance. Finally, resolution occurs when there is activation of cell-intrinsic and cell-extrinsic mechanisms that limit effector response and restore Teff/Treg balance.[2] The targeting of self-antigens leads to various diseases such as rheumatoid arthritis (RA),[3-8] multiple sclerosis (MS),[9-11] type 1 diabetes (T1D),[12-14] neuromyelitis optica,[8,9] and lupus.[10,11] Possibly by understanding similarities and differences between autoimmune diseases, novel therapies can be developed to regain tolerance.

Rheumatoid arthritis (RA) decreases the quality of life for 0.5-1% of adults of the world population. Individuals with RA suffer from CD4+ T cells, B cells and macrophages targeting the joint lining, known as the synovium, leading to inflammation, and proinflammatory markers lead to degradation of local cartilage and bone.[3] Individuals with class II major histocompatibility-DR4

(HLA-DR4) alleles account for 70% of all RA patients.[4] Foreign antigens, which share strong homologous peptide sequences with humans, are suspected as possible initiators to RA. Examples of these foreign antigens include heat-shock proteins, Epstein-Barr virus (EBV) trans-actin factor, and *Escherichia coli* dnaj.[5] The precise autoantigen that leads to the pathogenesis of RA is not known, however, the following autoantigens have been identified: Type II collagen, human chondrocyte glycoprotein 39, aggrecan, cartilage link protein, heat shock proteins, citrullinated filaggrin, immunoglobulin G, *N*-Acetylglucosamine-6-sulfatase, and filamin A.[6,7]

Multiple Sclerosis (MS) is a neurological disability that affects 2.5 million individuals internationally.[8] The exact mechanism of disease progression is unknown for MS, but the current hypothesis is that the immune system incorrectly targets proteins, such as myelin basic protein (MBP) and proteolipid protein (PLP), which are located within the protective myelin sheath surrounding the neurons of the central nervous system (CNS). The inflammatory response leads to demyelination and progressive loss of motor functions.[9] It has been reported that individuals with changes in HLA-DRB1 gene have the highest risk of developing MS.[10] Environmental factors that increase an individual's chance of developing MS include: EBV, smoking, and low levels of vitamin D.[11]

Type 1 Diabetes (T1D) is most commonly diagnosed among young children and young adults, affecting 2 in 1000. First, an abnormal immune response targeting beta cells in the pancreas leads to a reduction in insulin production. Insulin plays an important role in regulating blood sugar and fat storage. Second, a buildup of proinflammatory cytokines leads to further functional suppression on B cells resulting in elevated blood glucose levels. Finally, the regulatory control of the aberrant immune response fails, leading to further chronic destruction of B cells and complete loss of insulin production.[12] The exact cause that starts the cascade of events that leads to the

development of T1D is not known. It has been reported that individuals with HLA-DR3-DQ2 and/or HLA-DR4-DQ8 halotypes have a higher probability of developing T1D, accounting for 90% of individuals with T1D.[12,13] The cause for T1D for the remaining patients without genetic predispositions may be related to an yet discovered environmental factor[12,14] Currently, the following autoantigens are implicated in T1D: insulin,[15] non-specific islet cell (ICA),[16] insulinoma antigen-2 (IA-2),[17] and glutamic acid decarboxylase 65 (GAD-65).[18]

1.2. Current treatment approaches for autoimmune disorders

Treatments for autoimmune diseases are categorized into the following four categories: general immunosuppressants, mobility and transport inhibitors, immune cell activation inhibitors, and antigen mimics. Most of these therapies are not antigen specific and cause global immune modification or inhibition, leading to an increase in susceptibility of being infected by a foreign pathogen. Immunosuppressants are effective for many individuals afflicted with autoimmune disorders, however, they have been shown to have toxicity problems and other adverse effects.[19] Mobility and transport inhibitors prevent auto-reactive immune cells or antibodies from migrating to their site of action; however, these classes of therapies also suffer from adverse side effects that result in retraction of immune cells that may be needed to fight off foreign pathogens.[20] Immune cell activation inhibitors work by blocking costimulatory pathways required for an antigen-specific immune response. It has been reported that the lack of costimulation can inhibit immune activation and move the immune response toward tolerance.[21-23] Antigen mimics aim to induce an antigen-specific immune response without anaphlaxysis that can be associated with the native antigen.[24] A few of examples of each category will be highlighted.

Two small molecules teriflunomide (Aubagio) and lefunomide (Arava), to treat MS and RA respectively, are anti-inflammatory compounds that inhibit immune cell proliferation by blocking the synthesis of DNA necessary for cell division.[25] The pathway for pro-inflammatory cytokine IL-2 can be disrupted by the small molecule ciclosporin, which is used in the treatment of RA and T1D.[26] Glucocorticoids, such as prednisolone and prednisone, are meant to treat RA and SLE, however the mechanism of action is not known. These class of drugs show promising pleiotropic immunosuppression but they may reduce the robustness of the immune response by reducing the expression of cellular receptors.[27] The above examples and other global immune suppressants all lack specificity and do not cure the disorder but only manage symptoms by reducing damage done by the immune system.[26, 28]

The monoclonal (mAb) antibody natalizumab (Tysabri), approved by the FDA in 2004, is used to treat MS by targeting vascular cell adhesion molecule-1 (VCAM-1). Natalizumab inhibits binding of cell adhesion molecules and decreases the number of auto-reactive T-cells in the CNS tissue through reducing leukocyte trafficking across the blood brain barrier.[20] In addition, the mobility and transport inhibitor efalizumab (Raptiva) is an anti-LFA-1 antibody used to treat chronic psoriasis.[21] Both natalizumab and efalizumab have been shown to cause progressive multifocal myelencephalopathy (PML), which led to their removal of approval and withdrawn from clinical use, respectively. Upon determination of JC virus antibodies as risk factors for the development of PML in individuals with MS, for those who did not test positive for the JC virus, natalizumab was reapproved in 2006 as a last resort treatment.[29] Several other mAb meant to target CD20 to help treat autoimmune disorders, such as, veltuzumab, TRU015, ocrelizumab, and ofatumumab, are currently being studied in the clinic. [30] Immune cell activation inhibitor such as rituximab (Rituxan), is a chimeric IgG1 anti-CD20 mAb meant to target B-Cell activation, has

been approved for the treatment of MS, RA, and SLE.[31] Clinical success has been seen for B-cell depletion by rituximab in both MS[31] and SLE[32]. T-cell mediated autoimmune disease have been targeted with biologicals such as abatacept (Orencia) for RA, T1D, SLE, and psoriasis. Abatacept is a biological, CTLA-4 IgG1 fusion protein meant to target the B7 pathway, which leads to tolerance to antigen or immunosupresion.[33-34] In addition, belatacept (Nulojix) is also used to treat RA and T1D have been approved by the FDA.[33] Belatacept is another biological, CTLA-4 IgG1fusion protein that has been shown to have even greater binding affinity to B7 than abatacept.[34] Neither biological is antigen-specific in their B7 pathway inhibition. Alternatively, the small molecule fingolimond (Gilenya) used to treat MS patients worked by inhibiting the internalization of S1P-receptor on immune cells, thus preventing autoreactive lymph nodes from trafficking to the CNS.[25]

1.3. Antigen-specific immunotherapy (ASIT)

In order to combat the lack of specificity of the previously mentioned therapies, scientists have begun implementing the use of autoantigen delivery systems to induce an antigen-specific immune response for the treatment of autoimmune diseases. Antigen-specific immunotherapy (ASIT) are designed to treat specific autoimmune diseases by using implicated autoantigen.[35] The most successful ASIT, hyposensitization therapy, has been used to treat allergies by inducing an antigen-specific immune response to induce tolerance.[36] Occasionally, some hyposensitization therapy can lead to life threatening anaphylaxis, thus requiring a trained professional to administer treatment. Since hyposensitization therapy is a successful example of ASIT, similar approaches have been used to develop ASIT for autoimmune diseases.[35, 37-38]

A ‘decoy’ strategy, known as antigen mimics, is meant to induce an antigen-specific immune response by drawing the attention of the immune system away from the native antigen. Antigen mimics, insulin and insulin analogous have been used in the treatment of T1D but clinical trials have not been successful.[24] Similar to antigen mimics, altered peptide ligands (APLs) have emerged as a therapeutic subclass. They are composed of amino acids from the native antigenic epitope but with substituted amino acids. A polymer therapy known as glatiramer acetate (Copaxone®) was designed to emulate MBP epitopes and has been approved to treat MS. It is hypothesized to be a competitive MHC class II molecule that causes a T-helper type 2 immune response and it may be an antagonist for MBP specific T cells.[39-40] Thus, possibly making the mechanism of action both antigen-specific and non-specific in its effect on the immune response. However, further studies are required to obtain a better understanding of the mechanism of action.

The Dintzis group reported that in order to induce tolerogenic immune responses, the antigen-delivery vehicle must include certain antigenic (peptide antigen length/size and target affinity) and pharmaceutical (size, hydrophilicity and stability) characteristics.[5-8] Many antigen-specific immunotherapies exhibit characteristics similar to traditional vaccines. Vaccines are designed to initiate a directed adaptive immune response to specific antigens to provide a robust “protective” immunological response upon re-challenge. This is accomplished by co-delivering antigen in an adjuvanted matrix, typically comprised of insoluble alum particulates. Vaccines often contain particles within the size range of 1- 10 μm and are postulated to form a depot at the injection site, providing a high local concentration of antigen and initiating specific recruitment of immune cells. Additionally, these insoluble adjuvants make the adsorbed antigen more particulate in nature, comparable to that of a virus or bacteria, and help enhance antigen recognition and uptake, and thus more readily undergo phagocytosis by antigen-presenting cells (APCs).

Conversely, allergy shot therapies commonly use soluble allergens to hyposensitize the immune response and establish tolerance.[9] This is typically accomplished by delivering low doses of soluble antigens via subcutaneous injection over an extended period of time. These allergen antigens tend to be much smaller (< 50-70 kDa) than the much larger particulate vaccines and are not delivered as part of an adjuvanted matrix. Interestingly, these characteristics of the allergens would be conducive to transport and draining into lymph nodes. Allergen-specific immunotherapies are known to hyposensitize immune responses, thus providing a benchmark for design of autoimmune ASIT delivery systems that has yet to be explored. Traditional allergen desensitization requires multiple treatments over an extended period of time, typically months to years. Recent allergen desensitization approaches have investigated intranodal injection of ASIT and results have shown that it is a highly efficacious, safe, and reduces the treatment duration dramatically, sometimes to as few as 3 injections.[10]

1.3.1. ASIT by means of combination strategies for autoimmunity

Combination strategies for ASIT have emerged as a way to combine the specificity of antigen-only therapies and potency of immunomodulators. Two different combination strategies exist to treat autoimmunity, either by co-administration or via co-delivery. Co-administration therapies allow for the flexibility of dosing different compounds (i.e. an antigen and an immunomodulator) in similar period of time and frequently by the same route of administration without a co-delivery vehicle. Co-delivery ASIT, either chemically or physically, keeps both the immunomodulator and antigen near one another, thus, delivering both components at the same time and into the same environment.

The Kang group reported the use of a co-administration approach by co-injecting the small molecule immunosuppressant dexamethasone (Dex) and the antigen ovalbumin (OVA), which were able to cause long-term antigen-specific tolerance in T1D murine model.[41] The same group later reported co-injecting Tacrolimus (FK-506), an immunosuppressant, along with a plasmid DNA encoded with autoantigen. Their co-administration strategy resulted in the expansion of Tregs and thus treating autoimmunity.[42] Co-administration is not limited to small molecules, biologics have also been reported to be used in co-administration ASIT. The majority of these therapies use a plasmid encoding an immunomodulatory biologic component and a plasmid DNA encoding autoantigen. Glinka and coworkers reported the use of a plasmid encoding a fusion protein composed of preproinsulin (PPI) and Glutamate decarboxylase 65 (GAD65), which are both suspected autoantigens associated with T1D, and plasmid encoding an immunomodulator compound mutant B7, a known CTLA-4 inhibitor. This co-administration therapy was reported to improve the disease state of non-diabetic mice (NOD). Other have reported similar therapies such as the Garren group and Lewis group for MS[43] and T1D[44] respectively. Drawbacks to co-administration ASIT include the non-specific immune suppression by rouge immunomodulator or complete loss of efficacy if the autoantigen and immunomodulator drift away from the microenvironment meant to be targeted.

Co-delivery addresses the major drawback associated with co-administration for the treatment of autoimmunity by the using a co-delivery vehicle that insures the delivery an immunosuppressant and autoantigen at the same time and microenvironment. This strategy can be broken up into three distinct categories for the delivery of autoantigen and an immunosuppressant: first, plasmid DNA can co-encoded both components; second, the components are absorbed or co-

encapsulated; and finally, an autoantigen and immunosuppressant can be chemically linked together.

A single plasmid DNA encoding the autoantigen GAD65 and the immunomodulator IL-4[45] or the pro-apoptotic protein BAX,[46] have been co-delivered as a treatment for NOD mice, a T1D mouse model mimic. Both of these co-delivery therapies have been successful in the suppression and prevention of the disease.[45-46] Numerous types of particulate delivery vehicles (ie. liposomes,[47] nanoparticles,[48] microparticles[49]) either co-absorb or co-encapsulate autoantigen and immunosuppressants for the treatment of autoimmune diseases. The co-delivery by co-encapsulation of Dex and the MS autoantigen MOG_{35-55} in acetylated dextran nanoparticles were reported to improve the disease state of EAE mice.[49] When compared to co-administration work by Kang and coworkers[41] with the same autoantigen and immunosuppressant in the same mouse model, the co-delivery treatment was shown to be more efficacious.[49] Finally, bifunctional peptide inhibitors (BPIs) such as PLP chemically linked to ICAM-1, a cell adhesion molecule, has been shown to improving the disease state in a MS animal model;[50] and the BPI GAD65 chemically linked to $CD11a_{237-247}$, an immunomodulator, helped reduce immunogenicity in a T1D[51] mouse models. A drawback for co-delivery ASIT is the requirement of a delivery vehicle for an immunosuppressant and an autoantigen, since the delivery vehicle may be difficult to be formulated, encoded, or conjugated. This work will focus on the bioconjugation of autoantigens to an immunosuppressants and the synthesis of a novel antigen-only delivery system for the treatment of autoimmunity, and therefore, a brief review and explanation of bioconjugation strategy for the synthesis of our ASIT will be presented.

1.4. Introduction into Bioconjugation

In 2001 the Sharpless group—inspired by nature's ability to produce enormous biological diversity from a limited number of monomers—proposed the development of a set of robust, high yielding, selective, and broad ranging methods that can be performed under benign reaction conditions for coupling molecular fragments together.[52] Sharpless coined this class of reactions "click chemistry," a strategy which supplied a library of molecules with selectively-reactive handles for efficient synthesis of various conjugates. This convenient and efficient synthesis strategy allows for rapid construction of various bioconjugates or non-biological molecules to probe and reveal new information about biological systems or cause a desired biological effect (i.e. via an ASIT). The selectivity of click chemistry encouraged Bertozzi and co-workers to apply the strategy in living systems and develop "bioorthogonal" reactions.[53]

Several click reactions are present in the literature, such as Diels-Alder,[54] Staudinger ligation,[55] thiol-Michael addition,[54, 56] oxime ligation reactions,[57] and copper-catalyzed azide-alkyne cycloaddition reaction (CuAAC) to name a few. CuAAC is the most widely applied click reaction that has been developed. Various disciplines have applied this highly efficient coupling reaction for the synthesis of drugs, biomolecules, polymers, advanced biomaterial, and surfaces. Strain-promoted azide-alkyne cycloaddition reaction (SPAAC) was developed to improve upon the disadvantages of CuAAC by eliminating the need for copper, thus eliminating cell toxicity and allowing the reaction to become biorthogonal.

This work utilizes azide-alkyne cycloaddition (AAC) reactions for the synthesis of ASIT and therefore a literature review of the history, reaction conditions, methods for installation of reactive handles, and utilization in peptide or protein bioconjugates, with an emphasis on practical examples as well as challenges and limitations with this approach, will be covered. Finally, a

section outlining the trends of non-AAC linkers, which was extrapolated in our implementation of AAC chemistry bioconjugation will be discussed.

1.5. Azide-Alkyne Cycloaddition Reaction

In 1961 Huisgen was the first to report the formation of 1,2,3-triazoles via AAC (Table 1).[58] This heterocyclic bioisostere—a chemical group or substituent with similar chemical or physical properties to another substituent or group—is a potential replacement for an amide. 1,2,3-triazole's are more resistant to enzymatic degradation, oxidizing or reducing conditions, and pH. Specifically, the 1,4-substituted triazole constitutional isomer, is similar to an *E*-amide in both electronic properties and topology; the triazole isomer exhibits spacing of 5.0 Å as compared to 3.9 Å in the *E*-amide bond;[59]it also has a dipole moment of 5 Debye as compared to 4 Debye in the amide.[60] The 1,5-substitued triazole and *Z*-amide are geometrically analogous because they both have a bond distance of 2.4 Å.[61] While the triazole ring is appealing, the Huisgen reaction is limited in its application because of its drawbacks: lack of regioselectivity, elevated pressure, high temperatures, and long reaction time required to furnish a triazole mixture (Table 1).

Both the Sharpless[52] and Meldal[62] groups simultaneously and independently reported the use of catalytic amounts of Cu^{1+} led to regiospecific formation of 1,4-substituted triazoles under mild reaction conditions. In the absence of Cu, they reported rates 10^6-10^7 times slower in producing the mixture of 1,4- and 1,5-substituted products. The reaction can be performed at various temperatures (0-160 °C), in numerous solvents (including water), and at a wide range of pH values (4-12).[63-67] During the initial application of the CuAAC reaction, several drawbacks where discovered, where the problems were predominately associated with Cu. The active catalyst in CuAAC reaction is Cu^{1+}, which can be oxidized to the more stable Cu^{2+} in solution. To counter

this problem, Cu^{2+} is used with excess reducing agent to make Cu^{1+} *in situ*. The most common reducing agent used for CuAAC is sodium ascorbate in a 3- to 10-fold excess relative to Cu.[68] Other reducing agents, such as hydrazine[69] and hydroxylamine,[70] have also been used. Sodium ascorbate and Cu^{1+} however, have been reported to promote the oxidation of histidine and arginine residues.[71] These unintended side reactions have led to the introduction of Cu-stabilizing ligands (Table 1) to both limit degradation of these amino acids, as well as, to accelerate the rate of the CuAAC reaction.[72-73] The drawback of the toxic effect of Cu on cell viability has limited its use. Finally, the inability to perform CuAAC reactions in biological systems, due to the need of Cu, has restricted it use as a possible bioorthogonal reaction.

Table 1. Summary of various types of AAC reactions and their limitations

Reaction Type	Reagent 1	Reagent 2	Catalyst	Product	Limitations
Huisgen AAC	R_1-N_3	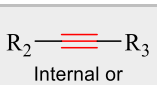 Internal or terminal alkyne		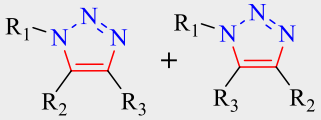	>100°C Days-Weeks Not regiospecific
CuAAC	R_1-N_3	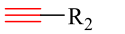	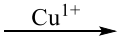	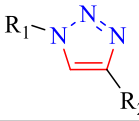	Requires catalyst, reducing agent, and stabilizing agent*
RuAAC	R_1-N_3	 Internal or terminal alkyne	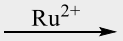	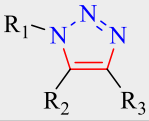	Requires catalyst Forms 1,5-regioisomer
SPAAC	R_1-N_3	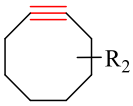		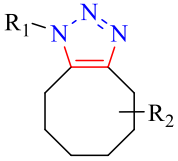	Not regiospecific Cyclooctyne reagents more expensive
*** Examples of Cu-stabilizing reagents commonly employed in the CuAAC reaction**		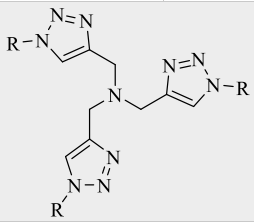		R = benzyl (**TBTA**) R = *tert*-butyl (**TTTA**) R = $CH_2CH_2CH_2OH$ (**THPTA**)	

To address the problems associated with CuAAC, Bertozzi and co-workers developed the SPAAC reaction in 2004 (Table 1).[74] This method does not require a catalyst because it uses the high degree of ring strain on the cyclooctyne ring (18 kcal/mol) and lowered activation energy due to the favorable geometry of the starting materials being similar to the transition state (sp^2 like in structure). Thus, the reaction is facile and works under mild reaction conditions and relatively fast reaction times.[75] However, the SPAAC has its own drawbacks, such as the lack of regiospecificity due to the absence of strong kinetic or thermodynamic preferences leading to a mixture of 1,4-substituted products. The aqueous solubility of the hydrophobic cyclooctyne reagents were of concern, but recent developments have seen the installation of hydrophilic moieties, such as polyethylene glycol (PEG) or sulfonate groups in the linker attached to the ring. Strained cyclooctyne reagents were initially cost-prohibitive to employ compared to their terminal alkyne counterparts. Alternative SPAAC reagents and synthetic routes[76] have recently been reported, thus making the reagents more cost effective. With greater access to SPAAC reagents, a number of strained alkyne moieties have been developed with varying reaction rates.[77] Photolabile "caged" cyclooctyne variants present an important added functionality to the reaction, revealing the reactive strained alkyne group under exposure to 350 nm light and enabling spatially-controlled conjugation (Figure 2A).[78] These reagents have predominately been used for surface functionalization applications where spatiotemporal control of conjugation is critical.[79-80]

Regioselective formation of 1,5-substituted triazoles has also been reported by the use of catalytic ruthenium (Ru) complexes.[81-86] Compared to Cu catalyst, Ru catalyst can uniquely react azides with internal alkynes.[87] Both steric and electronic considerations for the synthesis of 1,5-triazole have to be examined. The 1,5-triazole mimics the *Z*-amide bond, which is thermodynamically unfavorable compared to the *E*-amide bond due to steric repulsion of the

groups flanking the amide moiety. The value of the triazole as an amide bond surrogate relies on the oxygen lone pair, the acidic N-H bond and the polarized carbonyl carbon. The polarization of the 1,5-triazole, however, is such that the electrophilic carbonyl carbon is replaced by a negatively polarized nitrogen atom.[88] Therefore, despite the ability of Ru to catalyze reactions between internal alkynes and azides, the dissimilar electronic properties and unfavorable steric interactions compared to the naturally-occurring amide bond limits the implementation of Ru in bioconjugation approaches to make bioisostere of amides.[89] The facile synthesis of the 1,4-substituted triazole ring via AAC, and its stability and chemical properties has led to its implementation in bioconjugation applications. In order to exploit the utility of the triazole ring, one must first understand various ways to introduce reactive handles to molecules of interest, which will undergo subsequent AAC reactions.

1.6. Installation of Azide and Alkyne Functionalities on Intact Biomolecules

Two common approaches are used to functionalize biomolecules with azide or alkyne handles: *N*-hydroxysuccinimide (NHS) coupling reaction and thiol-maleimide reactions (Figure 1A, 1B). NHS ester mediated amide bond formation using an amine and carboxylic acid and are among the most popular compounds used to functionalize biomolecules due to their aqueous compatibility, commercial availability, and the ability to selectively target primary amines present on lysine residues or the *N*-terminus (Figure 1A). For biomolecules, reaction conditions generally employ aqueous buffers at pH 7-9. At a pH closer to 9, the reaction proceeds more efficiently due to greater amine deprotonation. However, at elevated pH, hydrolysis of the activated NHS ester also occurs at a greater rate. Conversely, at neutral pH, the reaction between primary amines and NHS esters proceeds with reduced hydrolysis of the NHS ester, but the reaction occurs at a slower

rate. Thus, a pH between the range 7-9 is commonly employed to balance the reaction rate and hydrolysis rate of the NHS ester. Typically, NHS esters reactions are performed at room temperature over 1-2 hours. Reactions involving sensitive biomolecules can proceed at 4°C overnight, in order to minimize or eliminate degradation.

Selective *N*-terminal functionalization has been shown at pH values below 7, with pH 6.3 being ideal. This is due to the difference in acidity between the α-amino group of the *N*-terminus (pK_a ~ 8) and the ε-amino group of lysine residues (pK_a ~ 10).[90] Amine-containing buffers such as tris or glycine must be absent, however, these can be useful as quenching buffers to ensure no additional reactive NHS ester is available after achieving the desired degree of functionalization. NHS ester reagent solutions should be prepared in anhydrous organic solvents to limit hydrolysis prior to initiating the reaction, provided that all reaction components remain compatible. However, excess NHS ester reagent can be use in anhydrous organic solvents. Unfortunately, NHS ester reagents are typically not stable for more than a few hours in solution, even when prepared in anhydrous solvents. Thus, if the NHS ester reagent is the limiting reagent, anhydrous solvents should be used to maximize yield.

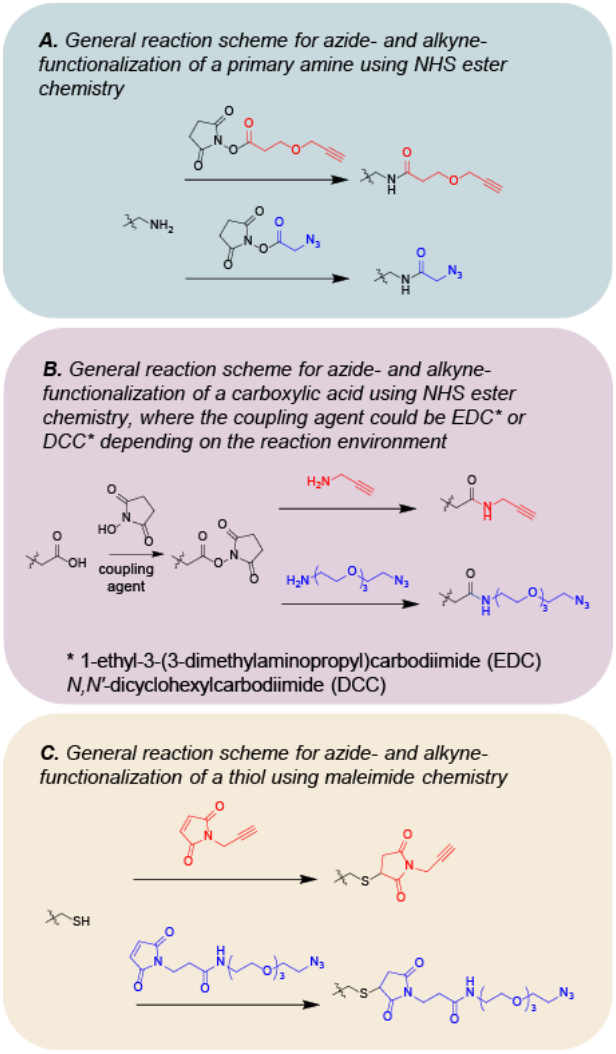

Figure 1: General reaction schemes to functionalize biomolecules with azides and alkynes.

For NHS ester-containing small molecules that do not require aqueous solvents to dissolve, it is best to use anhydrous organic solvents such as *N,N*-dimethylformamide (DMF), dimethyl sulfoxide (DMSO), acetonitrile (MeCN), and dichloromethane (CH_2Cl_2). The reduction of the possibility of aqueous hydrolysis generally results in higher yields and better selectivity for amino functional groups. In the absence of an amine, NHS esters can be used to conjugate other nucleophilic groups such as deprotonated hydroxyl or thiol moieties. Finally, coupling between a nucleophilic moiety (i.e. amines, thiols, alkoxides) and a carboxylic acid can be achieved by forming an NHS ester *in situ.* First, by either using the coupling reagent 1-ethyl-3-(3-dimethylaminopropyl)carbodiimide (EDC) or *N,N'*-dicyclohexylcarbodiimide (DCC) to modify the carboxylic acid, then by adding NHS to form the NHS ester *in situ*, and finally by adding the nucleophilic component to produce the amide bond to connect the two components. (Figure 1B).

The thiol-maleimide reactions can be used when a cysteine residue is present in a biomolecule. This reaction yields a thioether bond via a Michael addition reaction (Figure 1C). Thioethers have been reported to undergo thiol exchange reactions, as well as to convert back to the starting thiol and substituted maleimide.[91] Similar to the NHS ester reactions, maleimide reactions are pH-controlled in aqueous media. Generally, the pH range of 6-8 and at lower pH values, the reaction proceeds at a slower rate, but favors thiol functionalization over hydrolysis. However, at higher pH values, the reaction proceeds at a faster rate, but hydrolysis of the maleimide is of greater concern. Thiol-containing reaction buffers, such as dithiothreitol (DTT) or β-mercaptoethanol (BME), should be avoided, but are useful post-reaction to quench any remaining maleimide after achieving the desired conjugation levels. Mechanistic studies have revealed three main factors that affect the thiol-maleimide reactions: solvent, initiator (base), and the thiol selected.[92]

Biomolecule functionalization with the goal of attaching an azide or alkyne are most commonly performed using NHS ester or thiol-maleimide chemistry. There are a variety of commercially available heterobifunctional linkers other than just NHS esters or maleimides shown in Figure 2. Such monomers can be used for the following four major areas: final *N*-terminus functionalization during peptide or protein synthesis, residue-specific functionalization, post-translational modification, and nucleic acid modifications.

1.6.1 Unnatural amino acid Strategies for Azide-Alkyne Instillation

Selectivity and reproducibility of bioconjugation via NHS ester or maleimide chemistries on larger proteins have proven to be challenging, since the surface-exposed lysine and cysteine residues targeted can be abundant on larger proteins.[87, 93] To overcome the challenge, unnatural amino acids (UAAs) bearing azide or alkyne functionalities (Figure 2C)[54-56, 94] have been used in solid-phase peptide synthesis (SPPS) or by metabolic labeling during expression in cell systems, respectively. UAA modifications are generally divided into site-specific and residue-specific categories. Site-specific functionalization refers to the modification of a single amino acid, whereas residue-specific functionalization allows for partial or quantitative replacement of a particular amino acid. For smaller peptides, site-specific functionalization using SPPS is relatively simple. A wide range of UAAs are commercially available with both azide and alkyne functional groups and protected versions of these compounds (Figure 2B) can be used to enable selective incorporation of the desired handle during SPPS.[58] In residue-specific labeling, UAAs are included in cell growth medium and incorporated into the primary sequence of the expressing protein. In a review, Budisa *et al.*[95] outlines the biology of the metabolic labeling methods, as well as, some issues that arise with the incorporation of UAAs. Peptides bearing azide and alkyne handles also

present an attractive way to make cyclic peptides, which have literature precedence.[57, 60, 96] Site-specific installation of click reactive handles has been utilized for many functions such as fatty acid conjugation,[66] conjugation of an antibody to a drug,[67-68] or for fluorophore labeling of a protein.[72]

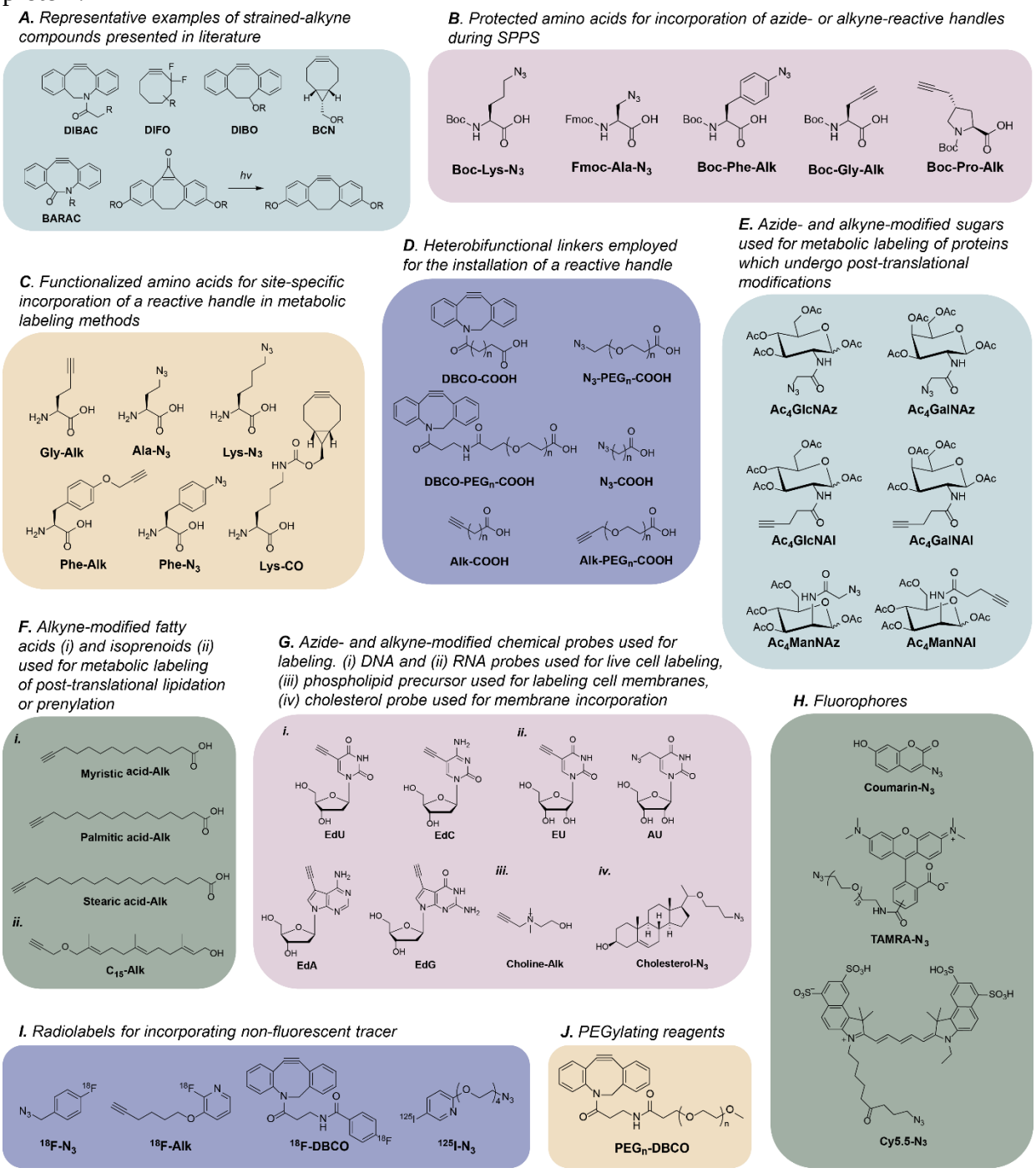

Figure 2. Commercially-available materials for biomolecule functionalization via azide or alkyne reactive handles.

1.6.2. Heterobifunctional Linker, Post-Translation, and Nucleic acid Modifications

Installation of azide or an alkyne can also be achieved with the desire for reactive handles using heterobifunctional reagents such as modified sugars, or nucleic acids. Heterobifunctional reagents are selected when the C-terminus amino acids of a peptide or protein are required to maintain activity. They are installed on the *N*-terminus as the final step of SPPS. Since these linkers do not contain a nucleophilic functionality such as a primary amine, there is no need for the use of protecting group chemistry. The heterobifunctional linker generally contains a carboxylic acid moiety on one end and on the other end either an azide or alkyne handle (Figure 2D). In order to alleviate potently increased hydrophobicity upon installation of a heterobifunctional linker, a variety of heterobifunctional linkers are commercially available with different solubilizing groups such as PEG and sulfate groups. PEGylated forms of the heterobifunctional linkers are available in various lengths, which permits precise spacing of the reactive handle.

Post-translational glycosylation has been exploited as a meant for site-specific conjugation during protein expressed in cell systems. For example, modified acetylated sugars may be added to growth medium, which first needs to be internalized by host bacteria, followed by the removal of the acetate groups by non-specific hydrolases or esterases prior to being available for incorporation into the protein sequence (Figure 2E). Upon incorporation of a sugars into proteins, 'click' chemistry can be performed either *in vitro* or following protein isolation.[79-81, 83, 85-86] Similarly, incorporation of alkyne-modified fatty acids can be done during other biosynthetic pathways such as post-translational lipidation, prenylation, farnesylation,[78, 80, 82, 84, 87, 89] (Figure 2F*i*) or isoprenoid precursors[87-88, 90] (Figure 2F*ii*). Protein and fatty acid incorporation of AAC

handles is also useful for the facile conjugation to AAC fluorophores (Figure 2H), which allows for direct measurement of biological activity.

DNA,[58, 60, 91] RNA,[59] and components on a cell membrane[60] can also have modifications to install azide and alkyne nucleic acids (Figure 2G*i-ii*) and cell surface molecules. (Figure 2G*iii-iv*). These modifications are primarily used for imaging applications. However, such modifications can be used to enhance targeting, alter binding,[58] or modify expression to provide significant therapeutic potential. Neef and co-workers[59] reported that an unnatural nucleic acid in DNA labeling resulted in a difference in incorporation efficiency and toxicity. However, they postulated that the difference was possibly due to the particular cell type used in their studies.

1.7. Payload Molecules for Probing or Modulating Biomolecule Function

In order to study biological function in real time, both azide and alkyne modified fluorophores (Figure 2H) and radiolabels (Figure 2I) have been reported. Predominately, biomolecules are tagged with a fluorescent component for imaging inside of a cell and/or quantitation using techniques such as flow cytometry. Sivakumar *et al*.[97] developed a pro-fluorescent hydroxyl-coumarin molecule (coumarin-N_3, Figure 2H), which had insignificant fluorescence when unconjugated, and became fluorescent upon successfully AAC by the formation of the extended conjugated system.[98] Due to the fluorescent hydroxyl-coumarin pro-fluorescent quality, various studies utilized the fluorophore to optimize the reaction and to study kinetics of the click reaction.[99-100] Similarly, radiolabels (Figure 2I) have been reported and used to enable access to both targeted radiotherapy and *in vivo* visualization and quantitation techniques that are not possible with fluorescent labels, such as positron emission tomography (PET)[101] and single photon emission computed tomography (SPECT).[102] In order to modify clearance or alter

biodistribution, PEGylation reagents (Figure 2J) can also be utilized by making significant changes to its molecular weight (MW), and thus significantly changing the biophysical properties of the bioconjugate. Van Geel *and coworkers.*[69] reported that AAC reaction efficiency can be increased by increasing PEG chain length, up to 12 units.

AAC chemistry has also been utilized in the field of biopharmaceutics as a facile method for the synthesis of antibody-drug conjugates (ADCs). Currently, ADCs used clinically or in clinical trials utilize thiol-maleimide chemistry to bioconjugation. Unlike AAC, this process thiol-maleimide chemistry is reversible and is not as specific as AAC reactions. This lack of specificity for thiol-maleimide chemistry leads to heterogenous product mixture.[103] In order to improve efficacy of ADCs that use thiols for bioconjugation, both site-specific modification and improved stability have been implemented.[104] In order to further improve ADCs, scientist are exploring click chemistry for conjugation of payloads to antibodies. Azide or alkyne functionalized UAA have been incorporated into antibodies then conjugated to an azide or alkyne functionalized payload[59-60, 104] using a variety of linker types including a cleavable linker.[60] Cytotoxic drugs auristatins and maytansinoids, commonly used in ADCs, have

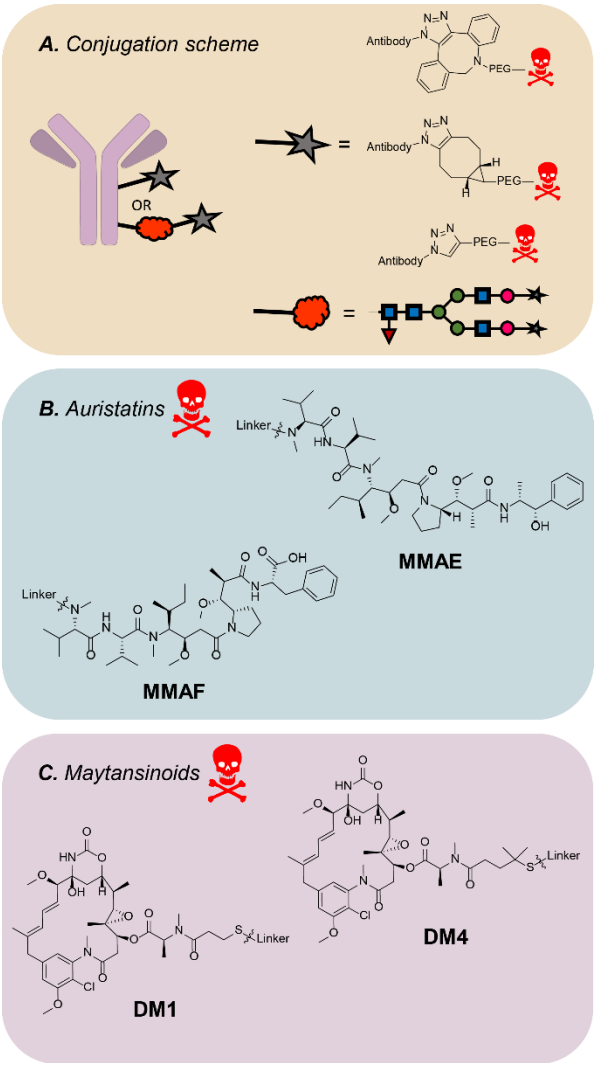

Figure 3. General conjugation in the construction of ADCs.

been functionalized with handles for AAC chemistry (Figure 3). Currently, Twenty-two of the ADCs currently in clinical trials or on the market incorporate monomethyl auristatin E (MMAE) or monomethyl auristatin F (MMAF).[103] Similarly, the maytansinoids are used in 13 ADCs either in the clinic or commercially-approved.[103] Heterobifunctional linkers (Figure 2D) have also been used to functionalize the payload molecule.[1, 103] The incorporation of azide-UAAs into a monoclonal antibody (mAb) allows for site-specific conjugation of modified payloads,[58-60] but requires careful optimization for each payload, linker, and mAb.[59] Another approach which does not alter the primary sequence exploits post-translational modifications by attaching click handles onto glycans of the heavy chain.[69, 100, 105-106] More information on payload conjugation in click chemistry and in ADCs can be found in Meyer *et al.*,[107] Beck *et al.*,[103] and Akkapeddi *et al*.[108]

1.8. Challenges Associated with Bioconjugates: Synthetic and Analytical Considerations

Bioconjugates can exploit the benefits of multiple molecules with different properties, but their complexity often brings new challenges with respect to the synthesis and analysis of these constructs. Synthetic complications typically center on solubility or stability of the parent molecules or resulting conjugate. Proteins and other biomolecules are generally more sensitive than the payload to temperature and other environmental factors such as organic solvents, thereby limiting the approaches available to the traditional synthetic chemist.[6,109] In addition to reaction condition considerations, analytical hurdles reside around heterogeneity, deconvolution of data, and limited sample quantities due to high costs of proteins, which requires adaption of methods and techniques to comply with these demands.

Solubility of the biomolecule and payload are required for the success of the conjugation reaction. Payload molecules with minimal aqueous solubility require assistance from an organic

solvent to ensure the conjugation reaction can proceed. Typically, DMSO, DMF, and MeCN are used in these situations. However, one must also bear in mind the effect of organic solvent on the biomolecules. Biomolecules with higher order structure can be conformationally altered in the presence of organic solvents and may have limited solubility as the organic concentration increases. Therefore, minimizing the overall organic solvent concentrations used in the reaction is often essential.[6,110] As covered previously, NHS ester and related chemistries which target surface-exposed lysines or other charged amino acids can have a great impact on the overall solubility of the product as these amino acids will lack a charge following conjugation, thereby decreasing solubility of the bioconjugate. To negate some of the deleterious effects of conjugation on solubility, linkers which have solubilizing moieties can either counteract or enhance solubility as desired in the conjugate.

Importantly, a thorough understanding of the stability and degradation mechanisms of the parent molecules will guide the chemist in selecting the appropriate reaction conditions while maintaining the integrity of the functional entities involved. These studies must assess both the physical and chemical stability of the molecules, since mechanisms leading to instabilities in small molecules are different than those seen for larger biomolecules. Proteins have a frequent propensity to aggregate in solution, a phenomenon which can be reversible or irreversible. Aggregation can be especially problematic during synthesis, leading to precipitation and lower yields if not properly controlled. Aggregation during a chemical reaction can generally be limited by excipient addition, modification of the reaction environment (pH or ionic strength), decreasing reaction temperature, and limiting the amount of time the biomolecule is in solution. Any aggregates that form during the reaction should be separated from the product prior to final isolation, typically by filtration, centrifugation, or other size exclusion methods. Analytical

techniques employed for studying aggregation in biomolecules include size exclusion chromatography (SEC), gel electrophoresis, or various spectrophotometric and light scattering particle sizing methods appropriate for the aggregate size involved. Liquid chromatography coupled with tandem mass spectrometry (LC-MS/MS), often preceded by enzymatic digestion, is a powerful technique for understanding chemical degradation products in biomolecules. Small molecules are generally more robust than biomolecules and the degradation products can be more easily understood using LC-MS and NMR techniques. When designing bioconjugates that utilize the AAC reaction, the chemical and physical stability of the biomolecule, linker, payload, and any intermediates or catalysts must be taken into consideration and monitored appropriately.

Purification of bioconjugates constructed via the AAC reaction often require additional considerations. When employing the CuAAC variant, residual Cu is undesirable in the final products due to the toxic and oxidative effects in living systems. Fortunately, removal through common techniques appropriate for the compounds involved is generally adequate. For small molecules, Cu-binding resins such as Cuprisorb or chelators such as ethylenediaminetetraacetic acid (EDTA) are added following the reaction, which can also serve to quench the reaction.[6] However, metal binding resins such as Cuprisorb have a tendency to bind to biomolecules and should be avoided during purification. Purification for peptides and proteins is typically completed by chromatographic techniques such as reverse phase high pressure liquid chromatography (HPLC), or through size exclusion methods such as dialysis, where appropriate. Following purification, inductively coupled plasma mass spectrometry (ICP-MS) is a useful technique for assessing residual Cu levels. Fortunately, Cu-free approaches such as SPAAC can be used to avoid problems associated with residual Cu.

Limiting side reactions with amino acid residues of biomolecules is a necessity to maintaining activity in the final conjugate. CuAAC reactions employing the common Cu^{2+} and sodium ascorbate catalyst system are known to lead to the formation of reactive oxygen species, which can degrade amino acids such as histidine, arginine, cysteine, and methionine.[6] Cu-chelating ligands such as THPTA or TBTA and side chain surrogates, such as aminoguanidine (surrogate for arginine) can assist in limiting degradation. In addition, cyclooctyne compounds are known to react with reduced cysteine residues through a thiol-yne mechanism. However, pre-incubation with iodoacetamide has been shown to mitigate this side reaction.[6] In order to verify the structure of the chemically altered biomolecule, analytical methods such as reverse phase HPLC, LC-MS/MS, and peptide mapping can be utilized.[111]

The CuAAC and SPAAC reactions have been employed extensively in construction of hydrogels due to high yields, mild conditions (aqueous solutions, physiological pH, ambient temperature), and minimal formation of byproducts.[112-115] An added complication of bioconjugation to polymers is the tendency for intra- or inter-molecular entanglement, limiting the accessibility to reactive sites. Reduction of this phenomenon can occur through the addition of organic solvents known to denature the polymer,[6] addition of heat to induce thermal unfolding, or altering pH or ionic environment to disrupt specific interactions causing entanglement.[116] In other cases, limited reactive site availability is due to the viscosity of high MW polymers, requiring more dilute reaction conditions. In general, conjugation efficiency will decrease as MW increases due to reduced collisions with appropriate geometry and sufficient energy to react, especially for polymers such as hyaluronic acid which are self-associating or have secondary structure.[117]

1.9. Lessons Learned from Other Bioconjugation Chemistries: Linker Stability

Another critical component of bioconjugates is the stability of the linker, since this can also have a dramatic impact on the efficacy of the bioconjugate. Both cleavable and non-cleavable linker strategies have been used in the ADC field as well as in other bioconjugates. Zimmerman and coworkers[58] incorporated the azide UAA *p*-azidomethyl-L-phenylalanine (pAzF) into trastuzumab (Tmab), conjugated via SPAAC chemistry to DBCO-PEG-MMAF. The resultant ADCs were highly potent when tested in *in vitro* cell cytotoxicity assays (Figure 3). The authors proposed that their ADCs were released during lysosomal degradation, which has been observed in other non-cleavable Tmab-maytansinoid ADCs. Some ADCs with non-cleavable linkers are active without cleavage and release of the drug, but the mechanisms of non-cleavable ADCs can be more complicated and must be determined experimentally.[58, 118-119] Cleavable linkers typically exploit environmental factors present in the cellular environment where payload release is desired, which involves pH, oxidizing/reducing conditions, or the presence of a relevant enzyme. While this approach is attractive in theory, and may be necessary for successful action of the payload, the mechanisms that release the payload may not be specific to only the desired target location.[120] For example, pH-sensitive linkers present in the bioconjugate can encounter acidic microenvironments during trafficking to the target location, and could release the payload in unintended locations throughout the body, yielding adverse side effects for the patient.[120-122] The site of conjugation of a payload onto the antibody can affect properties of the ADCs such as stability, immunogenicity, antigen binding, and pharmacokinetics. Careful optimization of conjugation site can lead to ADCs with desirable properties over ADCs made via random conjugation.[59, 123]

Some ADCs suffer from the 'bystander effect', which is when the conjugated toxin is released from the antibody following internalization in antigen-positive cells, crosses the cellular

membrane as a neutral species, and kills surrounding cells that may have lower expression of cell-surface antigen. In these cases, an understanding of the drug release mechanism is essential. ADC may not be sufficient to eliminate all of the solid tumor because cell populations with limited surface antigen expression will also be exposed to the toxin.

Brentuximab vedotin utilizes a cathepsin cleavable linker to conjugate MMAE to the antibody, which results in the release of this toxin in a neutral form capable of crossing biological membranes of adjacent cells not targeted by the ADC. Conversely, when the structural analogue, MMAF, is conjugated to an antibody and released in active form as a charged species, diffusion across membranes is limited, and the bystander effect is reduced. Payloads attached using cleavable linkers, such as those present in Tmab duocarmazine[124] are more prone to the bystander effect[125] than those containing non-cleavable linkages, such as the thioether linkage in Tmab emtansine. This underlines the importance of a thorough understanding of the stability of the linker and payload release, since the bystander effect provides an added mechanism to tune therapeutic specificity that must be accounted for in the design of ADCs with cleavable linkers. Jain and coworkers[126-127] have published a more detailed review on ADCs and associated linkers.

1.10. Lessons Learned from Other Bioconjugation Chemistries: Biological Consequence of the Linker

To date, comparative studies focused on the impact of different AAC linkers on biodistribution are largely absent from the literature. Fortunately, studies have been conducted using alternative bioconjugation chemistries, and the trends for those studies can be extrapolated to provide useful insight into the design of bioconjugates that utilize AAC chemistry. Tmab emtansine is an ADC used to treat patients with HER2-postitive metastatic breast cancer, and it is

composed of an anti-HER2 antibody Tmab linked via a thioether linkage to the maytansinoid DM1 (Figure 4*i*).[128] The thioether-linked 4*i* has been reported to be slightly more efficacious in mouse models than the disulfide-linked 4*ii*,[120] contrary to other maytansinoid-containing ADCs where the disulfide-linked drugs showed greater efficacy.[98-99, 120, 129] Erickson *et al.*[101] compared how the thioether and disulfide linkages in 4*i* and 4*ii* affected the mechanism of action and anticancer activity. In Tmab-sensitive breast cancer cell lines, both ADCs showed similar potency in terms of cell viability, but in Tmab-insensitive cell lines, 4*i* showed slightly greater potency than 4*ii*, although the cause was not fully understood. The clearance of 4*i* in plasma (Figure 4B) and in tumor cells (Figure 4C) was approximately two-fold slower than 4*ii*, which is most likely a result of improved linker stability. The payload delivery to tumors, however, was similar for both bioconjugates (Figure 4D). While the linker had an impact on pharmacokinetics (PK) and the rate of metabolism, both ADCs were successful in payload delivery and antitumor activity. Thus, much remains to be learned regarding the implications of linker design.

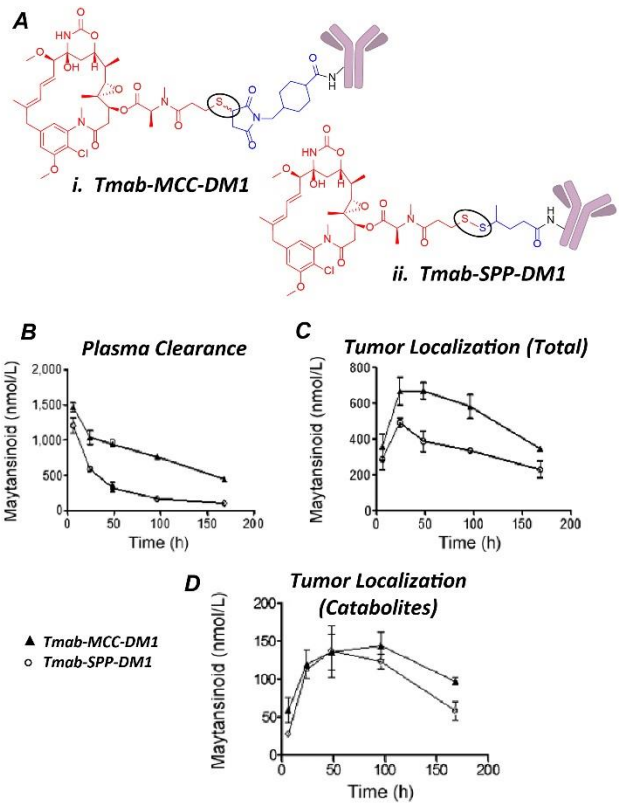

Figure 4: (A) Parent linker compounds: maleimidomethyl cyclohexane-1-carboxylate (MCC) and *N*-succinimidyl 4-(2-pyridyldithio)pentanoate (SPP). Tmab-MCC-DM1 (Ai) and Tmab-SPP-DM1 (Aii) structures, with DM1 in red, linkers in blue, and thioether and disulfide bonds circled. (B) Plasma clearance of ADCs, (C) Accumulation of ADCs in tumors, (D) Accumulation of ADC catabolites in tumors. (Figure adapted from Erickson et al.[124] with permission.)

Efflux pumps, such as multidrug resistance (MDR) proteins, target molecules for export out of cells. These pumps are more effective at transporting hydrophobic molecules than hydrophilic molecules. In addition, there is a strong correlation between MDR expression and poor clinical response.[102] Specifically, studies have shown that Tmab linked to DM1 via a hydrophilic PEGylated linker is more efficacious towards MDR^+ cells than those containing the more hydrophobic maleimidomethyl cyclohexane-1-carboxylate (MCC) linker.[130] Again, the relative hydrophobicity of the linker contributed to differences in activity as well as PK properties of the molecules.

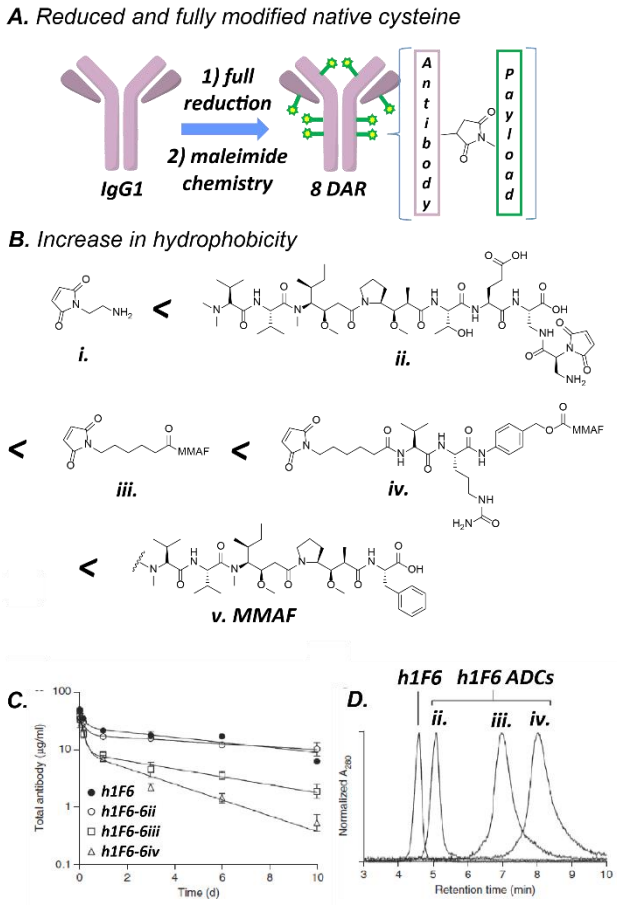

Figure 5: (A) Modification of native cysteine residues to make homogenous ADCs with DAR of 8, (B) Rank-order of increasing hydrophobicity of molecules conjugated to h1F6 C) Plasma clearance of h1F6 and h1F6 ADCs in mice, (D) Determination of hydrophobicity using hydrophobic interaction chromatography. (Figure adapted from Lyon et al.[130] with permission.)

In the context of ADCs, most drugs conjugated to the antibody are relatively hydrophobic and have minimal aqueous solubility, while the antibody typically has good aqueous solubility. Therefore, the resulting conjugate generally has intermediate solubility, often proportional to the MW contribution of the parent compounds in the overall conjugate. This can provide a significant benefit to the drug since hydrophobic drug molecules are more likely to enter cells via passive diffusion. On the other hand, ADCs often exploit the active transport mechanisms used to internalize

antibodies. Therefore, an increase in drug-to-antibody ratios (DAR) of ADCs leads to increased potency *in vitro,* but highly loaded ADCs often suffer from more rapid *in vivo* clearance.[131] Multiple studies report that by limiting the average DAR to the range of 2-4, potency can be maximized without negatively impacting *in vivo* performance.[104, 131-132] Methods have been developed to allow for DAR values of up to 8 by utilizing native cysteine residues on human IgG1 (Figure 5A). Using conventional hydrophobic drug-linker chemistries to make ADCs with a DAR of 8 resulted in fast plasma clearance.[104, 131-132] Lyon *et al.*[133] reported that by reducing hydrophobicity of ADCs through linker design, a DAR of 8 could indeed be achieved without accelerating plasma clearance. The authors conjugated 8 MMAF (5*v*) to an anti-CD70 antibody h1F6, using the protease cleavable linker 5*iv*. PK studies showed faster clearance of the h1F6-5*iv* than the unconjugated h1F6 (Figure 5C). They hypothesized that the difference in clearance maybe due to the loss of interchain disulfide bonds, leading to destabilized h1F6. However, the clearance of 5*i* conjugated to h1F6 and unconjugated h1F6 used as a control was similar. Therefore, the authors implicated linker hydrophobicity as the cause of accelerated clearance of h1F6-5*iv*. The relative hydrophobicity of h1F6 and conjugates was determined by hydrophobic interaction chromatography (HIC), revealing the following trend of increasing hydrophobicity: h1F5<5*ii*<5*iii*<5*iv* (Figure 5D). When a modified hydrophilic MMAF version (5*ii*) was conjugated directly to h1F6 with no linker, it had similar hydrophobicity to the parent antibody and both showed comparable plasma clearance *in vivo*. Similar *in vitro* potency was observed for h1F6-5*iv* and h1F6-5*iii*, however there was a >4-fold increase in *in vivo* activity for h1F6-5*iii* due to slower clearance (Figure 5C) of the more hydrophilic h1F6-5*iii*. Since h1F6-5*iii* is less hydrophobic than h1F6-5*iv*, it can be suggested that the reduction in hydrophobicity leads to improved plasma clearance of ADCs with high DAR of 8.

Solubility plays an important role in many physiological processes from biodistribution and clearance to immune recognition and response. Insoluble antigens are often processed by macrophages, while dendritic cells tend to process soluble materials.[1] Therefore, modification of the solubility of biomolecules through conjugation can perturb native function, altering recognition, trafficking, or uptake events. An understanding of aggregation propensity, with the associated decrease in solubility, is of critical importance in protein therapeutics. Aggregated proteins have the potential to induce an undesired immune response and lead to potentially serious adverse events for the patient.[134] In 2014, the FDA issued guidance on immunogenicity assessment as a key parameter in the development of therapeutic protein products. Recent studies have also shown that anti-drug antibodies formed upon repeat administration of biologic treatments such as rituximab have led to an immunogenic response in the patient.[135-136]

1.11. Utilizing AAC for the synthesis of chemical probes for the development of ASIT

With the brief overview of autoimmune diseases, their currently understood mechanism, and the lack of current viable treatments; ASIT has emerged as a viable strategy for the development of novel treatments for autoimmune disease. In this work, AAC library is synthesized and utilized for the construction of novel probes and potentially as ASIT for T1D. Both a co-delivery strategy ASIT and antigen-only delivery system for the treatment of autoimmunity will be reported.

CHAPTER 2:

DEVELOPMENT OF CHEMICAL BIOLOGY TOOLS FOR PROBING ANTIGEN SPECIFIC IMMUNOTHERAPY

CHAPTER 2: DEVELOPMENT OF CHEMICAL BIOLOGY TOOLS FOR PROBING ANTIGEN SPECIFIC IMMUNOTHERAPY

2.1. Introduction

The immune system is designed to defend against pathogens and environmental threats. Autoimmune diseases develop as a result of the loss of tolerance to self-antigen, leading to an improperly functioning immune system that targets its own tissues, organs, and cells.[137] Currently over 80 autoimmune diseases have been identified, afflicting over 5% of the world's population.[1] Current clinically available therapies either slow down the progression of autoimmunity or treat symptoms associated with the disease. Such therapies suffer from lack of specificity and has led to the development of antigen-specific immunotherapy (ASIT) as a potential therapeutic strategy for the treatment of autoimmune diseases.[138] We have designed a potentially novel ASIT know as antigen drug conjugates (AgDCs) to induce tolerance in autoimmune disease.

Taking inspiration from antibody drug conjugates (ADC) that have been successful in targeted drug delivery to specific receptors in cancer therapy, AgDCs are designed to be an ASIT co-delivery system by chemically linking an antigen to a drug for the treatment of autoimmune diseases. AgDCs are composed of an antigen (vehicle) which allows for the specific delivery of a potent drug (cargo). AgDCs are designed to be conjugated via azide-alkyne chemistry (AAC) for facile and rapid construction of different combination of antigens and drugs. Thus, various AgDCs can be constructed and used to probe an autoimmune disease animal model for quick and rapid identification of the best antigen and drug. In order to construct an AgDC, the following criteria must be met: first, a potent drug with easy installation of an AAC handle without compromising the drugs potency; second, a known autoantigen of an autoimmune disorder with the corresponding animal model that recognized the autoantigen; finally, determining the type of linker that will be used to chemically link the drug and antigen (i.e. PEGylated).

In T1D, beta cells that produce insulin are targeted incorrectly by the immune system which leads to the decrease and eventual loss in the production of the glucose regulating insulin.[14, 139] In T1D animal model, non-obese diabetic (NOD) BDC2.5 transgenic mice T cells can recognize the peptide sequence known as p79 (AVRPWVRME). Thus, p79 can be used to induce an antigen specific immune response in NOD BDC2.5 mice. Another example of an autoimmune disease is multiple sclerosis (MS). MS is the most common neurodegenerative disorder believed to be caused by an aberrant immune system targeting proteins on the protective nerve covering known as the myelin sheath.[9] Relapsing-remitting (RR)MS is the most common disease course and is characterized by new and increasing symptoms by periods of partial recovery. Experimental autoimmune encephalomyelitis (EAE) is an RRMS mouse model where and an adjuvant composted of antigenic epitope, $PLP_{139\text{-}151}$ (HSLGKLGHPDKF) with Complete Freud's Adjuvant (CFA) can induce disease. Since, the $PLP_{139\text{-}151}$ (PLP) peptide sequence is recognized by antigen-specific cells, an AgDC with PLP may be able to induce a tolerogenic effect in EAE mice. This section is focused on the initial synthesis and optimization of various biological probes (ie. fluorophores, AgDCs) for the autoimmune diseases.

2.2. Materials and Methods

Boronic acid, sodium ascorbate (NaAsc), trimethylamine, rhodamine B, *N*-hydroxysuccinimide, 2,4-dihydroxy benzaldehyde, *N*-acetylglycine, *N*-terminal 4-pentynoic acid and propargyl-*N*-hydroxysuccinimidyl ester were purchased from Sigma-Aldrich (St. Louis, MO) and used as received without further purification. 11-azido-3,6,9-trioxaundecan-1-amine (NH_2-PEG_3-N_3), Copper (II) sulfate pentahydrate ($CuSO_4 \bullet 5H_2O$), and *N*,*N*'-dicyclohexylcarbodiimide (DCC) were purchased from Acros Organics (Geel, Belgium). Fluorescein 5-Isothiocyanate

(isomer I) was obtained from TCI America (Portland, OR). Propargylglycine functionalized peptide $pPLP_{139-151}$ (p-HSLGKWLGHPDKF-OH) and *N*-terminal 4-pentynoic acid (homopropargyl, hp) modification peptide hpP79 (hp-AVRPWVRME-OH) purchased from Biomatik USA, LLC (Wilmington, DE).

2.2.1. Synthetic procedures

2.2.1.1. Synthesis of Rhodamine B N-hydroxysuccinimide esters *(Rhod-NHS ester)*

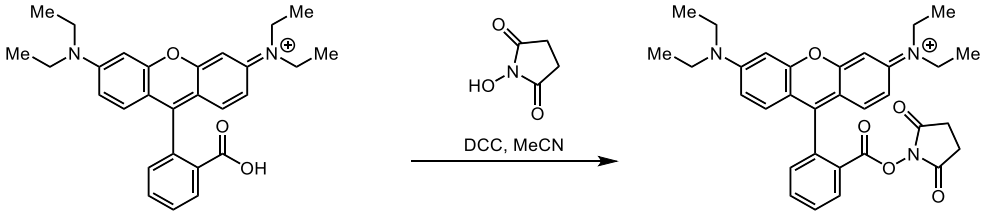

Figure 6: Reaction scheme for the synthesis of Rhod-NHS ester.

Synthesis of N-(6-(diethylamino)-9-(2-(((2,5-dioxopyrrolidin-1-yl)oxy)carbonyl)phenyl)-3H-xanthen-3-ylidene)-N-ethylethanaminium (Rhod-B) was adapted from Meng *et al.*[140] Both Rhod-B (2.4 g) and *N*-hydroxysuccinimide were dissolved in 100 mL of dry acetonitrile, heated to 45 °C, and stirred. Then a solution of dicyclohexylcarbodiimide (DCC) (1.2g in 50 mL dry acetonitrile) was added slowly to the reaction mixture. The reaction was started at elevated temperatures for 1h and then allowed to cool to room temperature for 20 h. Then the white precipitate was removed by filtration through Celite® and thefiltrate was concentration on the rotary evaporator, then residue was recrystallized in absolute ethanol, filtered and dried to give a solid purple product.; ^{1}H NMR (500 MHz, DMSO-d_6) δ 8.41 (dd, J = 7.9, 1.2 Hz, 1H), 8.09 (td, J = 7.6, 7.6, 7.2 Hz, 1H), 7.97 (td, J = 7.7, 7.7, 1.2 Hz, 1H), 7.67 (dd, J = 7.7, 1.2 Hz, 1H), 7.11 (d, J = 2.4 Hz, 1H), 7.08 (d, J = 2.4 Hz, 1H), 7.03 (s, 1H), 7.00 (s, 1H), 6.97 (d, J = 2.4 Hz, 2H),

3.65 (q, *J* = 7.14, 7.06, 7.06 Hz, 8H), 2.71 (br s, 4H), 2.69-2.65 (m, 2H), 8.44-8.40 (m, 2H), 1.20 (t, *J* = 6.99, 6.99 Hz, 12H); MS (TOF ESI+) expected $[M+H]^+$: 541.25 found: 541.25

2.2.1.2. Synthesis of Rhodamine B PEG$_3$ Azide (Rhod-N$_3$)

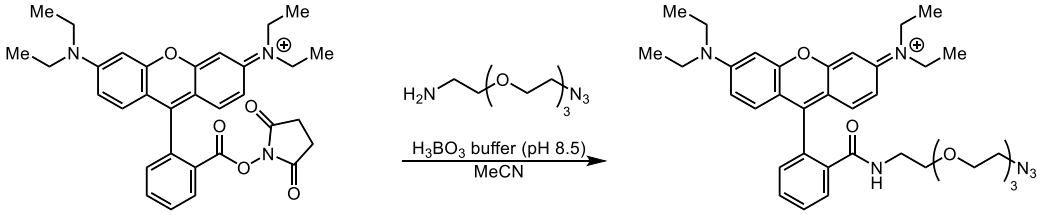

Figure 7: Reaction scheme for the synthesis of Rhod-N$_3$.

Synthesis of N-(9-(2-((2-(2-(2-(2-azidoethoxy)ethoxy)ethoxy)ethyl)carbamoyl)phenyl)-6-(diethylamino)-3H-xanthen-3-ylidene)-N-ethylethanaminium (Rhod-N$_3$) was adapted from Meng *et al*.[140] To a mixture of Rhod-NHS ester (0.737 mmol) in DMF (20 mL), NH$_2$-PEG$_3$-N$_3$ (6.60 mmol) in 20 mL H$_3$BO$_3$ buffer (pH = 8.5, 50 mM) was added and stirred at room temperature for 6 hours. The reaction mixture was frozen and lyophilized to give the crude product as an orange liquid. The crude product was dissolved in DMSO and purified by preparative RP-HPLC (Waters XBridge C$_{18}$, 5 µm, 10x250 mm, linear gradient from 5-95% MeCN (+ 0.05% TFA) in H$_2$O (+ 0.05% TFA) over 20 minutes, detection at 280 nm) to give the final product (57 mg, 18 %) as an orange-yellow solid; ^{1}H NMR (500 MHz, DMSO-*d*$_6$) δ 8.41 (dd, *J* = 7.9, 1.2 Hz, 1H), 8.09 (td, *J* = 7.6, 7.6, 7.2 Hz, 1H), 7.97 (td, *J* = 7.7, 7.7, 1.2 Hz, 1H), 7.67 (dd, *J* = 7.7, 1.2 Hz, 1H), 7.11 (d, *J* = 2.4 Hz, 1H), 7.08 (d, *J* = 2.4 Hz, 1H), 7.03 (s, 1H), 7.00 (s, 1H), 6.97 (d, *J* = 2.4 Hz, 2H), 3.65 (q, *J* = 7.14, 7.06, 7.06 Hz, 8H), 2.71 (br s, 4H), 2.69-2.65 (m, 2H), 8.44-8.40 (m, 2H), 1.20 (t, *J* = 6.99, 6.99 Hz, 12H); MS (TOF ESI+) expected $[M]^+$: 643.36, found: 643.36

2.2.1.3. Synthesis of alkyne-modified Pennsylvania Green (Penn Green-Alk)

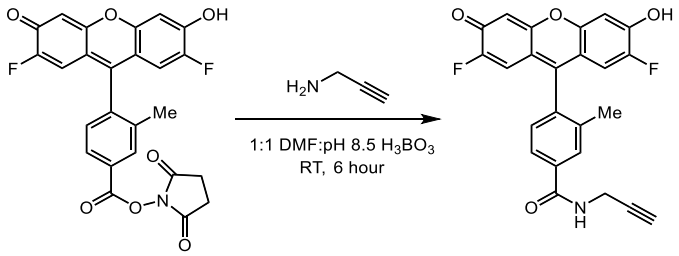

Figure 8: Reaction scheme for the synthesis of Penn Green-Alk.

Synthesis of 4-(2,7-difluoro-6-hydroxy-3-oxo-*3H*-xanthen-9-yl)-3-methyl-*N*-(prop-2-yn-1-yl)benzamide (Penn Green-Alk) was adapted from Meng *et al*.[140] To a mixture of Penn Green-NHS (55.3 µmol) in DMF (0.5 mL), propargylamine (61.2 µmol) in 0.5 mL H_3BO_3 buffer (pH = 8.5, 50 mM) was added and stirred at room temperature for 6 hours. The reaction mixture was frozen and lyophilized to give the crude product as an orange liquid. The crude product was dissolved in DMSO and purified by preparative RP-HPLC (Waters XBridge C_{18}, 5 µm, 10x250 mm, linear gradient from 5-95% MeCN (+ 0.05% TFA) in H_2O (+ 0.05% TFA) over 30 minutes, detection at 280 nm) to give the final product (22.5 mg, 84.7%) as an orange-yellow solid; ^{1}H NMR (400 MHz, DMSO-d_6) δ 7.99 (s, 1H), 7.93-7.87 (m, 1H), 7.40 (d, J = 7.9 Hz, 1H), 6.85 (br s, 2H), 6.63 (d, J = 11.2 Hz, 2H), 4.11 (dd, J = 5.6, 2.5 Hz, 2H), 3.17 (t, J = 2.5 Hz, 1H), 2.08 (s, 3H); HRMS (TOF ESI+) expected $[M+Na]^+$: 442.0867, found: 442.0870.

2.2.1.4. Synthesis of Rhodamine B alkyne (Rhod-Alk)

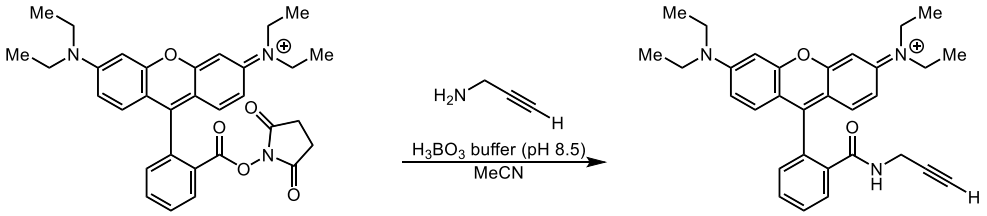

Figure 9: Reaction scheme for the synthesis of Rhod-Alk.

Synthesis of N-(6-(diethylamino)-9-(2-(prop-2-yn-1-ylcarbamoyl)phenyl)-3H-xanthen-3-ylidene)-N-ethylethanaminium was adapted from Meng *et al*.[140] To a mixture of Rhod-NHS (0.737 mmol) in DMF (20 mL), propargylamine (6.60 mmol) in 20 mL H_3BO_3 buffer (pH = 8.5, 50 mM) was added and stirred at room temperature for 6 hours. The reaction mixture was frozen and lyophilized to give the crude product as an orange liquid. The crude product was dissolved in DMSO and purified by preparative RP-HPLC (Waters XBridge C_{18}, 5 µm, 10x250 mm, linear gradient from 5-95% MeCN (+ 0.05% TFA) in H_2O (+ 0.05% TFA) over 20 minutes, detection at 280 nm) to give the final product (120 mg, 49%) as an orange-yellow solid; ^{1}H NMR (500 MHz, DMSO-d_6) δ 7.82-7.78 (m, 1H), 7.83-7.77 (m, 2H), 7.05-7.00 (m, 1H), 6.42-6.26 (m, 6H), 7.11 (d, J = 2.4 Hz, 1H), 7.08 (d, J = 2.4 Hz, 1H), 7.03 (s, 1H), 7.00 (s, 1H), 6.97 (d, J = 2.4 Hz, 1H), 3.65 (q, J = 7.14, 7.06, 7.06 Hz, 2H), 3.77 (d, J = 2.5 Hz , 2H), 2.70-2.63 (m, 8H), 2.66 (t, J = 2.5, 2.5 Hz, 1H)1.08 (t, J = 6.95, 6.95 Hz, 12H); HRMS (TOF ESI+) expected $[M]^+$: 480.2646, found: 480.2649.

2.2.1.5. Synthesis of 3-Azido-7-hydroxycoumarin (coumarin-N_3)

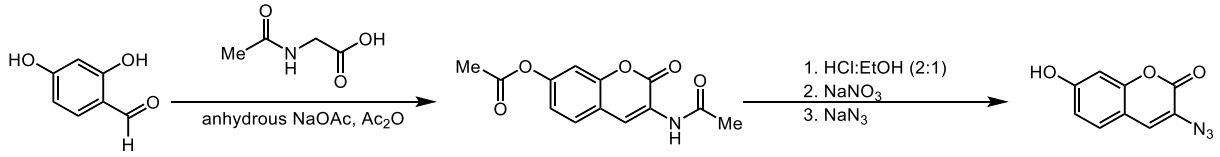

Figure 10: Reaction scheme for the synthesis of coumarin-N_3.

Synthesis of 3-azido-7-hydroxy-2H-chromen-2-one taken from Sivakumar *et al*.[97] A mixture of 2,4-dihydroxy benzaldehyde (2.76 g, 20 mmol), *N*-acetylglycine (2.34 g, 20 mmol), anhydrous sodium acetate (60 mmol) in acetic anhydride (100 ml) was refluxed under stirring for 4 h. The reaction mixture was poured onto ice to give a yellow precipitate. After filtration, the yellow solid was washed by ice water before it was refluxed in a solution of conc. HCl and ethanol (2:1, 30 mL) for 1 hour, then ice water (40 mL) was added to dilute the solution. The solution was then cooled in an ice bath and $NaNO_2$ (40 mmol) was added. The mixture was stirred for 5-10 minutes and NaN_3 (60 mmol) was added in portions. After stirring for another 15 minutes, the resulting precipitate was filtered off, washed with water, and dried under reduced pressure to afford a brown solid; 720 mg (18% overall yield). The product was pure enough for further reactions. ^{1}H NMR (DMSO-d_6, 500 MHz) δ 6.77 (d, J = 2.2 Hz, 1 H), 6.82 (dd, J = 8.5, 2.2 Hz, ^{1} H), 7.47 (d, J = 8.5 Hz, 1 H), 7.59 (s, 1 H). HRMS (TOF ESI+) expected [M]+ 203.0331; found 203.0326.

2.2.1.6. Synthesis of Fluorescein thiourea alkyne (FTU-Alk)

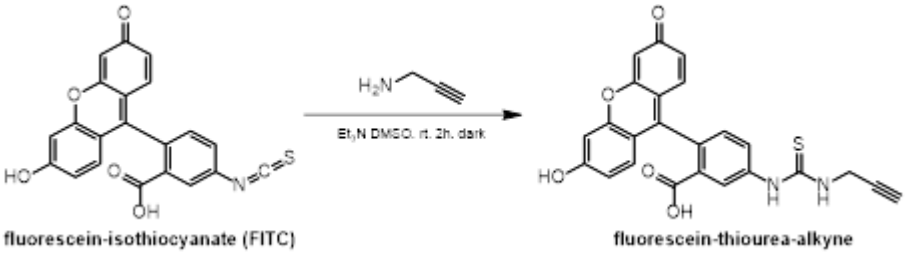

Figure 11: Reaction scheme for the synthesis of FTU-Alk.

Synthesis of 2-(6-hydroxy-3-oxo-3H-xanthen-9-yl)-5-(3-(prop-2-yn-1-yl)thioureido) benzoic acid (fluorescein thiourea alkyne; FTU-Alk; FTUA) was adapted from Meng *et al*.[140] To a mixture of FITC (200mg, 511.4 µmol) and 1-amino-11-azido-3,6,9-trioxa-undecane (131mg, 119.09 µL, 0.616 mmol) in DMSO (1 mL) was added triethylamine (75 µL, 0.514 mmol), and the mixture was stirred for 2 h at room temperature in the dark. The reaction mixture was then frozen at -20°C and lyophilized to afford a red oil. The crude product was dissolved in DMSO and purified by preparative RP-HPLC (Waters XBridge C_{18}, 5 µm, 10x250 mm, linear gradient from 5-95% MeCN (+ 0.05% TFA) in H_2O (+ 0.05% TFA) over 20 minutes, detection at 280 nm) to give the final product (176.5 mg, 77%) as an red-oil; ^{1}H NMR (500 MHz, DMSO-d_6) δ 7.82-7.78 (m, 1H), 7.83-7.77 (m, 2H), 7.05-7.00 (m, 1H), 6.42-6.26 (m, *6*H), 7.11 (d, *J* = 2.4 Hz, 1H), 7.08 (d, *J* = 2.4 Hz, 1H), 7.03 (s, 1H), 7.00 (s, 1H), 6.97 (d, *J* = 2.4 Hz, 1H), 3.65 (q, *J* = 7.14, 7.06, 7.06 Hz, 2H), 3.77 (d, *J* = 2.5 Hz , 2H), 2.70-2.63 (m, 8H), 2.66 (t, *J* = 2.5, 2.5 Hz, 1H)1.08 (t, *J* = 6.95, 6.95 Hz, 12H); HRMS expected $[M+H]^+$: 445.0853, found: 445.0858.

2.2.1.7. Synthesis of Fluorescein thiourea azide FTU-N_3

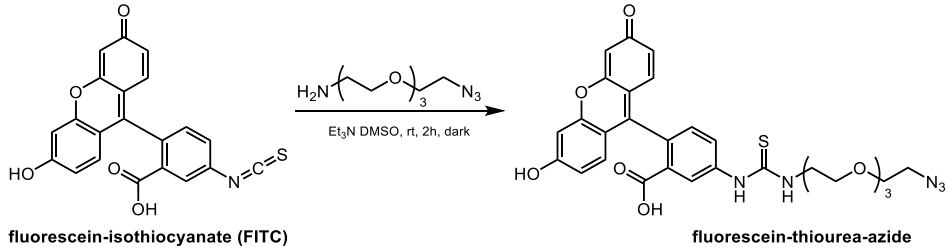

Figure 12: Reaction scheme for the synthesis of FTU-N_3

Synthesis of 5-(3-(2-(2-(2-(2-azidoethoxy)ethoxy)ethoxy)ethyl)thioureido)-2-(6-hydroxy-3-oxo-3H-xanthen-9-yl)benzoic acid (fluorescein thiourea azide; FTU-N_3) was adapted from Meng *et al.*[140] To a mixture of FITC (200 mg, 511.4 µmol) and NH_2-PEG_3-N_3 (33.92 mg, 0.616 mmol) in DMSO (1 mL) was added triethylamine (75 µL, 0.514 mmol), and the mixture was stirred for 2 h at room temperature in the dark. The reaction mixture was then frozen at -20 °C and lyophilized to afford a red-orange powder. The crude product was dissolved in DMSO and purified by preparative RP-HPLC (Waters XBridge C_{18}, 5 µm, 10x250 mm, linear gradient from 5-95% MeCN (+ 0.05% TFA) in H_2O (+ 0.05% TFA) over 20 minutes, detection at 280 nm) to give the final product (210.01 mg, 67%) as an orange-yellow solid; ^{1}H NMR (500 MHz, DMSO-d_6) δ 8.41 (s, 1H), 8.08 (s, 1H), 7.74 (d, J = 8.38 Hz, 1H), 7.18 (d, J = 8.0 Hz, 1H), 6.67 (d, J = 2.2 Hz, 2H), 6.62-6.54 (m, 3H), 3.64-3.53 (m, 14H); HRMS (TOF ESI+) expected $[M+H]^+$: 608.1815, found: 608.1811.

2.2.1.8. Synthesis of Dexamethsone-azide (Dex-N_3)

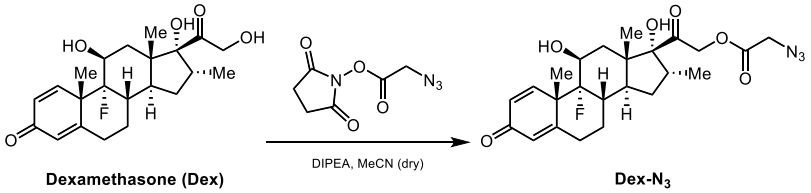

Figure 13: Reaction scheme for the synthesis of Dex-N_3

Dexamethasone (300 mg, 746.39 µmol) was added to a flame dried 250 mL round bottom flask with a stir bar and septa. Anhydrous MeCN (60 mL) was added under nitrogen, then DIPEA (720 µL, 3821.95 µmol) via glass syringe. The flask was stirred for 10 min before azidoacetic acid NHS ester (757.28 mg, 3821.95 µmol) was added as a powder. The reaction mixture was stirred overnight at room temperature before being analyzed by HPLC. Additional equimolar aliquots of azidoacetic acid NHS ester were added, followed by stirring for 2 hours at room temperature and analyzing by HPLC, until no additional benefit was observed. The crude reaction mixture was evaporated under reduced pressure, then dissolved in 4:6 MeCN:H_2O and purified by prep HPLC. The resulting column fractions were evaporated under reduced pressure to yield the final product as a white powder. ^{1}H NMR (500 MHz, DMSO-d_6) δ 7.30 (d, J = 10.2 Hz, 1H), 6.23 (dd, J = 10.1, 1.9 Hz, 1H), 6.01 (t, J = 1.7 Hz, 1H), 5.45 (dd, J = 5.0, 1.4 Hz, 1H), 5.23 (s, 1H), 5.17 (d, J = 17.5 Hz, 1H), 4.90 (d, J = 17.6 Hz, 1H), 4.32 – 4.19 (m, 2H), 4.19 – 4.11 (m, 1H), 2.88 (dqd, J = 11.5, 7.2, 4.1 Hz, 1H), 2.62 (tdd, J = 13.6, 6.0, 1.7 Hz, 1H), 2.44 – 2.32 (m, 1H), 2.35 – 2.28 (m, 1H), 2.22 – 2.05 (m, 3H), 1.77 (dt, J = 11.2, 5.2 Hz, 1H), 1.70 – 1.58 (m, 1H), 1.56 (dd, J = 13.8, 2.0 Hz, 1H), 1.49 (s, 3H), 1.35 (qd, J = 12.9, 5.0 Hz, 1H), 1.08 (ddd, J = 12.1, 8.2, 4.1 Hz, 1H), 0.89 (s, 3H), 0.80 (d, J = 7.2 Hz, 3H). ^{13}C NMR (126 MHz, DMSO-d_6) δ 204.36, 185.30, 168.28, 167.10, 152.77, 129.03, 124.12, 102.00, 100.61, 90.52, 70.63, 70.34, 69.00, 49.34, 48.09, 48.05,

47.87, 43.33, 35.69, 35.53, 33.67, 33.51, 31.92, 30.28, 27.32, 23.03, 22.98, 16.31, 15.15, 1.19. Expected $[M+H]^+$ = 476.2191 Da; Observed $[M+H]^+$ = 476.2067 Da.

2.2.1.9. Synthesis of Fluorescein Rhod –p79

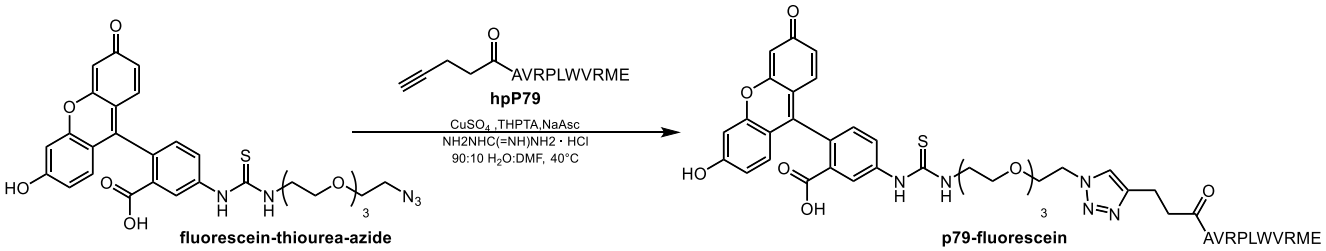

Figure 14: Reaction scheme for the synthesis of Rhod-p79.

To a solution of p79-Alk (28 μmol) in 37.5 mL deionized H_2O was added Fluorescein thiourea azide (42.82 μmol, 1.5 eq.) in 5.642 mL DMF, while protecting the reaction from light. Then 4,350 μL of a premixed solution of $CuSO_4$•$5H_2O$ (7.25 μmol) and Tris(benzyltriazolylmethyl)amine (THPTA; 62.9 μmol) in deionized H_2O was added to the reaction mixture, followed by 3200 μL of aminoguanidine•hydrochloride (578.0 μmol) in deionized H_2O. The reaction was allowed to stir at 40° C for 1-2 min before a 100 uL aliquot was removed for analytical HPLC to monitor reaction progress at 40° C. Then 5725 μL of NaAsc (578.0 μmol) in deionized H_2O was added to the reaction mixture. After 24 hours the reaction appears to no longer progress via HPLC analysis, the reaction mixture was purified by preparative HPLC on a Waters XBridge BEH C_{18}, 5 μm, 130 Å, 19x250 mm column using a gradient of MeCN in H_2O (constant 0.05% TFA). The isolated fractions were evaporated under reduced pressure to remove residual MeCN, then frozen at -20°C and lyophilized to yield a light pink oil. MS (TOF ESI+) expected $[M+2H]^{3+}$ = 656.9668 Da; Observed $[M+2H]^{3+}$ = 665.2963 Da

2.2.1.10. Synthesis of Dex-p79.

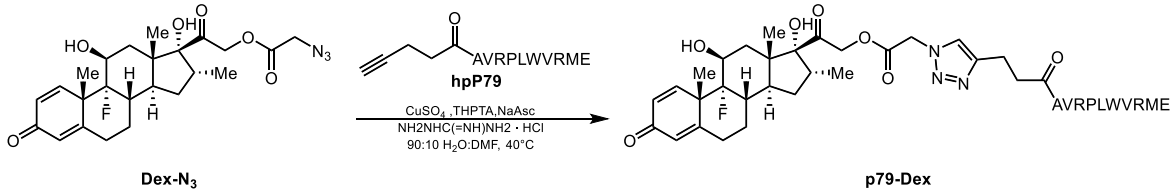

Figure 15: Reaction scheme for the synthesis of Dex-p79.

To a solution of p79-Alk (28 μmol) in 37.5 mL deionized H_2O was added Dexamethasone azide (42.0 μmol, 1.5 eq.) in 5.642 mL DMF. Then 4,350 μL of a premixed solution of $CuSO_4$•$5H_2O$ (7.25 μmol) and THPTA (62.9 μmol) in deionized H_2O was added to the reaction mixture, followed by 3200 μL of aminoguanidine•hydrochloride (578.0 μmol) in deionized H_2O. The reaction was allowed to stir at 40° C for 1-2 min before a 100 uL aliquot was removed for analytical HPLC to monitor reaction progress 40° C. Then 5725 μL of NaAsc (578.0 μmol) in deionized H_2O was added to the reaction mixture. After 2 hours the reaction appeared to be complete via HPLC analysis, the reaction mixture was purified by preparative HPLC on a Waters XBridge BEH C_{18}, 5 μm, 130 Å, 19x250 mm column using a gradient of MeCN in H_2O (constant 0.05% TFA). The isolated fractions were evaporated under reduced pressure to remove residual MeCN, then frozen at -20°C and lyophilized to yield a light brown powder. MS (TOF ESI+)

expected $[M+H]^+$ = 1812.94 Da, $[M+2H]2^+$ = 906.4 Da; Observed $[M+H]^+$ = 1812.8748 Da., Observed $[M+2H]2^+$ = 906.4775 Da.

2.2.2. Analytical characterization

NMR spectra were collected on a Bruker Avance AVIII 500 MHz spectrometer equipped with a dual carbon/proton cryoprobe, and all samples were dissolved in 600 μL of D_2O or DMSO-d_6. Data processing was completed using MestReNova 11.0 (Santiago de Compostela, Spain).

LC/MS sample analysis was completed on a Waters Xevo G2, employing linear elution gradients of 15-100% acetonitrile in water (constant 0.1% formic acid) over 45 min, on a Waters XBridge BEH C_{18}, 1.7 μm, 130 Å stationary phase (0.075 x 250 mm), with a 0.5 μL/min flow rate and 50°C column temperature. Electrospray ionization, operating in the positive mode (ESI+), was used as the ionization source with a QTof mass analyzer used for detection.

All HPLC chromatographic analysis was conducted on a Waters Alliance HPLC system equipped with either a diode array detector or dual wavelength UV/Vis detector. For RP-HPLC, general chromatographic conditions employed a linear elution gradient from 5-95% acetonitrile in water (constant 0.05% trifluoroacetic acid) over 50 min, on a Waters XBridge BEH C_{18}, 3.5 μm, 130 Å stationary phase (4.6 x 150 mm), with a 1.0 mL/min flow rate and a 35°C column temperature. For semi-preparative HPLC, a linear elution gradient of acetonitrile in water (constant 0.05% trifluoroacetic acid) over 20 min, on a Waters XBridge BEH C_{18}, 5 μm, 130 Å stationary phase (19 x 250 mm), with a 14.0 mL/min flow rate. Gradients were optimized for each run using the identical stationary phase in a 4.6 x 250 mm configuration.

2.3. Results and Discussion

2.3.1. Design and Rationale behind AgDCs

AgDCs were designed to selectively deliver a drug payload molecule which is chemically linked to an antigen-directing vehicle to antigen-specific cells. The selected drug must have the following qualities: high potency, known mechanism of action (MOA), and an available synthetic handle. These characteristics allow us to install an AAC handle at a position of the drug without losing potency. Dexamethasone (Dex) was chosen as our drug molecule because it meets all the required qualities to be used in AgDCs, and it has successfully been used in ADCs in literature.[141] For both PLP and p79, the C-terminus is required for immunological recognition, thus, the N-terminus was chosen as the site of AAC installation via the final step of solid-phase peptide synthesis preceding cleavage from the resin. By conjugating PLP or p79 to Dex, we expect a reduced inflammatory response in their respective autoimmune disease models. However, the focused of this section is to optimize AAC chemistry for the facile bioconjugation of a peptide to a drug. Finally, the linker that chemically connects the antigen and drug must be taken into consideration, specifically the following: linker flexibility, length, and stability. Long linkers may affect internalization of AgDCs into the immune cell, while a short linker may hinder binding to the cell surface. Thus, we employed a moderate length linker with the ability to be hydrolyzed in the cell to specifically release the potent drug.

2.3.2. Synthesis of chemical biology components for CuAAC reactions

For the facile and rapid construction of chemical biology probes we selected copper-catalyzed azide-alkyne cycloaddition (CuAAC) chemistry to be utilized in the final step in the synthesis of bioconjugates. CuAAC chemistry was selected because of its wealth in literature optimization[142-145] and its extensive use in bioconjugation[145-150]. Specifically, CuAAC reactions (Figure 16A) are known to be high yielding, produce benign side products, use mild reaction conditions, and are highly selective. Various small molecules and peptides with alkyne or azide handles were synthetized and utilized to make either AgDCs or other immunology active molecules in future chapters. (Figure 16B-D).

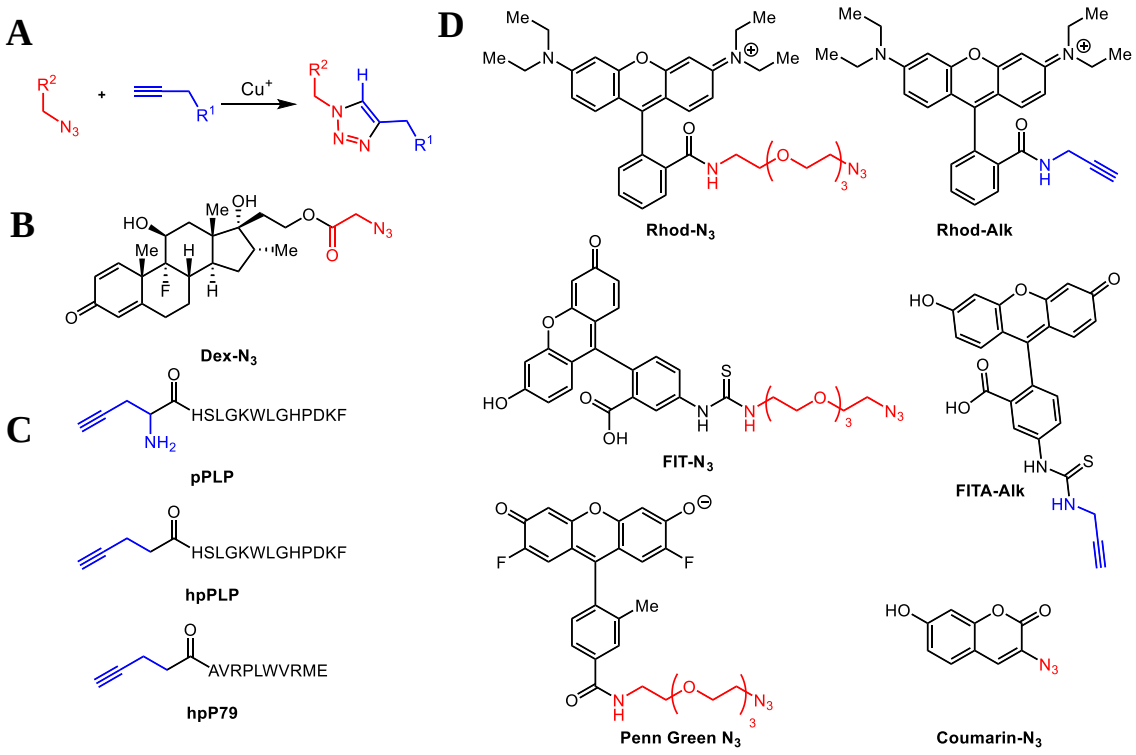

Figure 16: Chemical probes (A) Generic reaction scheme for a copper-catalyzed azide-alkyne cycloaddition. (B) Selected Drug Dexamethasone (Dex) for AgDCs. (C) *N*-termini modified antigens for AgDCs. D) Fluorophores with azide or alkyne handles for tracking bioconjugates.

Azide or alkyne handles were installed via three types of chemistry: *N*-hydroxysuccinimidyl activated esters (NHS ester) with corresponding nucleophile (primary amine), coupling reaction between electrophilic isothiocyanate and a nucleophile (primary amine),

and during solid-phase peptide synthesis by utilizing Hexafluorophosphate Azabenzotriazole Tetramethyl Uronium (HATU) to activate the carboxylic acid on 4-pentynoic acid for the installation of an alkyne handle on the N-terminus of PLP. The following section will discuss unique challenges faced when we first attempted to synthesize our bioconjugates and our final CuAAC optimization.

2.3.3. Optimization of CuAAC reactions for modified PLP and p79

Initial work in our group was focused on optimizing the CuAAC reaction between purchased propargylglycine-PLP (pPLP) and coumarin-N_3. Method development proved unsuccessful in 'clicking' pPLP to coumarin-N_3. In order to determine why the reaction did not proceed under various conditions, we chose to use a simpler alkyne substrate. Propargylglycine was selected as a substrate because it was the simplest reactive component in pPLP. Propargylglycine was also unsuccessful in conjugating to Dex-N_3 when stoichiometric or sub-stoichiometric copper was used. While it was not clear at the time why both pPLP and propargylglycine failed to conjugate to coumarin-N_3 (Table 2), we chose to simplify the CuAAC system even further and use propargylamine as a substrate.

Upon running the CuAAC reaction with propargylamine and couarmin-N_3, the reaction proceeded in less than 30 min at room temperature. The product was verified via ^{1}H NMR by identification of the unique resonance for the triazole proton (not shown). This result pointed toward a problem with the primary amine on both of the failed substrates. Significant literature presence exists for utilizing amines as ligands for copper. We hypothesized that the primary amine in propargylglycine chelated to copper and rendered the catalyst inactive. To test this hypothesis, we ran the reaction with super-stoichiometric copper to ensure available copper for the CuAAC

reaction to conjugate propargylglycine to coumarin azide. This method resulted in detectable product formation verified via ^{1}H NMR (not shown). To further test our hypothesis, we Boc-protected pPLP to make Boc-PLP, which was successful in conjugating to coumarin-N_3 via CuAAC chemistry. In order to avoid having to protect and deprotect pPLP, we decided to change our design of our PLP to not include a free primary amine near the alkyne handle. We decided to incorporate a homopropargyl handle on the N-terminus of PLP (hpPLP).

To determine if having a homopropargyl handle on the N-terminus would be feasible for CuAAC, we first tested if 4-pentynoic acid linker would conjugated to coumarin-N_3. To our delight, the reaction proceeded to form the triazole product. A new peptide was synthesized via solid-phase peptide synthesis to produce the homopropargyl-PLP (see analytical characterization). The CuAAC reaction between hpPLP and coumarin-N_3 proceeded with no major method

Table 2. Summary of failed and successful CuAAC reactions

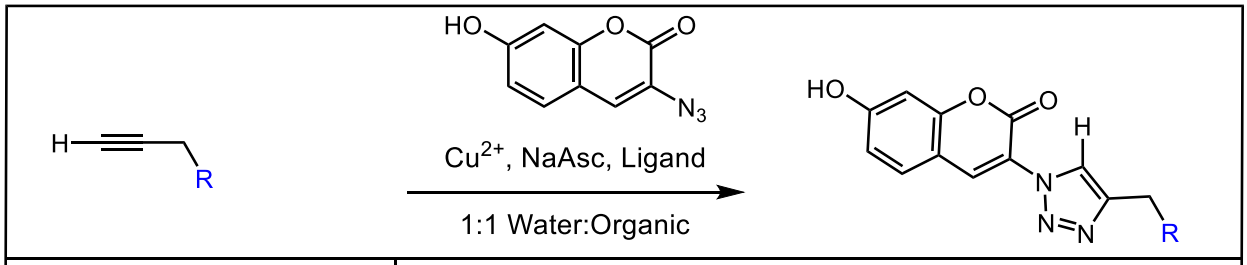

Failed	Succeeded
R= 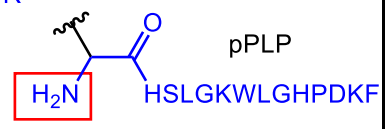 pPLP	R=  propargylamine 4-pentenoic acid
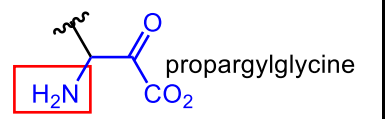 propargylglycine	 Boc-PLP hpPLP

development. With successful new design, the material was given to a fellow graduate student to synthesized AgDCs. The stark difference between pPLP and hpPLP may also be due to pPLP's primary amine and histidine nitrogen chelating to copper and thus inhibiting the CuAAC reaction.

The focus this work turned towards synthesizing T1D AgDCs by successfully conjugation homopropargyl-p79 (hpP79) to coumarin-N_3, Rhod-N_3, and Dex-N_3.

Optimization of CuAAC reactions were predominately done in aqueous media, however, when conjugating to less soluble organic compounds, the assistance of organic solvents (i.e. DMSO, EtOH, DMF) was used. Other components tested during the optimization of CuAAC reactions included balancing catalytic loading (Cu), using the stabilizing ligand THPTA, including aminoguanidine to help prevent the oxidation of methionine in p79, varying stoichiometric ratio to produce high yields, testing with elevated temperature. HPLC analysis proved to be the most useful technique in method development and product analysis due to the distinct hydrophobicity of starting materials and products.

2.3.4. Analytical Characterization

Synthesized molecules were characterized using various analytical technique such as, HPLC, NMR, LC/MS and other spectroscopic techniques. Small molecule (fluorophores and Dex-N_3) characterization (^{1}HNMR/MS) were straight forward and the data can be found in the material and methods section. The molecular heterogeneity of peptide containing material (PLP, Dex-p79, Rhod-p79) required additional characterization (HPLC; HSQC; LC/MS; LC/MSMS). HPLC analysis with UV/VIS detection of purified hpPLP provided purity values >96% (Figure 17). Analysis by LC/MS detection multiple charge state verified the synthesis of hpPLP (Figure 14) and LC/MS/MS was used to verify peptide sequence and modification (not shown). LC/MS

analysis for both purified AgDC Dex-p79 and purified Rhod-p79 detected multiple charge states that suggest the successful attachment of peptide antigen. $^{1}H/^{13}C$ heteronuclear single quantum coherence (HSQC) NMR was used as a qualitative analysis technique to verify successful bioconjugation of hpP79 and Dex-N_3. The resonance corresponding to the alkyne linker on the modified peptide (Figure 19A; $\delta(^{1}H) \approx 2.6$ ppm, $\delta(^{13}C) \approx 70$ ppm) is in a unique chemical environment and separated from other signals. Upon conjugation, the resonance shifts downfield upon successfully 'clicking" to Dex and being incorporated into the triazole ring (Figure 19B). With Dex-p79 in hand the next step would be to check whether our AgDC will have an immunological effect.

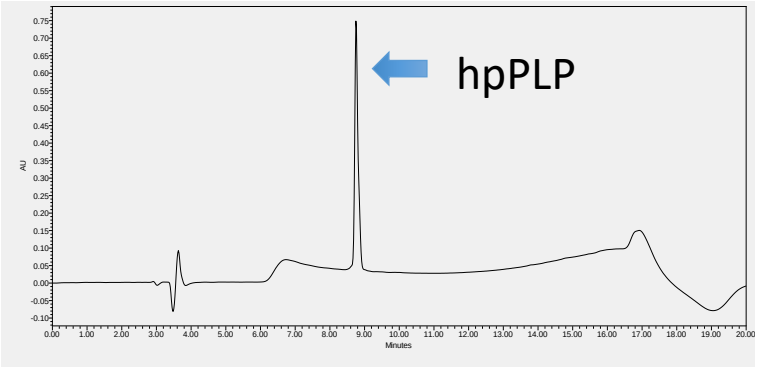

Figure 17: HPLC chromatogram showing single peak for purified hpPLP via an xBridge C18 5um (4.6X250mm) gradient 5:95 to 95:5 (Acetonitrile:Water) @ 220nM.

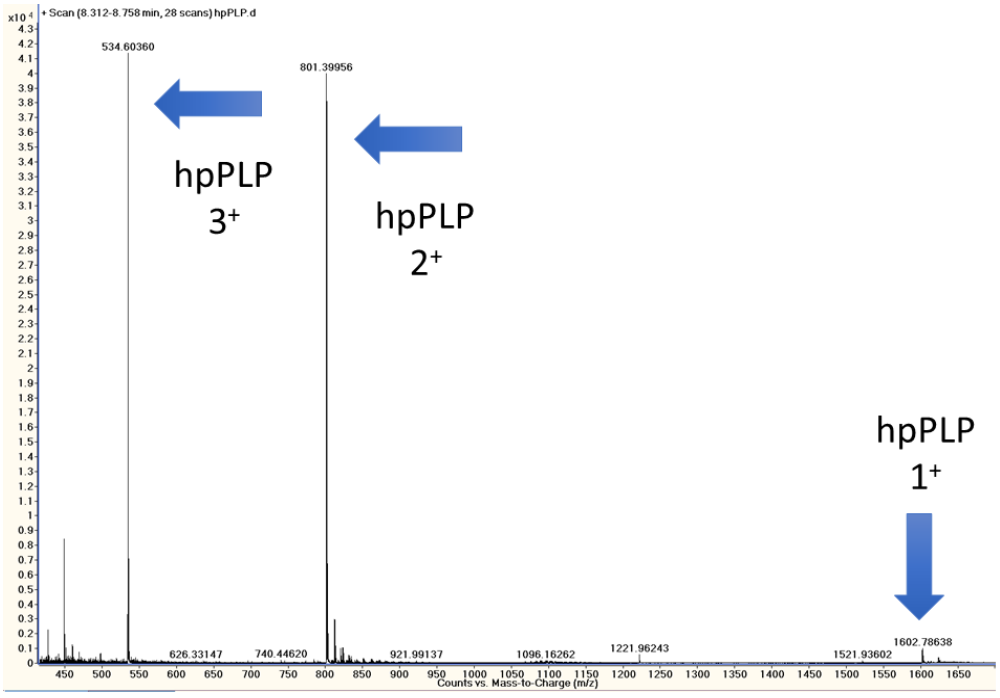

Figure 18: Mass Spectrum of Purified hpPLP verified with identification of multiple charge states (1^{+}, 2^{+}, 3^{+}).

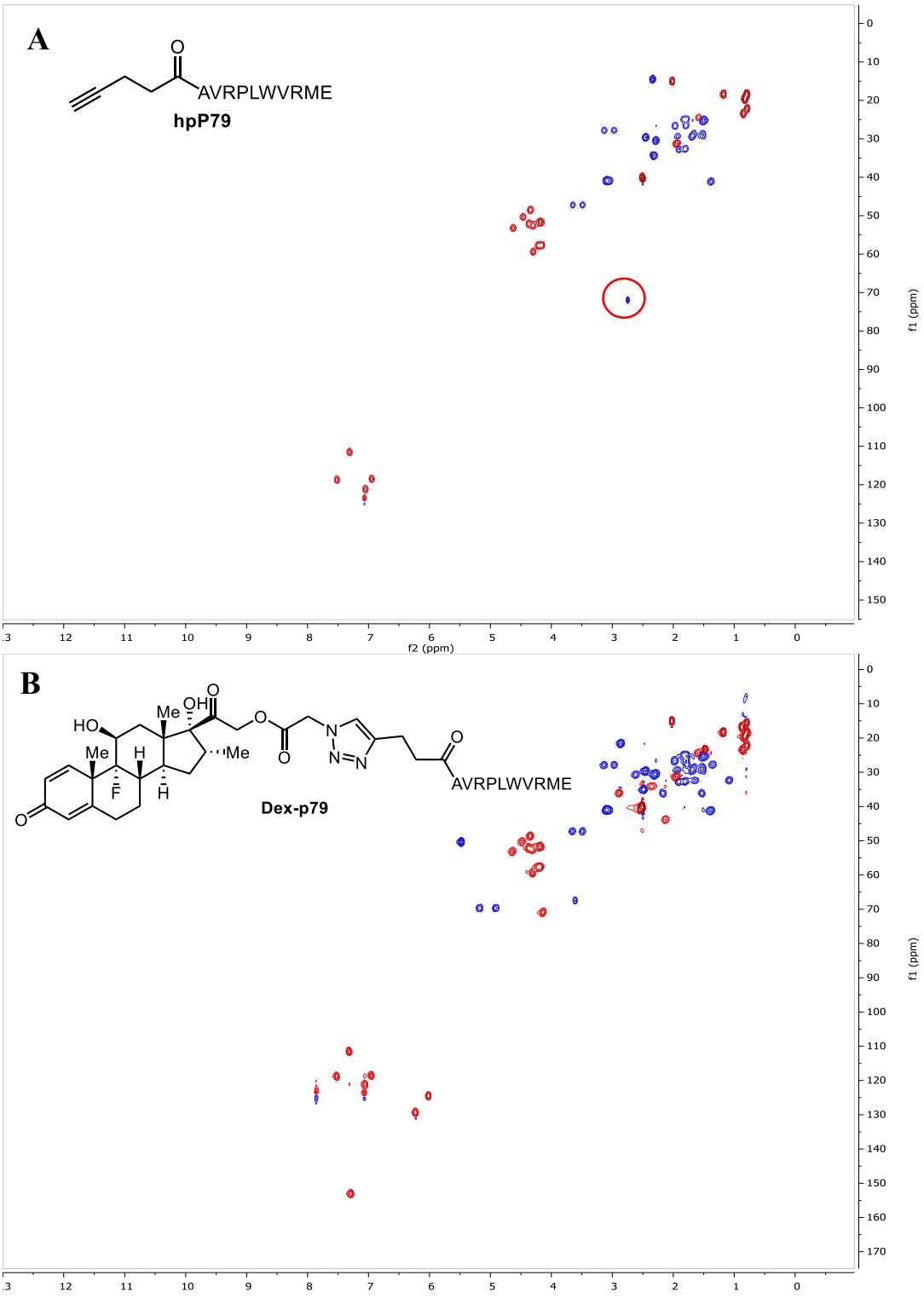

Figure 19: $^{1}H/^{13}C$ HSQC NMR data for hpPLP (top) and Dex-p79 (bottom)

2.4. Conclusion

Here we presented the successful synthesis of several azide/alkyne containing small molecules and peptides as well at the optimization of CuAAC chemistry for our purposes. For the installation of azide/alkyne handles, we utilized various synthetic techniques such as NHS chemistry, isothiocyanate chemistry, and solid-phase peptide synthesis. CuAAC optimization reviled our initial substrate pPLP may have been chelating copper and thus inhibiting the reaction. By redesigning our modified peptides to incorporate a homopropargyl linker, synthesis of various bioconjugates have been successful. All future work in our group has focused on utilizing a homopropargyl linker on peptides or proteins when trying to use CuAAC chemistry to construct bioconjugates. Our AgDCs for T1D need to be tested *in vitro* to determine if specificity has been retained and if they are able to induce tolerance in (NOD) BDC2.5 transgenic mice.

CHAPTER 3:

SOLUBLE ANTIGEN ARRAYS DISPLAYING A MULTIVALENT MIMOTOPES FOR THE TREATMENT OF TYPE 1 DIABETES

CHAPTER 3: SOLUBLE ANTIGEN ARRAYS DISPLAYING A MULTIVALENT MIMOTOPES FOR THE TREATMENT OF TYPE 1 DIABETES

3.1. Introduction

Type 1 diabetes (T1D) is an autoimmune disease that affects 2 in 1000 children and young adults.[139] It is an aggressive and devastating form of diabetes caused by an aberrant immune response resulting in the destruction of insulin-producing beta cells in the pancreas. The cause for the development of T1D is still unknown but a combination of genetic and environmental factors increase the susceptibility of developing the disease.[139, 151] Advancements over the last few decades have led to new diagnostics tools, novel therapies for managing the disease, and the discovery of causative antigens. Recent research has aimed to deliver antigens in a format that induces antigen-specific tolerance.[28, 38] Peptide-based approaches are more selective than protein-based therapies for delivery of specific epitopes including mimotopes, which target T cells clones for which the natural epitope is not known or for which the known epitope is recognized with poor affinity. However, a drawback of the administration of peptides *in vivo* is their rapid diffusion and dilution, which may result in insufficient uptake on a per cell basis.

Many current approaches to antigen-specific immunotherapy (ASIT) exhibit characteristics similar to traditional vaccines. Vaccines are typically particulate and designed to initiate a directed adaptive immune response to specific antigens in order to provide a robust "protective" immunological response upon re-challenge. Conversely, allergy shot therapies use soluble allergens to hyposensitize the immune response and establish tolerance.[152] This is typically accomplished by delivering low doses of soluble antigens via subcutaneous injection over an extended period of time. Allergen-specific immunotherapies are known to hyposensitize immune responses, thus providing a benchmark for design of ASIT delivery systems for autoimmune diseases that has yet to be explored.[153]

Scheme 1. Synthesis of SAgA and cSAgA Components and Molecules: (A) Alkyne-Functionalization of fluorescein

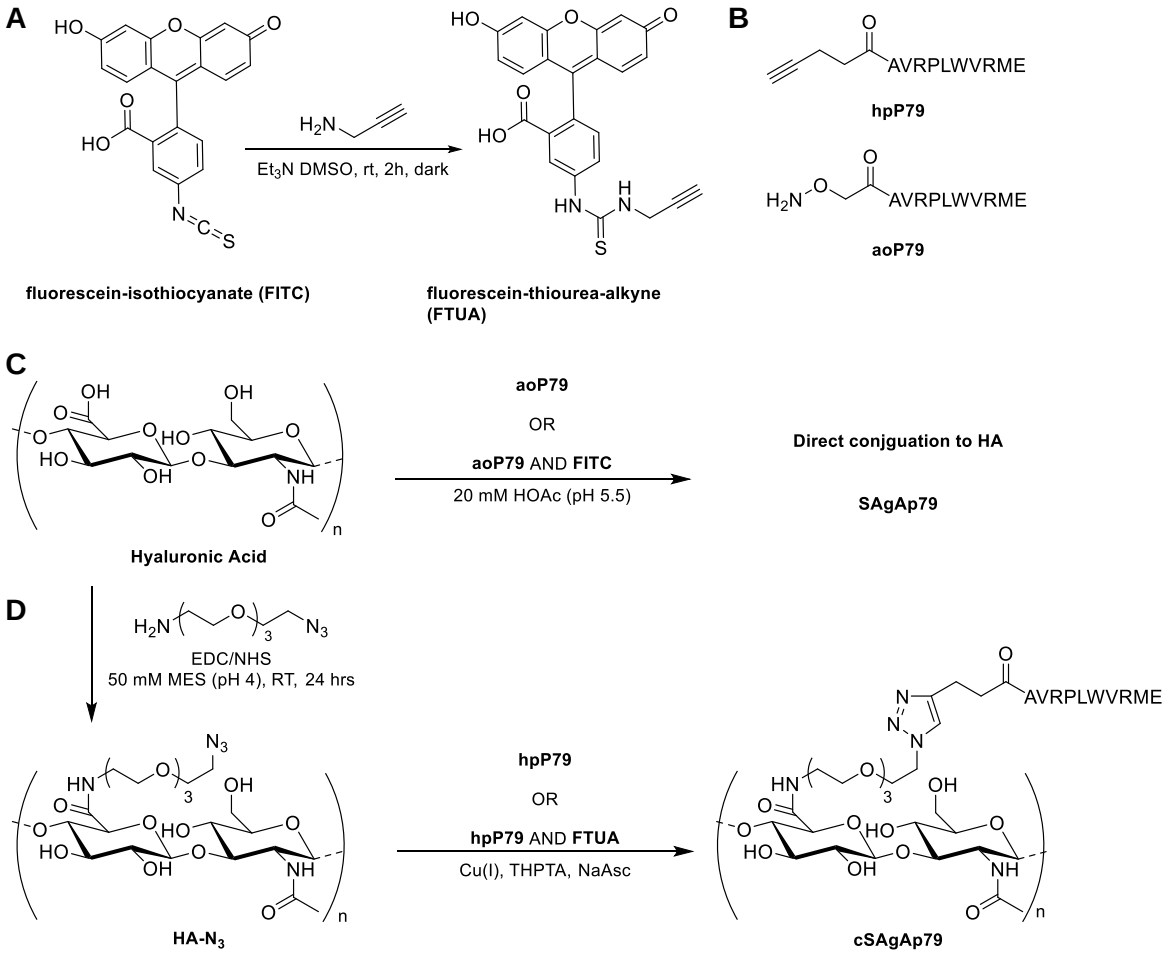

isothiocyanate; (B) structures of homopropargyl-modified peptide and aminooxy-modified peptide; (C) hydrolyzable Soluble Antigen Array (SAgA); (D) "click" Soluble Antigen Array (cSAgA)

SAgAs have been designed to bundle peptides together for more efficient uptake *in vivo* and, in some cases, achieve multivalent engagement of B cells.[64, 154] In addition, SAgAs uptake results in epitope presentation to targeted T cells in the absence of costimulation or proinflammatory cytokines, which may induce antigen-specific immune tolerance as a way to treat T1D. SAgAs are constructed using a hydrophilic linear polymer, hyaluronic acid (HA), grafted with multiple repeating epitopes from an autoantigen. Unlike spherical particles (i.e.,

nanoparticles, dendrimers) which are innately more ridged with fixed spacing and positioning of ligands, SAgAs are capable of contouring the receptor spacing on the cell surface. Thus, SAgAs are able to engage cell surface receptors with "high avidity multivalent antigen" by the molecules high conformational flexibility to allow for greater interactions with the cell surface to bind and cluster receptors.[155-162] We have previously reported utilizing soluble antigen arrays ($SAgA_{PLP}$) constructed by conjugating multiple repeating copies of autoantigen proteolipid protein peptide ($PLP_{139-151}$) to HA to induce tolerance in a multiple sclerosis (MS) mouse model known as experimental autoimmune encephalomyelitis (EAE). Both the hydrolyzable linked molecule $SAgA_{PLP}$ and non-hydrolyzable "clicked" molecule $cSAgA_{PLP}$ were able to cause B cell anergy, which was induced by BCR engagement and clustering in *in vitro* studies; as well as, the complete suppression of EAE disease symptoms compared to the control group results in *in vivo* studies. $cSAgA_{PLP}$ showed enhanced efficacy when compared to $SAgA_{PLP,}$ possibly due the stable covalent linkage in $cSAgA_{PLP}$.[64, 163-169]

While the immune response of MS is distinct from T1D, the mechanism of SAgAs is a novel strategy for the delivery of autoantigen. Here, we reported tailoring our SAgA technology as a therapeutic for another autoimmune diabetes, T1D. We synthesized two versions of SAgAs composed of HA polymer backbone with multiple repeating copies of the T1D autoantigen mimotope p79 (AVRPLWVRME) employing either a degradable or covalent linker. The p79 mimotope presented on the I-Ag7 MHC class II of non-obese diabetic (NOD) mice is recognized by CD4+ T cells from BDC2.5 T cell receptor (TCR) transgenic mice.[170] These T cells have been identified as islet-infiltrating T cells[171] and shown to also respond to the WE14 peptide from ChgA that has been modified by transglutaminase[172] and to hybrid insulin peptides resulting from the fusion of insulin C peptide and WE14 (aka 2.5HIP).[173] These T cells are pathogenic and rapidly

transfer disease when transferred as activated cells in NOD mice or as naïve T cells in NOD.SCID mice.[174-175] The bioconjugates were constructed via aminooxy chemistry (hydrolyzable: $SAgA_{p79}$) or copper-catalyzed alkyne-azide cycloaddition (CuAAC) chemistry (non-hydrolyzable: $cSAgA_{p79}$). Our ASIT technology was characterized via various analytical techniques: high-performance liquid chromatography (HPLC), nuclear magnetic resonance spectroscopy (NMR), circular dichroism (CD), dynamic light scattering (DLS), and fluorescence. The specificity and efficiency of T cell stimulation by these $SAgA_s$ was demonstrated by *in vitro* treatment of splenocytes from BDC2.5 versus NOD mice, and we identified conventional dendritic cells (cDCs) as the most efficient type of antigen-presenting cells (APCs) responsible for the presentation of SAgA-derived epitopes to T cells. We also observed that $cSAgA_{p79}$ are more stimulatory than $SAgA_{p79}$, a property that appears to be more associated with the N-terminal peptide modification than their peptide release properties. In summary, our results show that SAgA containing multiple copies of P79 can induce potent antigen-specific diabetogenic T cell responses in *in vitro* autoimmune diabetes models.

3.2. Materials and Methods

N-(3-dimethylaminopropyl)-*N′*-ethylcarbodiimide hydrochloride (EDC), 2-(*N*-morpholino)ethane-sulfonic acid sodium salt (MES), tris(3-hydroxypropyltriazolylmethyl)amine, sodium ascorbate (NaAsc), and Propargyl-*N*-hydroxysuccinimidyl ester were purchased from Sigma-Aldrich (St. Louis, MO) and used as received without further purification. Hyaluronic acid sodium salt (MW 16 kDa) was purchased from Lifecore Biomedical (Chaska, MN). 11-azido-3,6,9-trioxaundecan-1-amine (NH_2-PEG_3-N_3), *N*-hydroxysuccinimide, Copper (II) sulfate pentahydrate ($CuSO_4 \cdot 5H_2O$) was purchased from Acros Organics (Geel, Belgium). Alkyne-

functionalized peptide bearing an *N*-terminal 4-pentynoic acid (homopropargyl, hp) modification, hpP79 (hp-AVRPLWVRME-OH), aoP79 (aminooxy-AVRPLWVRME-OH) and an immunologically killed version (with two permuted amino acids) AV**PR**LWVRME (P79k) were obtained from Biomatik USA, LLC (Wilmington, DE).

3.2.1. Synthesis and Labeling of Soluble Antigen Arrays

Hydrolyzable $SAgA_{p79}$ and its fluorescein isothiocyanate (FITC)-labeled version ($_{f}SAgA_{p79}$), non-hydrolyzable cSAgAp79 and its fluorescein thiourea-labeled ($_{f}cSAgA_{p79)}$ were synthesized and characterized as previously reported. Peptide conjugation was determined through gradient reverse-phase analytical high-performance liquid chromatography (RP-HPLC).

Synthetic Procedures

3.2.1.1. Synthesis of Fluorescein thiourea alkyne (FTUA)

Synthesis of 2-(6-hydroxy-3-oxo-3H-xanthen-9-yl)-5-(3-(prop-2-yn-1-yl)thioureido) benzoic acid (fluorescein thiourea alkyne; FTUA; Scheme 1A) was adapted from Meng *et al*.[140] Triethylamine (75 µL, 0.514 mmol) was added to a mixture of FTUA (200mg, 511.4 µmol) and 1-amino-11-azido-3,6,9-trioxa-undecane (131mg, 119.09 µL, 0.616 mmol) in DMSO (1 mL) and the mixture was stirred for 2 h at room temperature in the dark. The reaction mixture was then frozen at -20°C and lyophilized to afford a red oil. The crude product was dissolved in DMSO and purified by preparative RP-HPLC (Waters XBridge C_{18}, 5 µm, 10x250 mm, linear gradient from 5-95% MeCN (+ 0.05% TFA) in H_2O (+ 0.05% TFA) over 20 minutes, detection at 280 nm) to give the final product (176.5 mg, 7%) as an orange-yellow powder; ^{1}H NMR (500 MHz, DMSO-d_6) δ 7.82-7.78 (m, 1H), 7.83-7.77 (m, 2H), 7.05-7.00 (m, 1H), 6.42-6.26 (m, 6H), 7.11 (d, J = 2.4

Hz, 1H), 7.08 (d, *J* = 2.4 Hz, 1H), 7.03 (s, 1H), 7.00 (s, 1H), 6.97 (d, J = 2.4 Hz, 1H), 3.65 (q, J = 7.14, 7.06, 7.06 Hz, 2H), 3.77 (d, *J* = 2.5 Hz , 2H), 2.70-2.63 (m, 8H), 2.66 (t, *J* = 2.5, 2.5 Hz, 1H)1.08 (t, *J* = 6.95, 6.95 Hz, 12H): HRMS expected $[M+H]^+$: 445.0853, found: 445.0858.

3.2.1.2. Synthesis of azide-functionalized hyaluronic acid (HA-N_3)

Synthesis of HA-N_3 (Scheme 1A) was adapted from Hu *et al* and Di Meo *et al*.[115, 140] Sodium hyaluronate (93.9 μmol, 16 kDa average MW) was added to a 250 mL round bottom flask with stir bar, followed by 100 mL of 50 mM MES buffer (pH = 4.0). The mixture was stirred until in solution (~15 minutes) before EDC (23.1 mmol) was added neat, then *N*-hydroxysuccinimide (18.8 mmol) added neat. The mixture was stirred for 5 minutes before H_2N-PEG_3-N_3 (4.51 mmol) in 20 mL MES buffer was added. The solution was then stirred for 24 hours at room temperature before being dialyzed in 6-8 kDa cutoff dialysis tubing against 4.5 L of 1.0 M NaCl solution for 24 hours, then 4.5 L of deionized water (4 x 12 hours). The volume in the bag was then transferred to vials, frozen, and lyophilized to yield a white powder (1.61 g, 95.0%).

3.2.1.3. Synthesis of Non-Hydrolyzable Soluble Antigen Arrays (cSAgAs $_{p79}$)

HA-N_3 (1.6 μmol) was added as a 30 μM solution in phosphate buffer (pH= 7.0) to a 250 mL round bottom flask with stir bar. Then hpP79 (40 μmol) was then added as a 3.52 mM solution in phosphate buffer (pH= 7.0), followed by a premixed solution of THPTA (70 μmol) and $CuSO_4 \cdot 5H_2O$ (14.5 μmol) in phosphate buffer (pH= 7.0). The solution was allowed to stir for 1-2 minutes before a 100 μL aliquot was removed for HPLC analysis. NaAsc (295 μmol) was then added to the reaction mixture as a 100 mM solution phosphate buffer (pH= 7.0). The reaction was allowed to 24 hours at room temperature. Additional 100 μL aliquots were removed throughout the course

of the reaction to determine the extent of conjugation. Then the reaction solution was quenched by adding 0.5 mL of 50 mM EDTA, then transferred to 6-8 kDa dialysis tubing and dialyzed against 4.5 L of 1.0 M NaCl (3 x 8 hours), then 4.5 L of deionized H_2O (6 x 8 hours). The volume in the bag was then transferred to vials, frozen, and lyophilized.

3.2.1.4. Synthesis of Non-Hydrolyzable Fluorescent Soluble Antigen Arrays ($_f$cSAgAs $_{p79}$)

HA-N_3 (2.0 μmol) was added as a 30 μM solution in phosphate buffer (pH= 7.0) to a 250 mL round bottom flask with stir bar. Then hpP79 (40 μmol) was then added as a 3.52 mM solution in phosphate buffer (pH= 7.0), followed by fluorescein thiourea alkyne (4 μmol), and then by a premixed solution of THPTA (70 μmol) and CuSO4 • 5H2O (14.5 μmol) in phosphate buffer (pH= 7.0). The solution was allowed to stir for 1-2 minutes before a 100 μL aliquot was removed for HPLC analysis. NaAsc (295 μmol) was then added to the reaction mixture as a 100 mM solution phosphate buffer (pH= 7.0). The reaction was allowed to 24 hours at room temperature. Additional 100 μL aliquots were removed throughout the course of the reaction to determine the extent of conjugation. Then the reaction solution was quenched by adding 0.5 mL of 50mM EDTA, then transferred to 6-8 kDa dialysis tubing and dialyzed against 4.5 L of 1.0 M NaCl (3 x 8 hours), then 4.5 L of deionized H2O (6 x 8 hours). The volume in the bag was then transferred to vials, frozen, and lyophilized.

3.2.1.5. Hydrolyzable Soluble Antigen Arrays (SAgA$_{p79;\ k}$)

Single-step grafting of aminooxy peptides to 16 kDa HA was performed as described previously.[168] Briefly, HA was dissolved in 20 mM acetate-buffered solution (pH 5.5 ± 0.1) and aminooxy reactive peptide was added simultaneously. After addition of the peptides, the reaction

solution was adjusted to pH 5.5 ± 0.1 and stirred at 500 rpm using a magnetic stir bar for 16 h at room temperature. The samples were then transferred to dialysis bags (MWCO 6000-8000 Da, Spectrum Laboratories, Inc., Rancho Dominguez, CA) and dialyzed against 2 L of deionized water for 24 h, with dialysis water exchanged every 6 h to remove unreacted peptides and residual buffer. After dialysis, the dialysate was frozen at −70°C and lyophilized.

3.2.1.6. Hydrolyzable Fluorescent Soluble Antigen Arrays ($_{f}SAgA_{p79}$)

Single-step grafting of aminooxy peptides to 16 kDa HA was performed as described previously.[168] Briefly, HA was dissolved in 20 mM acetate-buffered solution (pH 5.5 ± 0.1) and aminooxy reactive peptide and FITC were added simultaneously. After addition of the peptides, the reaction solution was adjusted to pH 5.5 ± 0.1 and stirred at 500 rpm using a magnetic stir bar for 16 h at room temperature. The samples were then transferred to dialysis bags (MWCO 6000-8000 Da, Spectrum Laboratories, Inc., Rancho Dominguez, CA) and dialyzed against 2 L of deionized water for 24 h, with dialysis water exchanged every 6 h to remove unreacted peptides and residual buffer. After dialysis, the dialysate was frozen at −70°C and lyophilized.

3.2.2. Analytical Characterization of Soluble Antigen Arrays

NMR spectra were collected on a Bruker Avance AVIII 500 MHz spectrometer equipped with a dual carbon/proton cryoprobe, all samples were dissolved in 600 μL of D_2O for examination. MestReNova 11.0 was used for NMR data analysis.

RP-HPLC analysis was done using a Waters Alliance HPLC system equipped with either a dual wavelength UV/Vis detector or diode array detector. For the quantitative determination of peptide conjugation by RP-HPLC, the following equation was used:

$$N_{con} = \left[\left(\frac{n_{pep}}{n_{HA}}\right)\left(\frac{V_{pre}-V_{sam}}{V_{pre}}\right)\right]\left(1-\frac{PA_t}{PA_{start}}\right) \qquad \textbf{Equation 1}$$

where N_{con} = number of conjugated peptides per backbone, n_{pep} = moles of peptide used in reaction, n_{HA} = moles of HA-N_3 used in reaction, V_{pre} = total reaction volume before NaAsc is added, V_{sam} = volume of "pre-NaAsc" sample removed from reaction mixture, PA_t = measured peak area of peptide at time *t*, PA_{start} = measured peak area of free peptide before NaAsc is added to the reaction. General chromatographic conditions employed a Waters XBridge C_4, 3.5 μm, 300 Å stationary phase under ion pairing (0.05% TFA in H_2O and MeCN) mobile phase conditions, utilizing a linear elution gradient (5-70%) with detection at 214 nm.

3.2.3. Biophysical Characterization

Determination of protein concentrations was done with $\varepsilon_{280\,nm}$ ($3\ mL \cdot g^{-1} \cdot cm^{-1}$) for p79. For derivatized polymers, the concentrations were determined on a total peptide basis (the same absorbance) so that the total concentration of p79 is unchanged. Other polymers and fluorescence concentrations were determined by weight.

3.2.3.1. Far UV Circular Dichroism (CD)

Far UV circular dichroism spectroscopy was performed using an Applied Photophysics Chirascan equipped with a 6-cell holder (Applied Photophysics, Leatherhead, UK).[176] Peptides were at concentrations of ~0.1 mg/ml, in phosphate buffer (pH= 7.0), in a 1-mm quartz cell. CD

was measured from 195 – 250 nm and using a 1 nm step size with a two second integration time at each step. Finally, corresponding buffers were subtracted for each sample.

3.2.3.2. Dynamic Light Scattering (DLS)

Dynamic light scattering was performed using a DynaPro Plate Reader (Wyatt Technology, Santa Barbara, CA).[177] Incident light was detected in a backscattering configuration and analyzed with an autocorrelator. 20 µL of sample, in phosphate buffer (pH= 7.0), was placed in a clear-bottomed 384 well plate and read at 20°C. Samples were measured 5 times with a 15 second acquisition time. Autocorrelation functions were fit using cumulant analysis and intensity averaged values are reported. Errors are reported as standard deviation of 3 replicates.

3.2.3.3. Intrinsic Fluorescence Spectroscopy

Intrinsic fluorescence was measured as described previously[176] using custom fluorescence plate reader (Fluorescence Innovations, Minneapolis, MN). Briefly, a 285 nm laser was used to excite samples and fluorescence was collected at 180° after passing through a 310 nm longpass filter to block excitation light. A prism dispersed light onto a CCD to quantify the fluorescence as a function of wavelength. 10 µL of sample, in phosphate buffer (pH= 7.0), was placed in a 384 well plate and covered with 2 µL of silicon oil to prevent sample evaporation. The fluorescence was measured from 10 to 90°C with a step-size of 1.25°C and an equilibration step of 2 min between each temperature. The total intensity from 300 to 400 nm was averaged for each temperature. Error bars represent the standard deviation of 4 replicates.

3.2.4. Mice

NOD (Jax #001976), BDC2.5 T cell receptor (TCR) transgenic mice (Jax #004460) and NOD.CD45.2 congenic mice (Jax #014149) were purchased from The Jackson Laboratory. NOD. IL-10/GFP ("Tiger") mice were kindly provided by Pere Santamaria[178]. BDC2.5.IL-10/GFP mice were produced by crossing NOD.IL-10/GFP mice with BDC2.5 mice. All mice were handled accordioning Columbia Center for Translational Immunology's animal barrier facility. Both male and female mice between 6-12 weeks of age were used as donors for the splenocytes used in all experiments. All mice used in this study were handled according Columbia University Institutional Animal Care and Use Committee recommendations and approved protocols.

3.2.5. T cell stimulation assay

Splenocytes from NOD and NOD.BDC2.5 mice were subjected to ACK (Ammonium-chloride-potassium) buffer to lyse red blood cells, filtered through a 70 μm cell strainer and resuspended into complete RPMI medium (containing 10% FBS, 50 IU/ml penicillin, 50 μg/ml streptomycin, 2 mM L-glutamine, 0.1 mM non-essential amino acids, 1 mM sodium pyruvate and 0.05 mM 2-Mercaptoethanol). The splenocytes were counted and labeled with a violet cell proliferation dye eFluor450 (VCPD) (10 μM for 15 min, eBioscience). VCPD-labeled splenocytes were cultured at $2x10^5$ cells/well with or without 100 nM of $SAgA_{p79,}$ $cSAgA_{p79}$ or HA in U bottom 96-well plates in triplicates. After 3 days of culture in a humidified CO_2 incubator at 37°C, the supernatants were collected and kept at -20ºC for cytokine analysis. The splenocytes were harvested and stained with antibodies to CD4, CD25, CD44 and CD69 (Biolegend) and CD4+ T cell responses were analyzed by flow cytometry (FCM) on BD Fortessa. From collected

supernatants, cytokine concentrations (IL-2, IL-10 and IFN-γ) were measured by ELISA (MAX kits, Biolegend) according to manufacturer guidelines.

3.2.6. Cellular uptake

Splenocytes were isolated from NOD or BDC2.5 mice as above, and cultured at $2x10^5$ cells per well (U-bottom 96-well plates) in complete RPMI medium with or without $_{f}cSAgA_{p79}$ at 0.1-1μM final concentration in humidified CO_2 incubator at 37°C. Cells were harvested at 12 or 24h time points, washed twice in FACS buffer (PBS, 2% bovine serum, 0.05% sodium azide) to remove unbound $_{f}cSAgA_{p79}$ and stained with antibodies to CD45, B220, CD11c, CD11b, CD8a, F4/80, CD40 and CD86 (Biolegend). Samples were then analyzed on Fortessa for $_{f}cSAgA_{p79}$ uptake by various cell types. Moreover, expression of costimulatory molecules CD86 and CD40 was measured to assess activation of various APCs.

3.2.7. APC subset-specific antigen presentation

Splenocytes from NOD mice were prepared as above and cultured at $2x10^5$ cells/well with/without $SAgA_{P79}$ or $cSAgA_{P79}$ at 1 nM concentration (limiting low dose to better identify the most efficient APCs). After 24h, the cells were harvested, washed twice, stained with antibodies against CD8, B220, CD11c, CD11b, CD45 and Gr1 and sorted into eight populations (BD Influx sorter). Finally, 10^3 sorted cells from each sorted population were co-cultured with 50,000 purified T cells/well (10% CD4+ CD25- T cells from BDC2.5 mice and 90% CD4+ CD25- and CD8+ T cells from NOD.CD45.2 mice) for 4 days. T cell purification was performed with MoJoSort magnetic cell separation kits (mouse CD4 T cell and CD3 T cell isolation kits, respectively, both

supplemented with biotinylated anti-CD25). The analysis of T cell response was performed by FCM as described above.

3.2.8. Peptide and SAgA titration

Splenocytes from NOD.BDC2.5.IL-10/GFP and NOD.CD45.2 mice were prepared as described above, labeled with VCPD (eBioscience) and mixed (10% and 90% respectively). The splenocytes were co-cultured ($2x10^5$ total cells/well) in the presence/absence of titrated $SAgA_{P79}$ or $cSAgA_{P79}$ or their corresponding free peptide at 10-fold serial dilutions ranging from 10 pM to 1µM concentrations. After 3 days of co-culture, the supernatants were removed for cytokine analysis and kept at -20°C. The splenocytes were collected, stained with antibodies to CD45.1 (to distinguish antigen-specific CD4+ T cells from bystander CD45.2+ T cells), to CD25 and CD44 (activation) and to Lag-3 and PD-1 (immune checkpoint markers) and analyzed by FCM. The gating strategy shown on Figure S5). Secreted cytokines (IL-2, IFN-γ and IL-10) in stored supernatants were quantified by ELISA (as above).

3.2.9. Statistical Analysis

GraphPad Prism was used to perform statistical analysis including sigmoidal nonlinear regression, ordinary one-way or two-way analysis of variance (ANOVA), and unpaired t-test. ANOVA was followed by Tukey's or Sidak's post-hoc test, where appropriate. The threshold for statistical significance was set to $p<0.05$.

3.3. Results and Discussion

3.3.1. Structural design of click soluble antigen arrays

Hydrolyzable multivalent soluble antigen arrays ($SAgA_{p79}$) and the non-hydrolyzable ($cSAgA_{p79}$) version are synthesized by conjugating approximately 10- 11 p79 peptides to a 16 kDa HA linear polymer. The valency was designed based on studies by the Dintzis group, which suggested a multivalent linear polymer with a valency of 10-20 antigens and a molecular weight (MW) less than 100 kDa could induce tolerogenic immune responses.[162, 179-180] Studies done by Judkowski et al. identified multiple sequences from a peptide library that were able to stimulate T cells from transgenic BDC2.5 NOD mice, with the most stimulatory one known as the p79 mimotope (AVRPLWVRME).[170, 181] We have previously reported hydrolyzable $SAgA_{PLP}$ and non-hydrolyzable $cSAgA_{PLP}$ constructed via aminooxy chemistry and CuACC linker chemistry, respectively, to conjugate $PLP_{139-151}$ peptide to HA. Our studies pointed to superior efficacy of non-cleavable $SAgA_{PLP}$ that can sustain BCR engagement, thus prolonged interaction on the cell surface of B cells in EAE model.[32] With our previous SAgA work in mind, our new SAgAs for T1D were designed by conjugating p79 (aoP79/hpP79) to HA via aminooxy chemistry or CuAAC chemistry. While the underlying pathogenesis and immune processes differ between MS and T1D, the novel delivery of autoantigen via SAgAs technology was expected to deliver similar benefits. Our ASIT was designed to target diabetogenic T cells implicated in disease initiation and progression in the NOD mouse model of T1D.

3.3.2. Analytical characterization of click soluble antigen arrays

Characterization was completed using various analytical techniques. ^{1}H NMR was utilized to confirm the successful CuAAC conjugation of all the starting materials to furnish $cSAgA_{p79}$

(Figure 20). The peak at 7.8 ppm for cSAgA$_{p79}$, highlighted in yellow, is consistent with previously reported proton chemical shift for a triazole proton. This peak was not seen in any of the starting

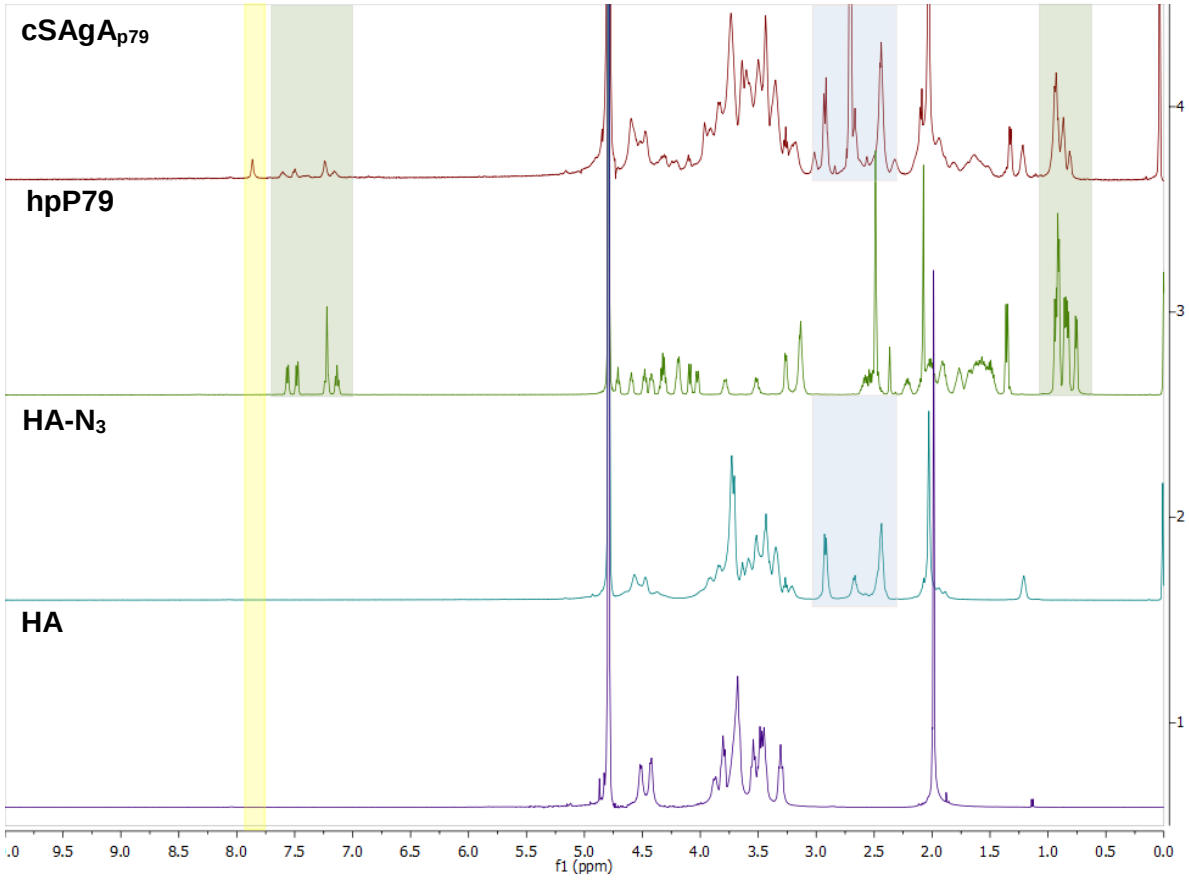

Figure 20: ^{1}H NMR spectra of starting materials and the reaction product. Resonances from the peptide starting materials are present in the final compound cSAgA$_{p79}$. A new peak only found in the product is highlighted in light yellow.

materials since it can only form after the successful CuAAC reaction between the azide (HA-N$_3$) and alkyne (hpP79). Resonance of both starting materials are seen in the final product highlighted in green (hpP79), purple (HA- N$_3$), and blue (PEG$_3$).

$^{1}H/^{13}C$ Heteronuclear Single Quantum Coherence (HSQC) NMR spectroscopy was used qualitatively to confirm the existence of resonances present in peptide sample hpP79 and HA-N_3, which were carried over to the final dialyzed products $cSAgA_{p79}$ and $_{f}cHA_{p79}$. These experiments affirm the complete absence of the terminal alkyne resonance from the terminal alkyne of the homopropargyl linker on the mimotope at (Figure 21A; $\delta(^{1}H) \approx 2.9$ ppm, $\delta(^{13}C) \approx 70$ ppm) in both the fluorescent and non-fluorescent $cSAgA_{p79}$ products. These experiments in combination with the ^{1}H NMR confirm the final product contains only the conjugated peptide of non-hydrolyzable

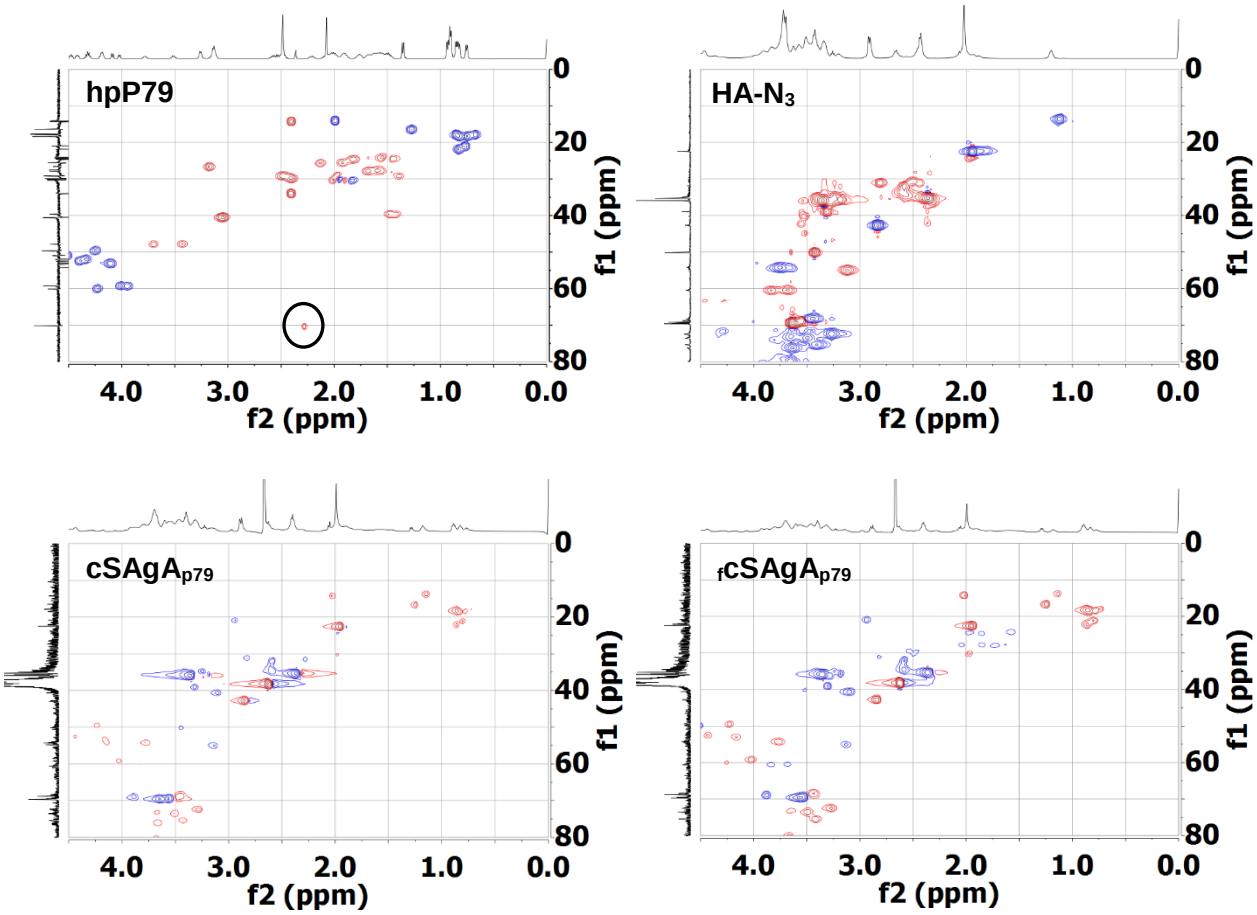

Figure 21: HSQC NMR spectra of starting materials and the product $_{f}cSAgA_{p79}$ and $cSAgA_{p79}$. Resonances from the peptide starting materials are present in the final compounds for both $_{f}cSAgA_{p79}$ and $cSAgA_{p79}$. The alkyne peak found only hpP79 is not found in any of the products, which implies complete no residual unconjugated p79.

cSAgAs. ^{1}H NMR was not used to confirm successful conjugation of hydrolyzable $SAgA_{p79}$ due lack of material, however, RP-HPLC was sufficient to show successful conjugation.

Quantitative analysis of peptide conjugation efficiency was done using a RP-HPLC by measuring the decrease in peak area of the peptide throughout the course of the reaction (Figure S1: Supplementary Info). In CuAAC chemistry, Cu^{1+}, which is a catalyst that allows the reaction to proceed, is generated *in situ* upon the addition of NaAsc, the reducing agent, to an inactive Cu^{2+} in solution. An aliquot of the reaction mixture was removed before the final NaAsc addition step, for HPLC analysis to establish a baseline response correlating to the molar excess of peptide used in the reaction. Thus, following the addition of NaAsc, any decrease in peak area of free alkyne-containing peptide (hpP79) was attributed to conjugation. A small aliquot pre-NaAsc was taken from the reaction mixture as a control sample. hpP79 displayed <5% degradation (2.7%) at 37°C for 24 hours, demonstrating a minimal impact of peptide degradation on the accuracy of the analytical methodology. Bioconjugation optimization, which is required to achieve the desired peptide conjugation to HA-N_3 (11 peptides), was performed by testing various conditions such as buffer type, temperature, reactant concentrations, and molar excess of free peptide. From these observations, the desired peptide valency in $cSAgA_{p79}$ (11 p79) and $_{f}cSAgA_{p79}$ (7:1; p79:FTUA) were identified. Similar to CuAAC reaction, the aminooxy reaction was tracked by measuring the decrease in peptide. The increased retention time of the bioconjugates following peptide conjugation (Figure S1) correlates with increased product hydrophobicity. The hydrophilic polymer backbone comprises only ~32% by mass of the SAgA but has a significant effect on hydrophilicity. Unlike the CuAAC, milder conditions were used thus negligible degradation of peptide was seen via RP-HPLC. The reaction between the aminooxy peptide (aoP79) and HA was

a one-step reaction resulting in the final desired peptide valence of $SAgA_{p79}$ (10 p79) and $_{f}SAgA_{p79}$ (8:2; p79:FITC). See Table 1 for more information.

To better understand the biophysical properties of the SAgAs, a few experiments were performed at physiologically relevant pH (7.4). Circular dichroism (CD) experiments were performed to evaluate the secondary structure of the bioconjugates (Figure 22A, 22B). CD revealed no significant secondary structure for the non-peptide components found in the SAgAs (data not shown), which include HA, HA-N_3, triazole, FTA, and FTUA. The CD spectra of hpP79

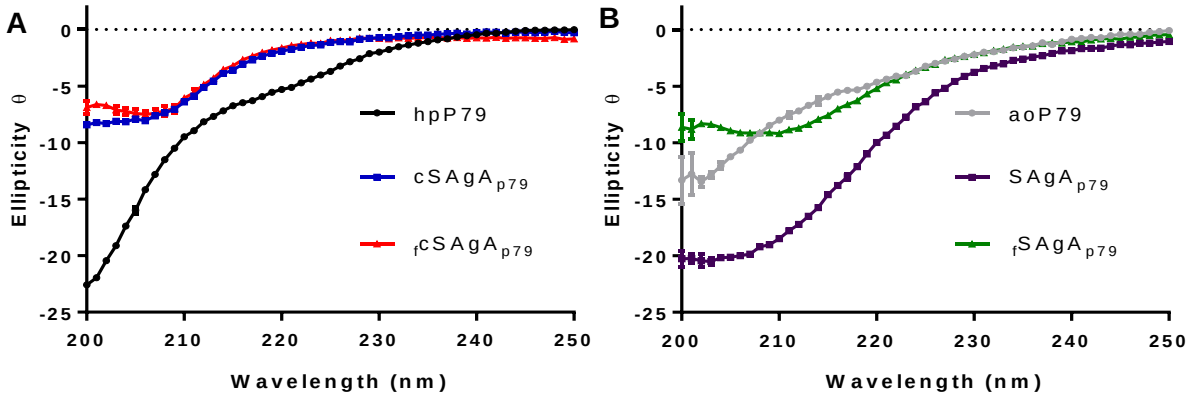

Figure 22: (A):Far-UV Circular Dichroism of $cSAgA_{p79}$ and (B): $SAgA_{p79}$

and aoP79 both exhibited the presence of random coil, which is consistent with small peptide secondary structure in literature. However, the modified peptides secondary structures were different, possibly because of the differences in the hydrophobicity of the modification. Both cSAgAs (Figure 22A) also exhibited a random coil structure but differ slightly from their parent peptide (hpP79). This may be due to the conjugation of peptides to HA resulting in loss of rotational freedom and decreased entropy of peptides in solutions. Both $SAgA_{p79}$ and aoP79 (Figure 22B) showed similar secondary structure to the cSAgAs. The loss of the hydrophobic homopropargyl linker upon conjugation to HA-N_3 makes the cSAgAs more hydrophilic, which

may explain the similar secondary structure to both aoP79 and $SAgA_{p79}$. $_{f}SAgA_{p79}$ did not follow this trend.

Experiments studying the intrinsic fluorescence (Figure S2) of the SAgA revealed no transition state change. $_{f}cSAgA_{p79}$ showed a significant difference in intensity due to the conjugated fluorophore. Finally, DLS data (Table 3) revealed reasonable increases in size of SAgAs compared to starting materials. Interestingly, HA (16 kDa) when compared to HA-N_3 (24.5 kDa) was shown to be larger (nm). All SAgAs showed a significant amount of aggregation in physiological pH (7.4) and high heterogeneity. Both the hydrolyzable $_{f}SAgAs$ and non-hydrolyzable $_{f}cSAgA$ showed a significant increase in average size when compared to their non-fluorescent counterparts, which may be due to the hydrophobic fluorophore causing significant aggregation of SAgAs.

Table 3. Peptide molar conjugation of hydrolyzable and click conjugates, as determined by RP- HPLC[a] .Dynamic light scattering (DLS) of SAgAs and components.

Sample	Approx. MW (kDa)[b]	Average Molar Ratio per Polymer[c]		DLS[d]	
		P79: HA	DYE: HA	Radius (nm)	%Polydispersity
hpP79 	1.335	0	0	0.82 ± 0.02	14.3
aoP79 	1.3287	0	0	0.82 ± 0.02	4.1
P79k 	1.3287	0	0	NA	NA
HA-N_3 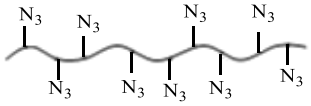	24.5	0	0	6.5 ± 0.03	24.5
HA 	16.0	0	0	7.3 ± 0.03	57.1

cSAgA$_{p79}$ 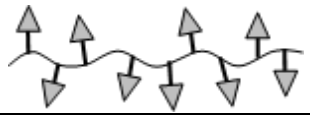	39.7	10.7	0	17.6 ± 0.01	Multimodal
$_{f}$cSAgA$_{p79}$ 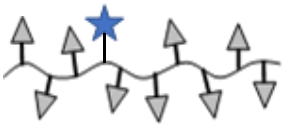	33.8	7	1	81.3 ± 0.03	Multimodal
SAgA$_{p79}$ 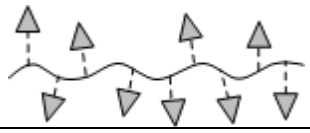	27.99	9.6	0	70.9	57.0
$_{f}$SAgA$_{p79}$ 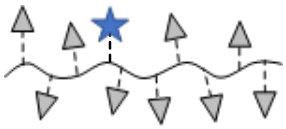	30.1	8.2	1.8	178.4 ± 5.5	53.8
SAgA$_{p79k}$ 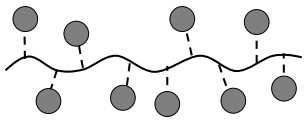	30.1	10	0	NA	NA

[a] Results are an average of triplicate injections from a single batch preparation. In the molecule schematics, dotted lines represent hydrolyzable oxime linker chemistry while solid lines represent non-hydrolyzable 'click' linker chemistry.
[b] Calculated from RP-HPLC data. MW, molecular weight.
[c] HA, hyaluronic acid; p79
[d] DLS data were collected in triplicate

★ represents florecent dye.

3.3.3. Specificity of T cell responses to SAgA-derived epitopes

To validate the ability of the p79 epitope grafted on SAgAs to elicit an antigen-specific T cell response, we cultured splenocytes from NOD and BDC2.5 mice with one of the p79-SAgAs or with the corresponding 'naked' HA molecule. The specificity was demonstrated by both the

lack of response of BDC2.5 T cells to HA and the lack of response of NOD T cells to cSAgA$_{P79}$ in terms of activation markers (Figure 23A,B) and cytokine production (Figure 23C-E).

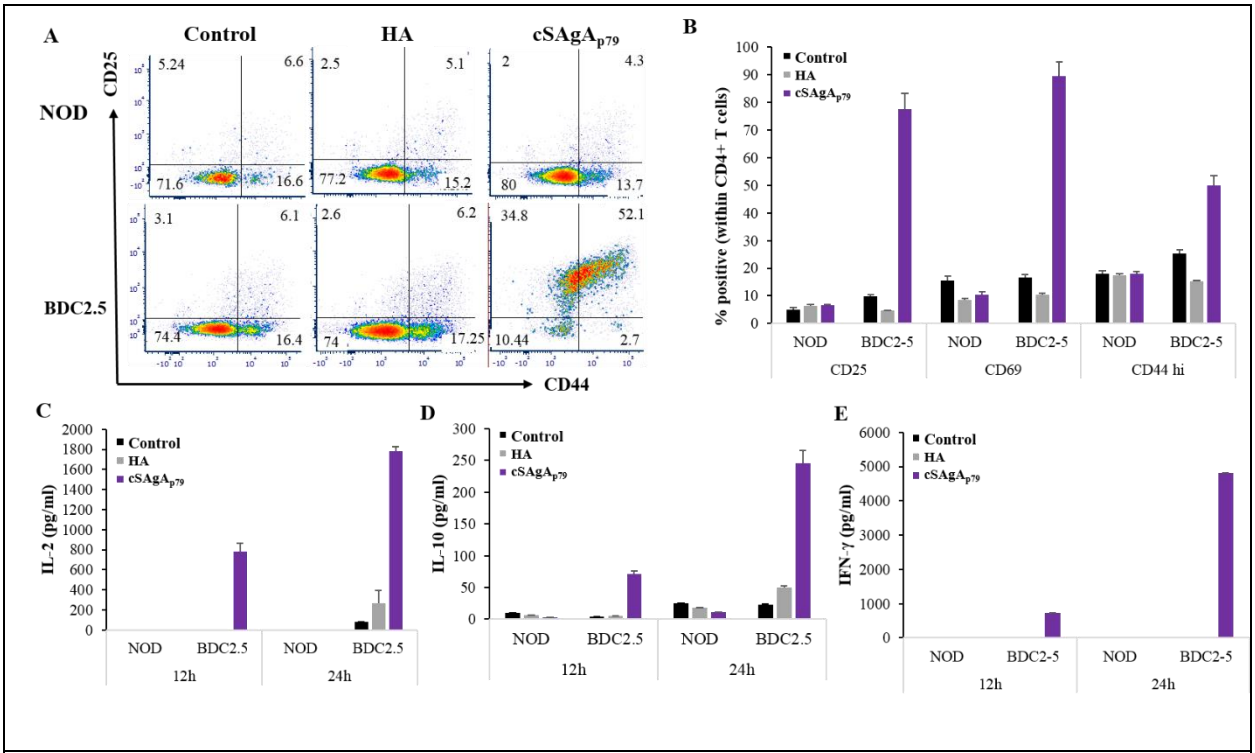

Figure 23. Antigen-specific CD4+ T cells responses to cSAgA$_{p79}$ in vitro. Representative plots (A) and summary of triplicates samples (B) showing upregulation of CD25, CD44 and CD69 in CD4+ T cells from BDC2.5 mice as compared NOD mice after 12h of culture. (C-E) Cytokine secretion at 12h and 24h of culture: IL-2 (C), IL-10 (D) and IFN-γ (E). The values are given as mean ± SD (n=3 technical replicates).

3.3.4. Uptake of SAgAs by different spleen cell populations

We then used FITC-conjugated SAgAs to compare the ability of different cell populations within the spleen to capture SAgAs (Figure S3). After up to 24h incubation *in vitro*, splenocytes were analyzed for FITC uptake.

Initially, all antigen-presenting cell (APC) populations (B cells, macrophages/monocytes, pDCs and cDCs) but not T cells from NOD splenocytes were found to take up SAgAs (Figures 24A,B; S5A,B). However, uptake by BDC2.5 splenocytes was increased as early as 12h for

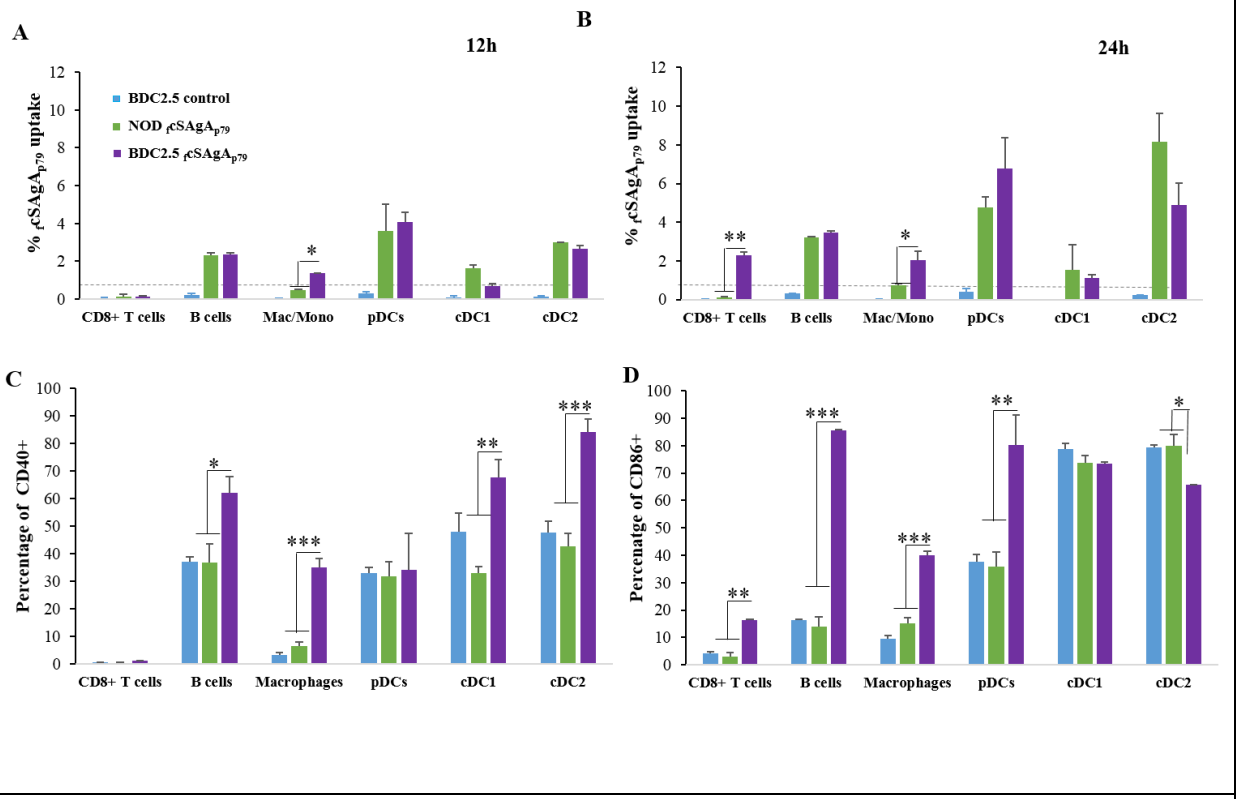

Figure 24. Uptake efficiency of $_{f}cSAgA_{p79}$ (1 μM) by different APCs at 12h (A) and 24h (B) time points and upregulation of costimulatory molecules CD40 (C) and CD86 (D) at 24h. Control cells from NOD mice are not shown (comparable to BDC2.5 control). The values are given as mean ± SD (n=3 technical replicates) and the data are representative of two experiments performed with $_{f}cSAgA_{p79}$, and experiments performed with FITC-conjugated $SAgA_{p79}$. MMN: monocytes, macrophages, neutrophils.

macrophages/monocytes, and later (by 24h) for other cells including T cells. Given that T cell activation was evident as early as 12h with BDC2.5 splenocytes (Figure 23), we hypothesized that antigen-specific T cell activation (possibly through cytokine release) stimulated other immune cells, leading to increase endocytosis. Indeed, the increased uptake of SAgA by BDC2.5 splenocytes was associated with increased expression of the maturation molecules CD40 and CD86 at 12-24h (Figures 24C,D; S5C) and increased cell size at 24h (Figures S5A vs S5B). Importantly, SAgAs were not responsible for APC maturation because they had no effect on NOD splenocytes in terms of CD40/CD86 expression (Figures 24C,D; S5C) and cell size (Figures S5A

vs S5B). Thus, these SAgAs do not have inherent immunogenic adjuvant properties, a prerequisite for tolerance induction.

3.3.5. Presentation of SAgA-derived epitopes by spleen APCs

Given that most cell types were able to take up SAgAs provided at high dose (100 nM – 1 µM), we then asked what APC subsets are most effective at processing and presenting SAgA-derived epitopes, using a limiting dose (1 nM) that would be more in line with *in vivo* conditions. Following culture of NOD splenocytes with $SAgA_{p79}$ or $cSAgA_{p79}$ (no noticeable T cell response), the cells were sorted into 8 populations, as shown on Figure S5, and each purified population was cocultured with purified CD4+ CD25- T cells from BDC2.5 mice. Antigen-specific T cell stimulation was only detected with cDC subsets (Figure 25). Moreover, $cSAgA_{p79}$ was more

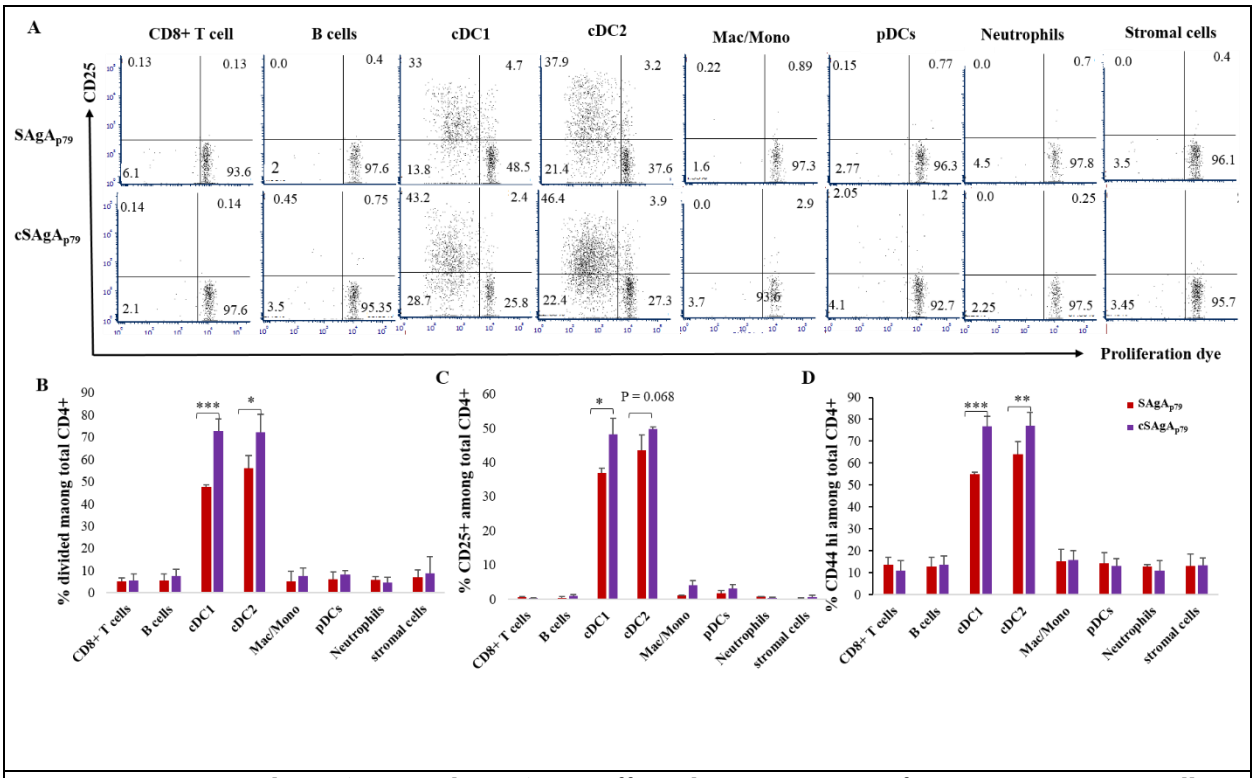

Figure 25: Conventional DCs (cDC1 and cDC2) most efficiently present epitopes from SAgA to CD4+ T cells as compared to other APCs. Representative dot plots depicting proliferation and CD25 upregulation by antigen-specific BDC2.5 CD4+ T cells (A), and summary bar graphs of BDC2.5 CD4+ proliferation (B) and upregulation of CD25 (C) and CD44 (D). The values are given as mean ± SEM (n=3 technical replicates).

stimulatory than $SAgA_{p79}$ (Figure 25). This was somewhat surprising as epitopes were not expected to be released as easily with the covalent link relative to the hydrolyzable link.

3.3.6. Stimulatory activity of SAgA variants and their corresponding peptides

In the light of apparent stimulatory superiority of $cSAgA_{p79}$ over $SAgA_{p79}$, we conducted a titration of these two SAgAs along with their respective peptides, which had different modifications prior to grafting to HA. CD4+ T cells (10%; from BDC2.5 mice with IL-10/GFP reporter) were diluted with non-specific T cells (90%; from NOD.CD45.2 mice) serving as internal negative controls for T cells (gating strategy shown on Figure S6).

As negative control for antigen, we use $SAgA_{p79k}$ containing an immunologically killed version of p79 with two amino acids permuted (p79k). Soluble peptides (aoP79 used to make $SAgA_{p79}$ and hpP79 used to make $cSAgA_{p79}$) were compared with the non-modified p79 and mixed together with the HA molecule used to make SAgA (HA with p79 and aoP79 and HA-N_3 with hpP79). Because each SAgA molecule bears 10-11 peptides, we represented all concentrations as peptide-equivalent (e.g. 1 nM SAgA = 10-11 nM peptide), and for free peptide / HA mixtures, we use 10-fold less HA than peptide to achieve the same relative amount as with SAgAs. The controls $SAgA_{p79k}$ and p79k+HA did not induce any T cell response (Figures 26 and S7), again highlighting the highly specific nature of the response. p79, aoP79 and $SAgA_{p79}$ induced a similar T cell response (based on proliferation and surface markers) that was most evident at 1-10 nM, while hpP79 and $cSAgA_{p79}$ were the most stimulatory, with T cell responses measurable at 10-100 pM (Figures 26A-E and S7-8).

We generally found that the free peptide was more stimulatory than its SAgA form at equivalent concentrations. However, at higher doses, SAgAs induced a greater PD-1 upregulation

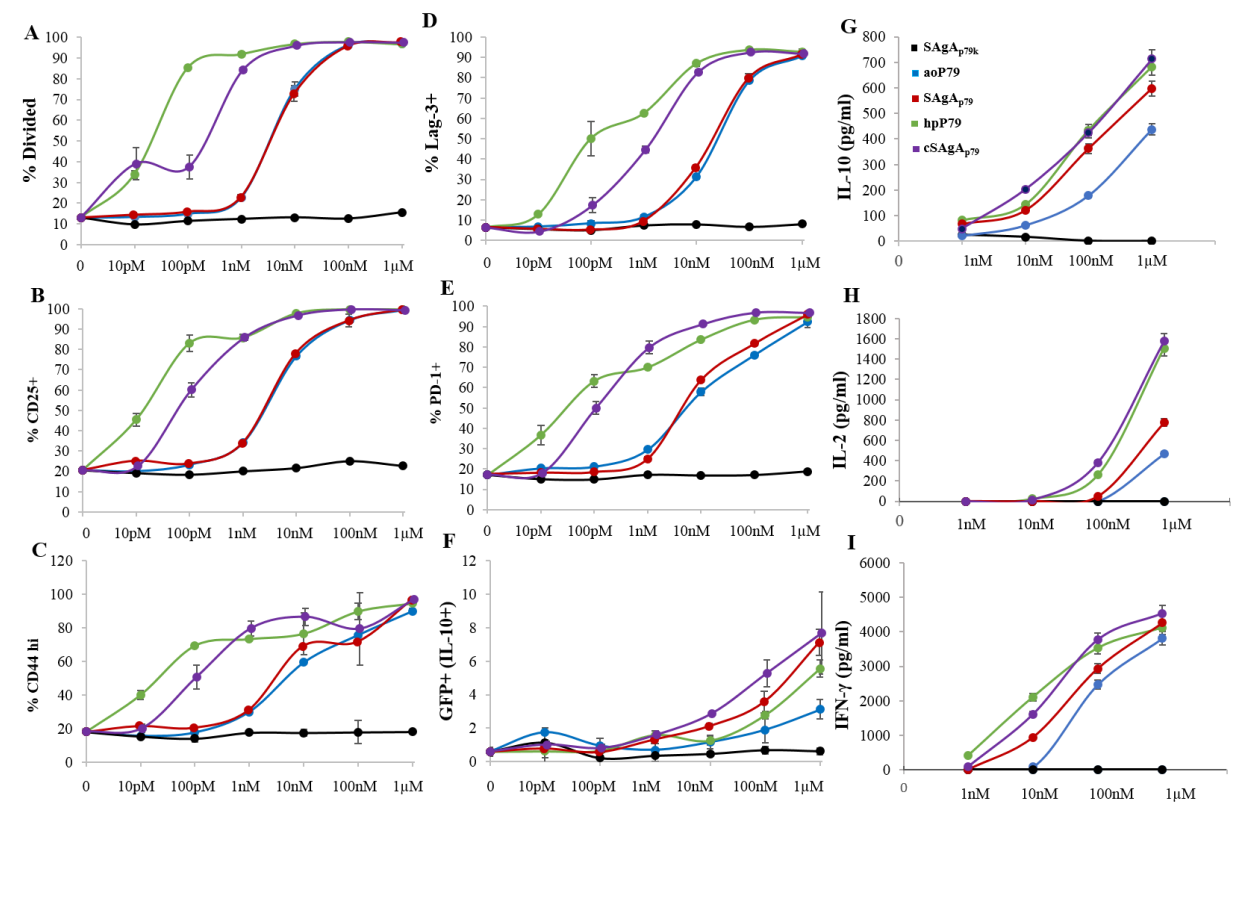

Figure 26: Dose-response curves of BDC2.5 CD4+ T cell responses (gated on CD45.1+ cells) induced by SAgA$_{p79}$ and cSAgA$_{p79}$ compared to their respective peptide aoP79 and hpP79 after 3 days *in vitro* culture: proliferation based on VCPD dilution (A), upregulation of CD25 (B), CD44 (C), Lag-3 (D), PD-1 (E), and IL-10/GFP (F), secretion of IL-10 (G), IL-2 (H) and IFN-γ (I). The values are given as mean ± SD (2-3 technical replicates per experiment). Data are representative of 2-3 experiments for each molecule with at least two batches tested for most showing comparable results. In other experiments, the free peptide was consistently more potent than its corresponding SAgA.

than their respective free peptide (Figure 26E). No significant stimulation was observed in bystander CD45.1- T cells (polyclonal T cells from NOD.CD45.2 mice; Figure S7). The cytokine response required higher doses of peptide or SAgA (at least 10 nM for IL-10 and IFN-γ, and 100 nM for IL-2), and in this case, SAgA were at least as stimulatory if not better than their corresponding free peptide (Figure 26F-I). Overall, the results suggest that cSAgA$_{p79}$ may be more

potent than $SAgA_{p79}$ not because of the difference in release mode but rather because of the *N*-terminal modification of p79.

3.4. Conclusion

Both hydrolyzable and non-hydrolyzable SAgAs were characterized and evaluated *in vitro* as therapeutic agents to target diabetogenic BDC2.5 T cells as representative autoreactive T cells in the NOD mouse model of T1D. Biophysical properties of both versions of non-fluorescent SAgA varied slightly. CD spectra for both hydrolyzable $SAgA_{p79}$ and non-hydrolyzable $cSAgA_{p79}$ were shown to be similar to the aoP79. Neither appeared to have any transition state when tested via a temperature fluorescent gradient. Both versions appeared to be heterogeneous and prone to aggregation.

Our *in vitro* immunoassays demonstrated that SAgA-derived epitopes were efficiently presented to specific T cells. T cell responses were generally greater with soluble peptide because of the high local concentration at which some free peptide may bind directly to MHC-II via spontaneous peptide exchange, whereas SAgAs require endocytosis, degradation and processing before loading onto MHC. We initially postulated that the distinct peptide grafting chemistries between $SAgA_{p79}$ and $cSAgA_{p79}$ would influence their immunological properties. Indeed, the ability of SAgAs to bring in bundled peptides inside the cells and release them should be affected by the balance of extracellular versus endosomal degradation. Excessive extracellular and/or insufficient endosomal degradation could limit the antigen load. Hydrolyzable SAgAs are expected to release their peptide cargo under the endosome's low pH, while the covalent linker is not expected to be broken down by any known enzymes. Both SAgAs and cSAgAs are susceptible to degradation at the level of the HA backbone by extracellular and endolysosomal hyaluronidases.

Thus, differences in stimulatory activity may be determined by how much peptide is effectively taken up and loaded on MHC. However, when comparing the stimulatory activity of two modified peptides used to produce these two forms of SAgAs, namely the aminooxy and alkyne versions, we observed that the alkyne form of the peptide was significantly more stimulatory. While the *N*-terminal aminooxy residue did not seem to have any effect on T cell stimulation relative to the unmodified p79 peptide, the *N*-terminal alkyne could possibly interact with the outside of the MHC-II molecule, forcing the peptide to bulge and facilitating interactions with the BDC2.5 TCR. As both hpP79 and $cSAgA_{p79}$ are more stimulatory, it would be surprising that both the alkyne motif (C≡C) and the cyclic motif resulting from reaction with azide would have the same effect on tweaking the overall epitope conformation.

In vitro, both SAgAs could promote the upregulation of immune checkpoint receptors like PD-1 and Lag-3, which may help predispose the targeted T cells to tolerance induction by their ligands. Nevertheless, further studies will be required to address how the antigen-specific T cells respond to those SAgAs in the *in vivo* environment in the context of T1D development. While *in vitro* stimulation was expected to favor soluble peptides for the reasons provided above, it is expected that SAgAs will be more stimulatory *in vivo* due to reduced diffusion, greater peptide uptake and improved lymph node drainage.

SUPPORTING INFORMATION

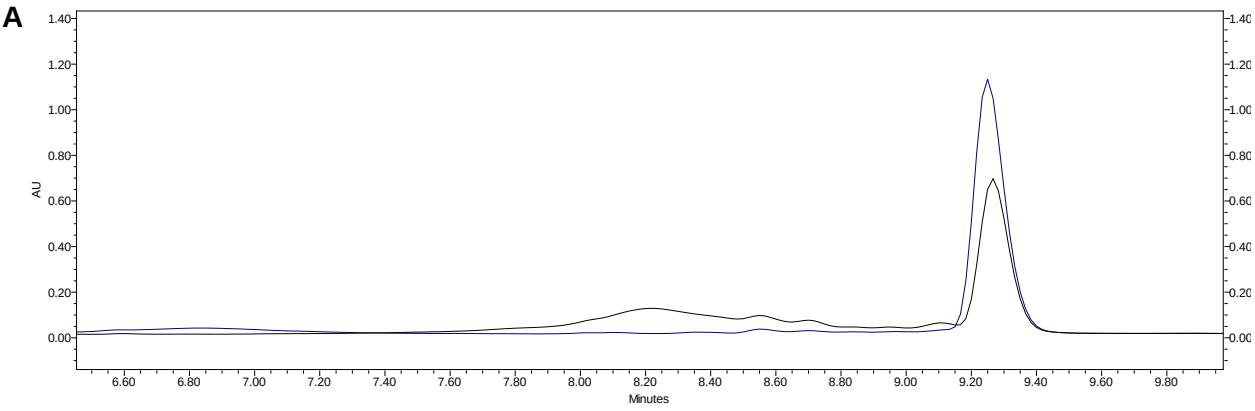

Figure S1 A: Reverse-phase analytical high-performance liquid chromatography (RP-HPLC) of $SAgA_{p79}$ formation (broad black peak at 9.20 min) compared to initial hpP79 (blue peak at 9.3min) on an xBridge C4 5um (4.6X250mm) gradient 5:95 to 95:5 (Acetonitrile :Water) @ 214 nM.

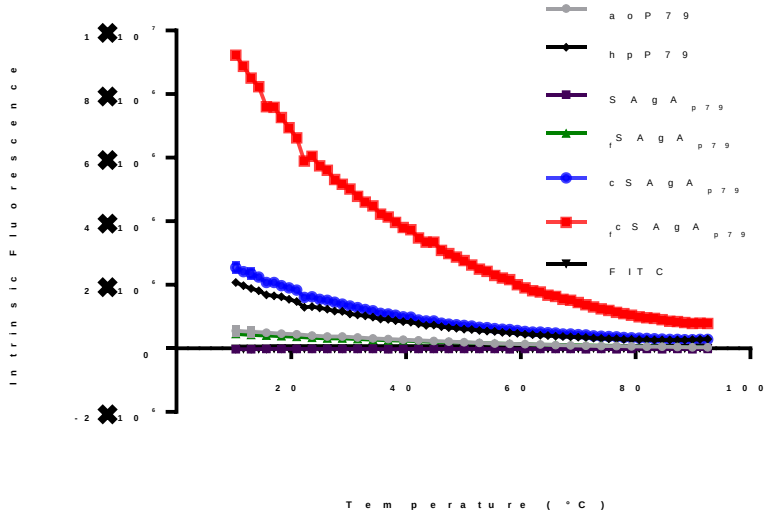

Figure S2: Intrinsic florescence of SAgA and components found within each SAgA

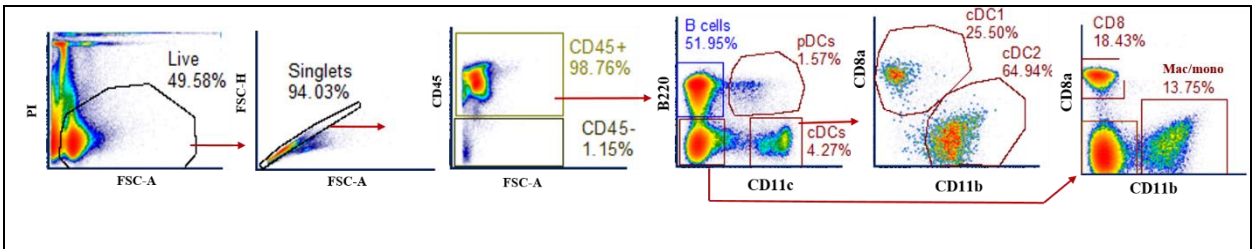

Figure S3. Gating strategy for different spleen populations assessed for fcSAgA uptake.

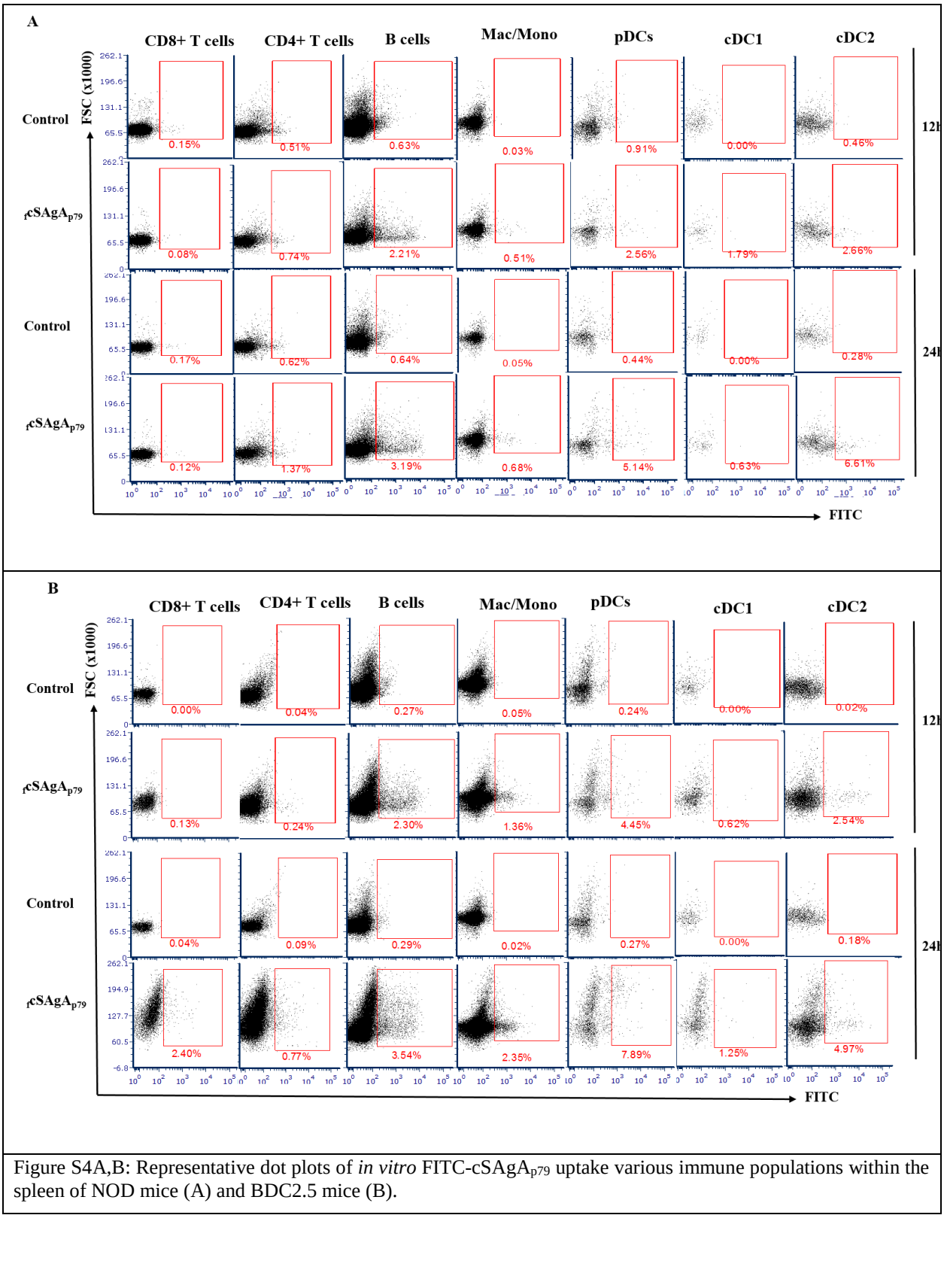

Figure S4A,B: Representative dot plots of *in vitro* FITC-cSAgA$_{p79}$ uptake various immune populations within the spleen of NOD mice (A) and BDC2.5 mice (B).

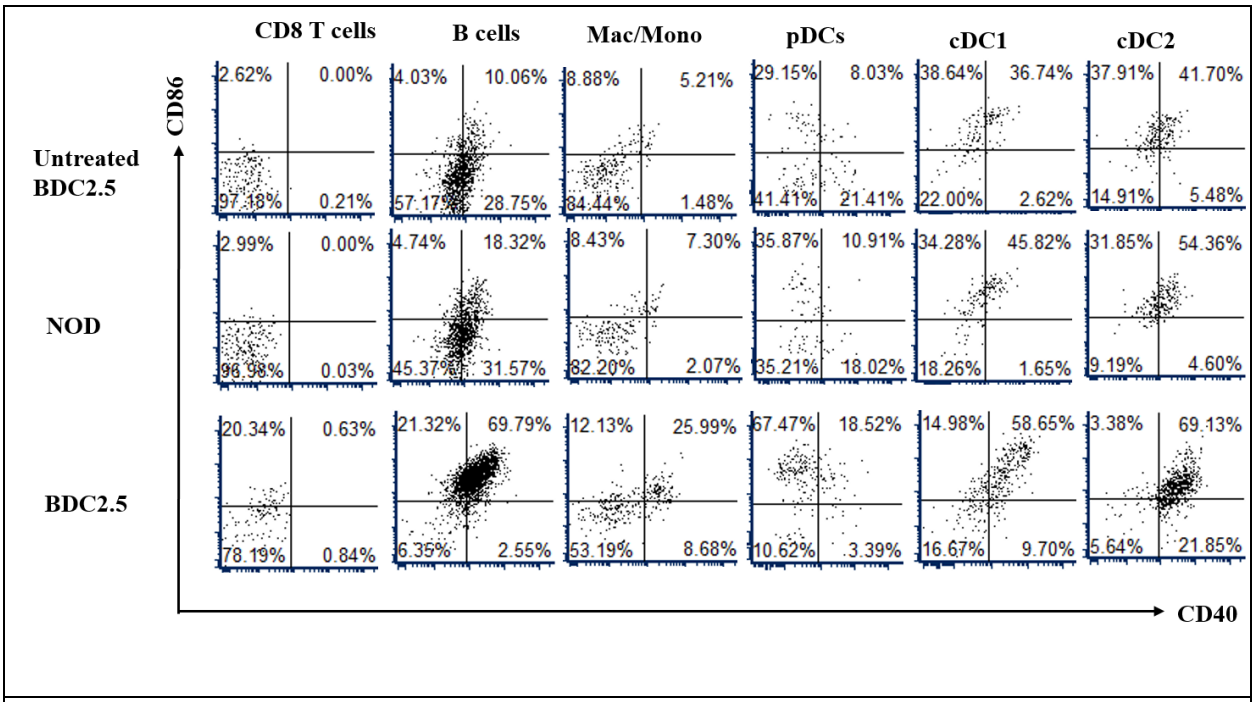

Figure S4C. Representative dot plots illustrating the activation of various NOD and BDC2.5 spleen cell populations based on upregulation of co-stimulatory molecules CD40 and CD86.

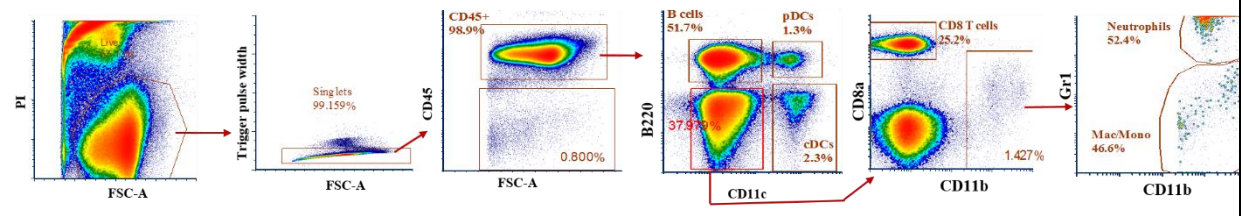

Figure S5. Gating strategy for the sorting of NOD splenocytes after incubation with p79-containing SAgAs for 24h and before coculture with BDC2.5 T cells to study their relative efficiency in presenting SAgAs to CD4+ T cells.

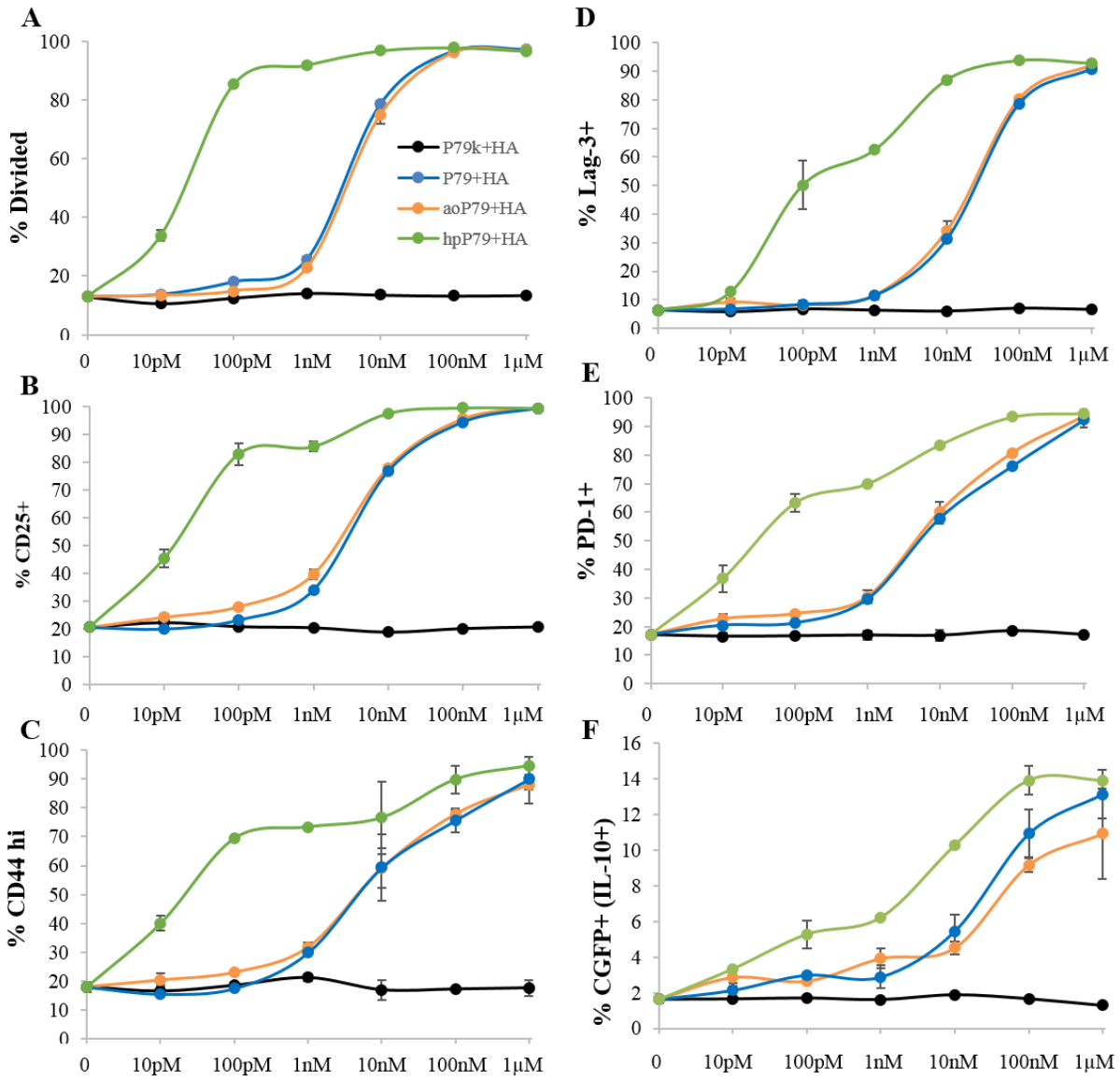

Figure S6. (A) Gating strategy to evaluate CD4+T cell responses to SAgAs and their respective peptides. (B-G) Dose-response curves of BDC2.5 CD4+ T cell responses (gated on CD45.1+ cells) induced by soluble peptides mixed with soluble HA, including unmodified p79, aoP79 (with linker for hydrolysable SAgA), hpP79 (with linker for covalent SAgA) and immunologically inactive P79k (with two amino acid permutations), at various concentrations. Splenocytes from BDC2.5 IL-10/GFP reporter mice were cultured with each peptide for 3 days. The values are given as mean ± SD (technical duplicates, with several batches tested).

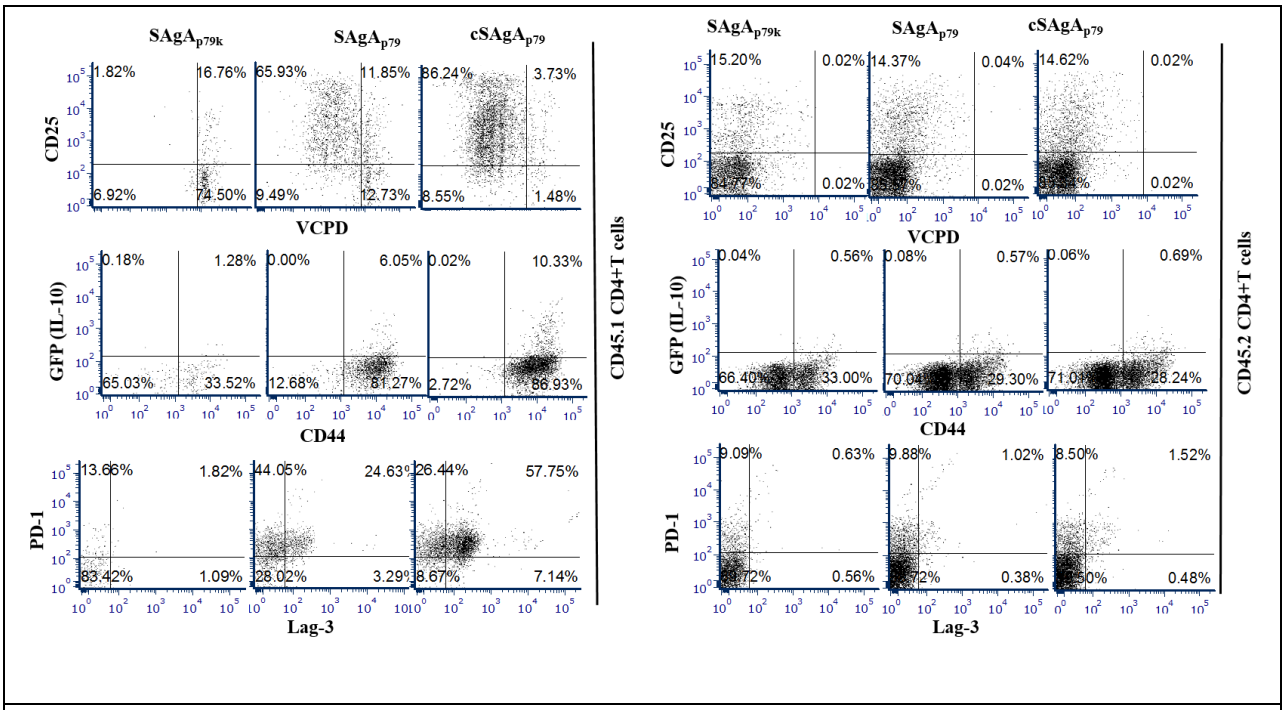

Figure S7. Representative dot plots for some of the markers measured at selected concentrations illustrating differences between SAgA$_{p79}$ and cSAgA$_{p79}$, and the response of antigen-specific T cells (CD45.1+) and polyclonal T cells (CD45.1-).

CHAPTER 4:

SYNTHESIS AND BIOPHYSICAL CHARACTERIZATION OF MULTIVALENT PROTEIN BASED SOLUBLE ANTIGEN ARRAYS FOR JUVENILE DIABETES

CHAPTER 4: SYNTHESIS AND BIOPHYSICAL CHARACTERIZATION OF MULTIVALENT PROTEIN BASED SOLUBLE ANTIGEN ARRAYS FOR JUVENILE DIABETES

4.1. Introduction

Autoimmune diseases, such as multiple sclerosis (MS),[182-183] type 1 diabetes (T1D),[184-188] neuromyelitis optica (NMO),[189-190] and systemic lupus erythematosus (SLE),[191-192] implicate loss of tolerance to self-antigen in autoreactive B cells, which leads to host tissue damage, disability, and death. In individuals afflicted by T1D, the insulin producing beta cells in the pancreas are targeted by an abnormal immune response, resulting in cell death.[184] It has been reported that autoantibodies are a strong predictor of the development of T1D. No studies have shown such antibodies to be pathogenic; studies have suggested B cells may contribute to the development of disease via their antigen presenting function and/or cytokine production.[184-188] Rituximab works by depleting B cells and has been used to treat certain autoimmune disease such as T1D. However, the monoclonal antibody causes global B cell depletion, leading to adverse side effects, and has limited efficacy.[193-195] Antigen-specific immune therapy (ASIT) has emerged as a potential means to selectively induce immune tolerance,[28, 38] via an intervention similar to allergy shot therapies, which use soluble antigens to restore tolerance towards specific antigens.[152] In particular, strategies to engage and selectively tolerize or delete autoreactive B cells offer a promising approach to ASIT.

Dintzis and co-workers studied the delivery of antigens bound to polymers, and they reported two different antigen-specific responses dictated by the following properties: polymer molecular weight, solubility, and antigen valency and spacing. An immunogenic response was seen when polymer delivering haptens were large (>100 kDa), rigid, and poorly soluble. A tolerogenic effect occurred when polymer delivering haptens were smaller (<100 kDa), flexible, soluble, and often with relatively lower hapten density.[162, 196-198] Interestingly, the molecular

properties that encourage immune tolerance are also favorable for accessing B cell compartments in secondary lymphoid organs (<100 kDa)[199-200] and promote selectivity to antigen-specific B cells over other professional antigen presenting cells (pAPCs). We rationalized an antigen delivery system exhibiting molecular properties capable of inducing tolerance by engaging antigen-specific B cells may be a viable therapeutic for T1D.

Our group has previously reported a novel antigen delivery system known as Soluble Antigen Arrays (SAgAs), which were originally designed with 'Dintzis rules' in mind as ASIT for MS. SAgAs are constructed via a hydrophilic linear polymer hyaluronic acid (HA) grafted with multiple repeating autoantigen (proteolipid protein peptide, $PLP_{139-151}$).[64, 154, 163-169] $SAgA_{PLP}$ induced tolerance and suppressed disease progression in many studies conducted in experimental autoimmune encephalomyelitis (EAE), a model used to mimic MS in humans. Our studies ultimately pointed toward SAgAs engagement of B cell receptor (BCR) in an antigen-specific manner. $cSAgA_{PLP}$ constructed via a non-hydrolyzable linker chemistry rather than a hydrolyzable linker ($SAgA_{PLP}$) showed greater binding *in vitro* to B cells and greater disease suppression *in vivo*.[64, 154]

We hypothesized that SAgAs composed of multiple repeating human insulin conjugated via non-degradable linker chemistry to HA may silence or delete B cells obtained from non-obese diabetic (NOD) mice transgenic for anti-insulin immunoglobulin heavy chain (VH125.NOD). Human insulin was conjugated onto HA via Copper-catalyzed Azide-Alkyne Cycloaddition (CuAAC) linker chemistry. $SAgA_{Ins}$ with different valency were synthesized and their biophysical properties were studied. Specificity of $SAgA_{Ins}$ was determined in B cells from both 125Tg (NOD) and VH125.NOD mice in order to confirm their ability to ligate to BCR on the surface of IBCs. To further validate specificity, B cells (CD43-) purified from spleens of VH125.NOD mice and

MD4 B cells (hen egg lysozyme (HEL) reactive) were mixed in at approximately the same frequency as IBCs. $SAgA_{Ins}$ was observed to block binding of insulin to IBCs but not HEL binding to MD4 B cells. Lastly, to determine if $SAgA_{Ins}$ can induce antigen-specific tolerance, and if there is valency dependence, *ex vivo* B cells from 125Tg mice were cultured *in vitro* with or without $SAgA_{Ins}$, or HA alone. These cells where subsequently assayed for surface levels of BCR as well as other markers to determine BCR stimulation or anergy.

4.2. Materials and Methods

Cell Prime™ r-insulin recombinant human insulin was purchased from EMD Millipore Corporation (Chicago, IL). *N*-(3-dimethylaminopropyl)-*N′*-ethylcarbodiimide hydrochloride (EDC), 2-(*N*-morpholino)ethane-sulfonic acid sodium salt (MES), tris(3-hydroxypropyltriazolylmethyl)amine, sodium ascorbate (NaAsc), and Propargyl-*N*-hydroxysuccinimidyl ester were purchased from Sigma-Aldrich (St. Louis, MO) and used as received without further purification. Hyaluronic acid (HA) sodium salt (MW 16 kDa) was purchased from Lifecore Biomedical (Chaska, MN). 11-azido-3,6,9-trioxaundecan-1-amine (NH_2-PEG_3-N_3), *N*-hydroxysuccinimide, Copper (II) sulfate pentahydrate ($CuSO_4 \bullet 5H_2O$) was purchased from Acros Organics (Geel, Belgium). Alkyne-functionalized peptide bearing an *N*-terminal 4-pentynoic acid (homopropargyl, hp) modification, $hpPLP_{139-151}$ (hp-HSLGKWLGHPDKF-OH) was originally synthesized in our laboratory via solid phase peptide synthesis. Larger quantities of hp $PLP_{139-151}$ peptide was obtained from Biomatik USA, LLC (Wilmington, DE). VH125.NOD and MD4 mice were purchased from The Jackson Laboratory and 125Tg mice were a kind gift from the laboratory of Dr. Rachel Friedman (National Jewish Health, Department of Biomedical Research). CD43 negative selections were purchased from

Miltenyi Biotec and Millipore Sigma respectively. B76 and HM79 were produced in the Cambier laboratory and were directly conjugated to fluorochromes (Thermo Fisher Scientific). 5 uM Indo-1 acetoxymethyl calcium indicator were purchased from Molecular Probes. All other chemicals and reagents were analytical grade and used as received.

4.2.1. Synthesis and Labeling of Soluble Antigen Arrays

Soluble antigen arrays (SAgAs)- and fluorescein isothiocyanate (FITC)-labeled SAgAs (fSAgAs) were synthesized and characterized as previously reported. Peptide conjugation was determined through gradient reverse-phase analytical high-performance liquid chromatography (RP-HPLC). Relative FITC fluorescence of labeled samples was determined spectrofluorometrically.

4.2.1.1. Synthesis of Alkyne-Functionalized Human Insulin (FTUA)

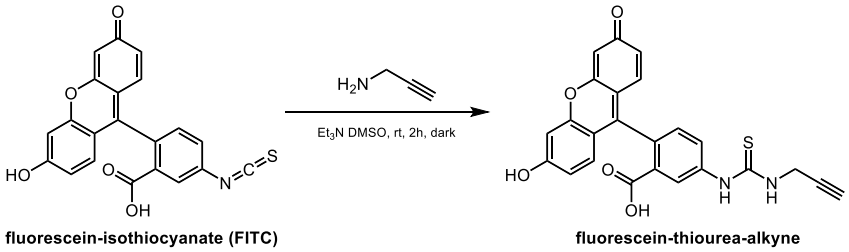

Figure 27: Reaction scheme for the synthesis of FTUA.

Synthesis of 2-(6-hydroxy-3-oxo-3H-xanthen-9-yl)-5-(3-(prop-2-yn-1-yl)thioureido) benzoic acid (fluorescein thiourea alkyne; FTU-Alk) was adapted from Meng *et al*.[140] To a mixture of FTUA (200mg, 511.4 µmol) and 1-amino-11-azido-3,6,9-trioxa-undecane (131mg, 119.09 µL, 0.616 mmol) in DMSO (1 mL) was added triethylamine (75 µL, 0.514 mmol), and the mixture

was stirred for 2 h at room temperature in the dark. The reaction mixture was then frozen at -20°C and lyophilized to afford a red oil. The crude product was dissolved in DMSO and purified by preparative RP-HPLC (Waters XBridge C_{18}, 5 µm, 10x250 mm, linear gradient from 5-95% MeCN (+ 0.05% TFA) in H_2O (+ 0.05% TFA) over 20 minutes, detection at 280 nm) to give the final product (176.5 mg, 7%) as a red-oil; ^{1}H NMR (500 MHz, DMSO-d_6) δ 7.82-7.78 (m, 1H), 7.83-7.77 (m, 2H), 7.05-7.00 (m, 1H), 6.42-6.26 (m, *6*H), 7.11 (d, *J* = 2.4 Hz, 1H), 7.08 (d, *J* = 2.4 Hz, 1H), 7.03 (s, 1H), 7.00 (s, 1H), 6.97 (d, J = 2.4 Hz, 1H), 3.65 (q, J = 7.14, 7.06, 7.06 Hz, 2H), 3.77 (d, *J* = 2.5 Hz , 2H), 2.70-2.63 (m, 8H), 2.66 (t, *J* = 2.5, 2.5 Hz, 1H)1.08 (t, *J* = 6.95, 6.95 Hz, 12H); HRMS expected $[M+H]^+$: 445.0853, found: 445.0858.

4.2.1.2. Synthesis of Alkyne-Functionalized Human Insulin (Ins-Alk)

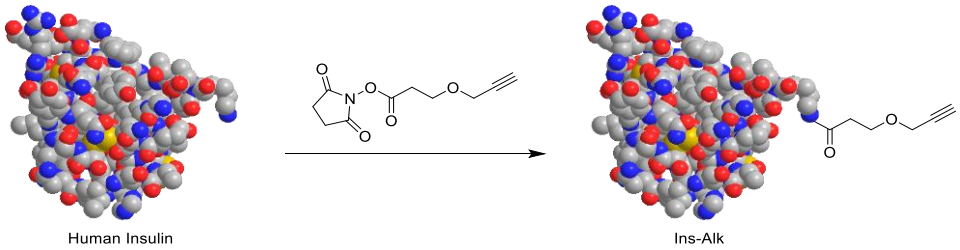

Figure 28: Reaction scheme for the synthesis of Ins-Alk.

Synthesis of Ins-Alk was adapted from Patent No.: US 8,906,850 B2. 120.00 mg of powdered human insulin is dissolved in 3000 µL of anhydrous DMSO at room temperature followed by the addition of 120 µL of triethylamine (TEA). The solution is stirred for 30 minutes at room temperature. Next, 1.2 equivalents (relative to human insulin) of propargyl-*N*-hydroxysuccinimidyl ester is slowly added to the insulin-TEA solution as a 1.0 M solution of the propargyl-*N*-hydroxysuccinimidyl ester in THF. The reaction is mixed for 1 h and then quenched

via the addition of 9.7 µL of a stock solution containing 250 µL of ethanolamine in 5,000 µl of DMSO followed by mixing for five minutes. (37.8 mg, 30.51%); MS (TOF ESI+) deconvoluted expected $[M]^+$: 5918.66, found: 5918.66.

4.2.1.3. Synthesis of Azide Functionalized hyaluronic Acid (HA-N_3)

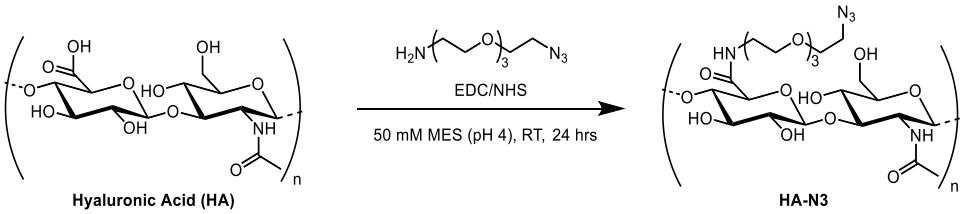

Figure 29: Reaction scheme for the synthesis of HA-N_3.

Synthesis of HA-N_3 was adapted from Hu *et al* and Di Meo *et al*. Sodium hyaluronate (93.9 µmol, 16 kDa average MW) was added to a 250 mL round bottom flask with stir bar, followed by 100 mL of 50 mM MES buffer (pH = 4.0). The mixture was stirred until in solution (~15 minutes) before EDC (23.1 mmol) was added neat, then *N*-hydroxysuccinimide (18.8 mmol) added neat. The mixture was stirred for 5 minutes before H_2N-PEG_3-N_3 (4.51 mmol) in 20 mL MES buffer was added. The solution was then stirred for 24 hours at room temperature before being dialyzed in 6-8 kDa cutoff dialysis tubing against 4.5 L of 1.0 M NaCl solution for 24 hours, then 4.5 L of deionized water (4 x 12 hours). The volume in the bag was then transferred to vials, frozen, and lyophilized to yield a white powder (1.61 g, 95.0%).

4.2.1.4. Synthesis of Florescent Hyaluronic Acid ($_f$HA-N3)

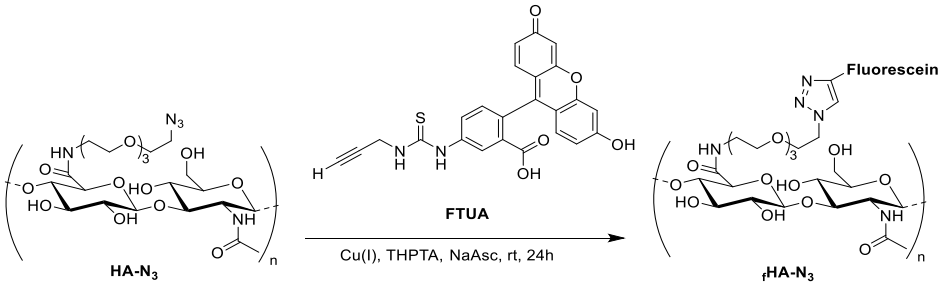

Figure 30: Reaction scheme for the synthesis of $_f$HA-N_3

HA-N_3 (2.0 μmol) was added as a 30 μM solution in phosphate buffer (pH= 7.0) to a 250 mL round bottom flask with stir bar. Then hpP79 (40 μmol) was then added as a 3.52 mM solution in phosphate buffer (pH= 7.0), followed by FTUA (4 μmol), and then by a premixed solution of THPTA (70 μmol) and $CuSO_4 \bullet 5H_2O$ (14.5 μmol) in phosphate buffer (pH= 7.0). The solution was allowed to stir for 1-2 minutes before a 100 μL aliquot was removed for HPLC analysis. NaAsc (295 μmol) was then added to the reaction mixture as a 100 mM solution phosphate buffer (pH= 7.0). The reaction was allowed to 24 hours at room temperature. Additional 100 μL aliquots were removed throughout the course of the reaction to determine the extent of conjugation. Then the reaction solution was transferred to 6-8 kDa dialysis tubing and dialyzed against 4.5 L of 1.0 M NaCl (3 x 8 hours), then 4.5 L of deionized H_2O (6 x 8 hours). The volume in the bag was then transferred to vials, frozen, and lyophilized.

4.2.1.5. Synthesis of SAgA Insulin ($SAgA_{Ins}$)

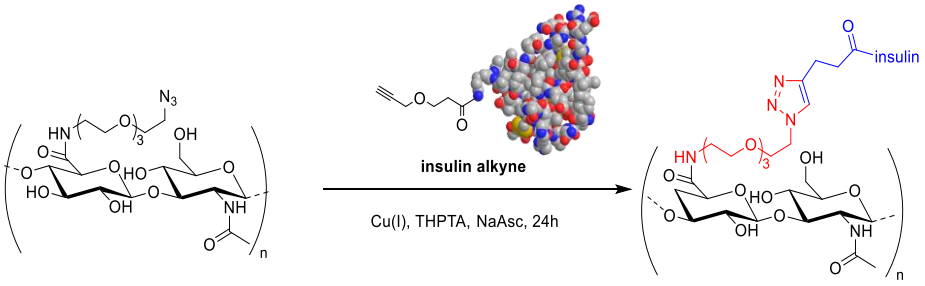

Figure 31: Reaction scheme for the syntheses of $_{lv}SAgA_{Ins}$, $_{mv}SAgA_{Ins}$ and $_{hv}SAgA_{Ins}$.

Three different reactions with 5 equivalents of Ins-Alk relative to HA-N_3 (to make $_{lv}SAgA_{Ins}$ and $_{mv}SAgA_{Ins}$) and 10 equivalents of Ins-Alk relative to HA-N_3 ($_{hv}SAgA_{Ins}$) were set up with the following conditions. HA-N_3 (0.81 μmol) was added as a 15 μM solution in phosphate buffer (50 mM, pH= 7.0) to a 100 mL round bottom flask with stir bar. Followed by the addition of insulin-alkyne, a 4.0 mM or 8.1 mM solution in DMF (5 and 10 equivalents relative to HA-N_3 respectively) was also added. Then a premixed solution of THPTA (60 μmol) and $CuSO_4 \cdot 5H_2O$ (12 μmol) in phosphate buffer (50 mM, pH= 7.0) was added to the alkyne/azide mixture. Then a 100 μL aliquot was removed for HPLC analysis. NaAsc (242 μmol) was then added to the reaction mixture as a 100 mM solution in phosphate buffer (pH= 7.0). One reaction with 5 equivalence of Ins-Alk relative to HA-N_3 was stirred at room temperature for 24h until some alkyne component was consumed to furnish $_{lv}SAgA_{Ins}$. While two other reactions were stirred at elevated temperature (40°C) for 24 h until all alkyne component was consumed to produce both $_{mv}SAgA_{Ins}$ and $_{hv}SAgA_{Ins}$. Additional 100 μL aliquots were removed throughout the course of the reaction to determine the extent of conjugation. Upon completion of the reaction, the solution was quenched by adding 0.5 mL of 50 mM EDTA, then transferred to 6-8 kDa dialysis tubing and dialyzed

against 4.5 L of 1.0 M NaCl (3 x 8 hours), then 4.5 L of deionized H_2O (6 x 8 hours). The volume in the bag was then transferred to vials, frozen, and lyophilized.

4.2.1.6. Synthesis of PLP Hyaluronic Acid (HA-$_{PLP}$)

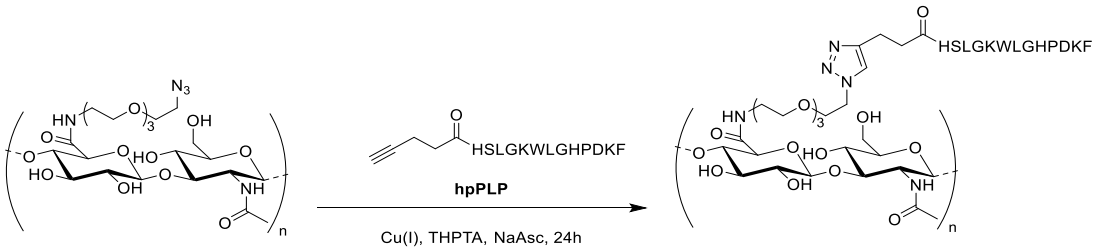

Figure32: Reaction scheme for the synthesis of HA-$_{PLP}$.

HA-N_3 (0.37 μmol) was added as a 56 μM solution in phosphate Buffer (50 mM, pH= 7.0) to a 150 mL round bottom flask with stir bar. Followed by the addition of hpPLP, a 1.7 mM solution in DMF (5.0 equivalents relative to HA-N_3) was also added to the solution. Then a premixed solution of THPTA (8.5 μmol) and $CuSO_4 \bullet 5H_2O$ (1.6 μmol) phosphate buffer (50 mM, pH= 7.0) was added to the solution. Then a 100 μL aliquot was removed for HPLC analysis. NaAsc (33 μmol) was then added to the reaction mixture as a 100 mM solution in phosphate buffer (50 mM, pH= 7.0). The reaction was stirred at room temperature for 24h until the alkyne component was partially consumed (~3PLP per HA). Additional 100 μL aliquots were removed throughout the course of the reaction to determine the extent of conjugation. Upon completion of the reaction, the solution was quenched by adding 0.5 mL of 50 mM EDTA, then transferred to 6-8 kDa dialysis tubing and dialyzed against 4.5 L of 1.0 M NaCl (3 x 8 hours), then 4.5 L of deionized H_2O (6 x 8 hours). The volume in the bag was then transferred to vials, frozen, and lyophilized.

4.2.1.7. Synthesis of Florescent Ins hyaluronic Acid (fHA-Ins)

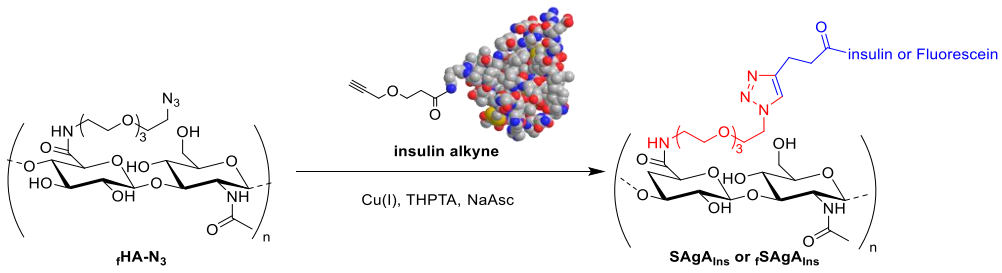

Figure 33: Reaction scheme for the synthesis of $_{f}SAgA_{Ins}$

$_{f}HA\text{-}N_3$ (0.81 µmol) was added as a 15 µM solution in phosphate buffer (50 mM, pH= 7.0) to a 100 mL round bottom flask with stir bar. Followed by the addition of insulin-alkyne, a 4.0 mM in DMF (5 equivalents relative to $_{f}HA\text{-}N_3$) was also added. Then a premixed solution of THPTA (60 µmol) and $CuSO_4 \bullet 5H_2O$ (12 µmol) in phosphate buffer (50 mM, pH= 7.0) was added to the alkyne/azide mixture. Then a 100 µL aliquot was removed for HPLC analysis. NaAsc (242 µmol) was then added to the reaction mixture as a 100 mM solution in phosphate buffer (pH= 7.0). The reactions were stirred at room temperature for 24h until the alkyne component was partially consumed (~2 Ins per HA). Additional 100 µL aliquots were removed throughout the course of the reaction to determine the extent of conjugation. Upon completion of the reaction, the solution was quenched by adding 0.5 mL of 50 mM EDTA, then transferred to 6-8 kDa dialysis tubing and dialyzed against 4.5 L of 1.0 M NaCl (3 x 8 hours), then 4.5 L of deionized H_2O (6 x 8 hours). The volume in the bag was then transferred to vials, frozen, and lyophilized.

4.2.2. Analytical Characterization of Click Soluble Antigen Arrays

NMR spectra were collected on a Bruker Avance AVIII 500 MHz spectrometer equipped with a dual carbon/proton cryoprobe (unless otherwise noted), and all samples were dissolved in

650 μL of D_2O for analysis. MestReNova 11.0 was used for NMR data analysis. The amide methyl resonance (δ ~ 1.90-2.05 ppm) of all ^1H NMR spectra was normalized to an integration of 3.0, and the sum of all other signals in the range of δ ~ 1.0-4.0 ppm was used to ratiometrically determine the number of azide functionalization sites during HA-N_3 synthesis.

RP-HPLC and SEC analysis were conducted using a Waters Alliance HPLC system equipped with either a diode array detector or dual wavelength UV/Vis detector. For the quantitative determination of peptide conjugation by RP-HPLC, the following equation was used:

$$N_{con} = \left[\left(\frac{n_{pep}}{n_{HA}}\right)\left(\frac{V_{pre}-V_{sam}}{V_{pre}}\right)\right]\left(1-\frac{PA_t}{PA_{start}}\right) \qquad \textbf{Equation 1}$$

where N_{con} = number of conjugated peptides per backbone, n_{pep} = moles of peptide used in reaction, n_{HA} = moles of HA-N_3 used in reaction, V_{pre} = total reaction volume before NaAsc is added, V_{sam} = volume of "pre-NaAsc" sample removed from reaction mixture, PA_t = measured peak area of peptide at time *t*, PA_{start} = measured peak area of free peptide before NaAsc is added to the reaction. General chromatographic conditions employed a Waters XBridge C_4, 3.5 μm, 300 Å stationary phase under ion pairing (0.05% TFA in H_2O and MeCN) mobile phase conditions, utilizing a linear elution gradient (5-70%) with detection at 214 nm.

4.2.3. Biophysical Characterization

Determination of protein concentrations was done with $\varepsilon_{280\,nm}$ (3 $mL \cdot g^{-1} \cdot cm^{-1}$) for human insulin. For derivatized polymers, the concentrations were determined on a total protein basis (the same absorbance) so that the total concentration of insulin is unchanged. Other polymers and fluorescence concentrations were determined by weight.

4.2.3.1. Far UV Circular Dichroism (CD)

Far UV circular dichroism spectroscopy was performed using an Applied Photophysics Chirascan equipped with a 6-cell holder (Applied Photophysics, Leatherhead, UK).[176] Proteins were at concentrations of ~0.1 mg/ml, in phosphate buffer (pH= 7.0) or acidic water (pH= 3.0), in a 1-mm quartz cell. CD was measured from 195 – 250 nm and using a 1 nm step size with a two second integration time at each step. Finally, corresponding buffers were subtracted for each sample.

4.2.3.2. Dynamic Light Scattering (DLS)

Dynamic light scattering was performed using a DynaPro Plate Reader (Wyatt Technology, Santa Barbara, CA).[177] Incident light was detected in a backscattering configuration and analyzed with an autocorrelator. 20 µL of sample, in phosphate buffer (pH= 7.0), was placed in a clear-bottomed 384 well plate and read at 20°C. Samples were measured 5 times with a 15 second acquisition time. Autocorrelation functions were fit using cumulant analysis and intensity averaged values are reported. Errors are reported as standard deviation of 3 replicates.

4.2.3.3. Intrinsic Fluorescence Spectroscopy[176]

Intrinsic fluorescence was measured as described previously using custom fluorescence plate reader (Fluorescence Innovations, Minneapolis, MN).[176] Briefly, a 285 nm laser was used to excite samples and fluorescence was collected at 180° after passing through a 310 nm longpass filter to block excitation light. A prism dispersed light onto a CCD to quantify the fluorescence as a function of wavelength. 10 µL of sample, in phosphate buffer (pH= 7.0), was placed in a 384 well plate and covered with 2 µL of silicon oil to prevent sample evaporation. The fluorescence

was measured from 10 to 90°C with a step-size of 1.25°C and an equilibration step of 2 min between each temperature. The total intensity from 300 to 400 nm was averaged for each temperature. Error bars represent the standard deviation of 4 replicates.

4.2.4. Mice

Female mice, aged 6-8 weeks, were used in all experiments. VH125.NOD mice express, by virtue of knock-in, the variable heavy-chain region from the insulin specific 125 hybridoma, on the NOD background. Together with endogenous light chains, these mice bear ~3 % insulin reactive B cells in the periphery. 125Tg mice express both the heavy- and light-chain from the 125 hybridoma, rendering 100 % of their peripheral B cells reactive to insulin. MD4 mice express both a heavy- and light-chain specific for hen-egg lysozyme (HEL); the sole antigen specificity of all B cells in this mouse. Mice were housed and bred at the University of Colorado Denver Anschutz Medical Campus Vivarium or in the Biological Resource Center at National Jewish Health. All experiments involving mice were performed in accordance with the regulations and with approval of the University of Colorado Denver Institutional Animal Care and Use Committee and National Jewish Health.

4.2.5. Tissue harvest

Spleens were harvested in IMDM supplemented with 5 % FCS, 1 mM sodium pyruvate, 50 ug/mL gentamicin, 100 U/mL penn/strep, 2 mM L-glutamine, and 5E-5 M beta-mercaptoethanol; single cell suspensions were prepared by mechanical disruption. RBC's were lysed with 1mL ACK (150 mM NH_4Cl, 10 mM $KHCO_3$, 100 mM Na_2EDTA) for 1 min at room temperature (RT). Cells were subsequently washed and resuspended in either complete medium

containing 0.1 % NaN_3 or complete medium alone for staining or calcium measurement, respectively. For staining of VH125.NOD + MD4 B cells, B cells were purified via CD43 negative selection before mixing MD4 B cells (~1%) into the VH125.NOD B cells.

4.2.6. Flow cytometry

Cells were resuspended at 1E7 cells/mL in cold complete medium containing 0.1 % sodium azide (NaN_3). 100 uL aliquots containing 1E6 cells were stained with fluorescently-conjugated monoclonal antibodies. Antibodies against the following cell-surface molecules were used: B220 (RA3-6B2; BD), IgM-AF488 (B76) and, CD79b-PE (fab; HM79). B76 and HM79 were produced in the Cambier laboratory and were directly conjugated to fluorochromes according to the manufacture's protocol. For the detection of B cells expressing insulin reactive B cell receptors, cells were first incubated with or without $SAgA_{Ins}$ molecules or hyaluronic acid (HA) alone [0.5 ug] for 20 min at 4 degrees C. After two washes and resuspension in 100 uL medium, cells were stained with monomeric biotinylated insulin (ins-bt) (1:50), and HEL-AF488 (1:200) for VH125.NOD + MD4 experiment, for 20 min at 4 degrees C. Cells were washed again before adding anti-B220 (APC, PE, or BUV396), anti-IgM, fab anti-CD79 and, fab anti-biotin-AF647. Following final incubation and washing, cells were analyzed on a Fortes X-20 flow cytometer (BD) and analyzed using FlowJo software (Tree Star).

4.2.7. Calcium mobilization

For measurements of relative intracellular free calcium concentration ($[Ca_{2+}]_i$), 125Tg RBC-lysed splenocytes (1E7/ mL in complete medium containing 2 % FCS) were incubated with or without $SAgA_{Ins}$ or HA, for 4 hours at 37°C and 5 % CO_2. For an additional hour at RT, cells

were simultaneously stained with anti-B220-APC (1:500), fab anti-CD79b-PE (1:500) and, loaded with 5 uM Indo-1 acetoxymethyl. After washing once in medium, cells were resuspended at 5E6 cells/ mL in RT medium in 500 uL aliquots. Indo-1 was excited with a 355-nm UV laser, Ca^{2+} - bound Indo-1 was detected with a 379/28 bandpass filter; unbound Indo-1 was detected with a 524/40 bandpass filter. Relative free intracellular calcium concentration was determined by calculating the ratio of bound/unbound Indo-1. After acquiring data for 30 s, to establish a baseline, cells were stimulated with the indicated dose of $SAgA_{Ins}$ molecules, anti-IgM [B76] and/or ionomycin and data collected for an additional 2 min 30 sec. Relative mean $[Ca_{2+}]_i$ was measured on a Fortessa X-20 flow cytometer and analyzed with FlowJo software.

4.2.8. Statistical Analysis

GraphPad Prism was used to perform statistical analysis including sigmoidal nonlinear regression, ordinary one-way or two-way analysis of variance (ANOVA), and unpaired t-test. ANOVA was followed by Tukey's or Sidak's post-hoc test, where appropriate. The threshold for statistical significance was set to $p<0.05$.

4.3. Results and Discussion

Structural Design of Click Soluble Antigen Arrays

SAgAs were synthesized by conjugating multiple modified autoantigen (human insulin alkyne; Ins-Alk) molecules to a 16 kDa linear polymer hyaluronic acid (HA) to produce the following conjugates: low valency $_{lv}SAgA_{Ins}$ (2 insulin per HA), medium valency $_{mv}SAgA_{Ins}$ (4 insulin per HA), high valency $_{hv}SAgA_{Ins}$ (9 insulin per HA). SAgAs are designed to induce a tolerogenic effect by draining into secondary lymphoid organs to access B cells. To achieve the

desired immunological effect, SAgAs are designed by following Dintizis' reported antigen structure properties to induce tolerance in B cells: < 100 kDa, flexible, and highly soluble. We hypothesize that SAgAs with >5 insulin molecule per HA will induce anergy of insulin-specific B cells (IBCs) in the T1D non-obese diabetic (NOD)mouse model, and as a result, re-tolerating the mice to the autoantigen insulin and blocking T1D progression. We have previously reported that non-cleavable $cSAgA_{PLP}$ constructed via copper-catalyzed azide-alkyne cycloaddition (CuACC) covalent linker chemistry through conjugation of homopropargyl-$PLP_{139-151}$ to HA-azide to be superior to hydrolyzable linker chemistry with the same basic components in suppression of disease severity in the multiple sclerosis (MS) mouse mode experimental autoimmune encephalomyelitis (EAE). Our studies pointed to superior efficacy of non-cleavable $SAgA_{PLP}$ to sustained B cell receptor (BCR) engagement, thus prolonged interaction on the cell surface of B cells.[38] SAgA platform modular antigen design, allows for targeted ASIT in partnership with selected antigens using currently validated animal models to predict clinical success of the therapeutic SAgA platform. We chose the T1D autoantigen human insulin and the VH125 NOD mouse model. We selected CuAAC chemistry to conjugate modified human insulin to modified HA. CuAAC chemistry allows for high control over valency and stability.

4.3.1. Synthesis and Analytical Characterization of Click Soluble Antigen Arrays

Both quantitative and qualitative analytical techniques were used to characterize SAgAs and their components. The amine pegylated azide (H_2N-PEG_3-N_3) was conjugated to HA via EDC/NHS coupling chemistry. ^{1}HNMR was used to quantify azide functionalization of HA-azide revealing an average of 41 azides per HA (Figure 34). This was done by integrating a peak form the HA backbone, highlighted in yellow, and a peak in HA-N_3 that corresponds to a methylene peak, highlighted in blue. Due to manual integration performed to determine conjugation and the heterogeneity of HA, this analysis should be considered semi-qualitative. Modification of the autoantigen human insulin was conducted by conjugating an alkyne linker (Propargyl-N-hydroxysuccinimidyl ester) via NHS chemistry to furnish insulin-alkyne (Ins-Alk). LC-MS verified the successful synthesis of Ins-Alk and further characterization of the modified protein led to the identification of the site of modification. LC/MS analysis determined that two species of Ins-Alk existed. Either B29 lysine was modified or modification occurred on *N*-terminus on the A chain (Figure 35A; 35B).

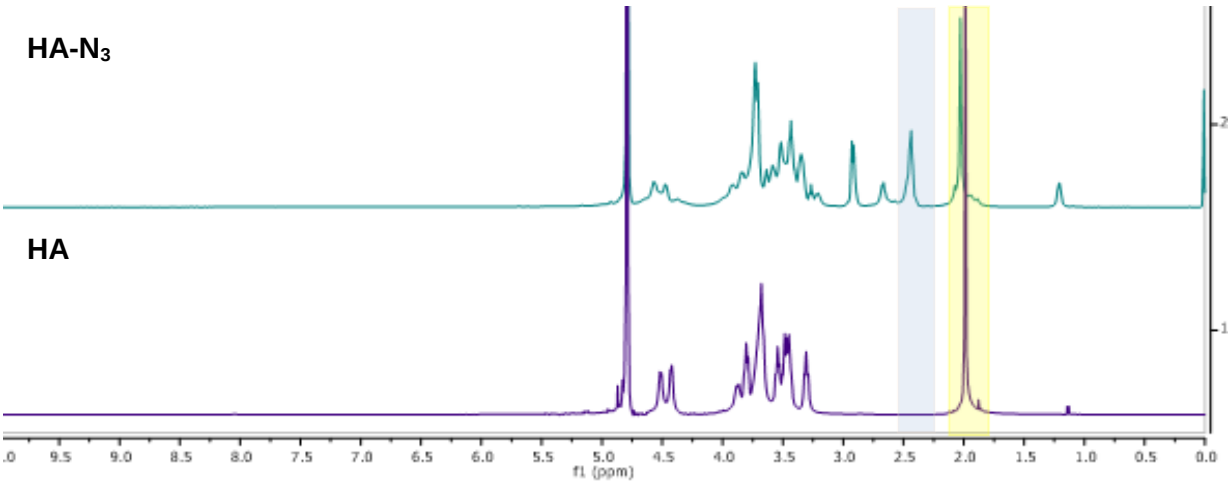

Figure 34: ^{1}H NMR spectra of hyaluronic acid (HA) and hyaluronic acid azide (HA-N_3). Peaks used to determine the average number of azides in HA-N_3 are highlighted in yellow and blue.

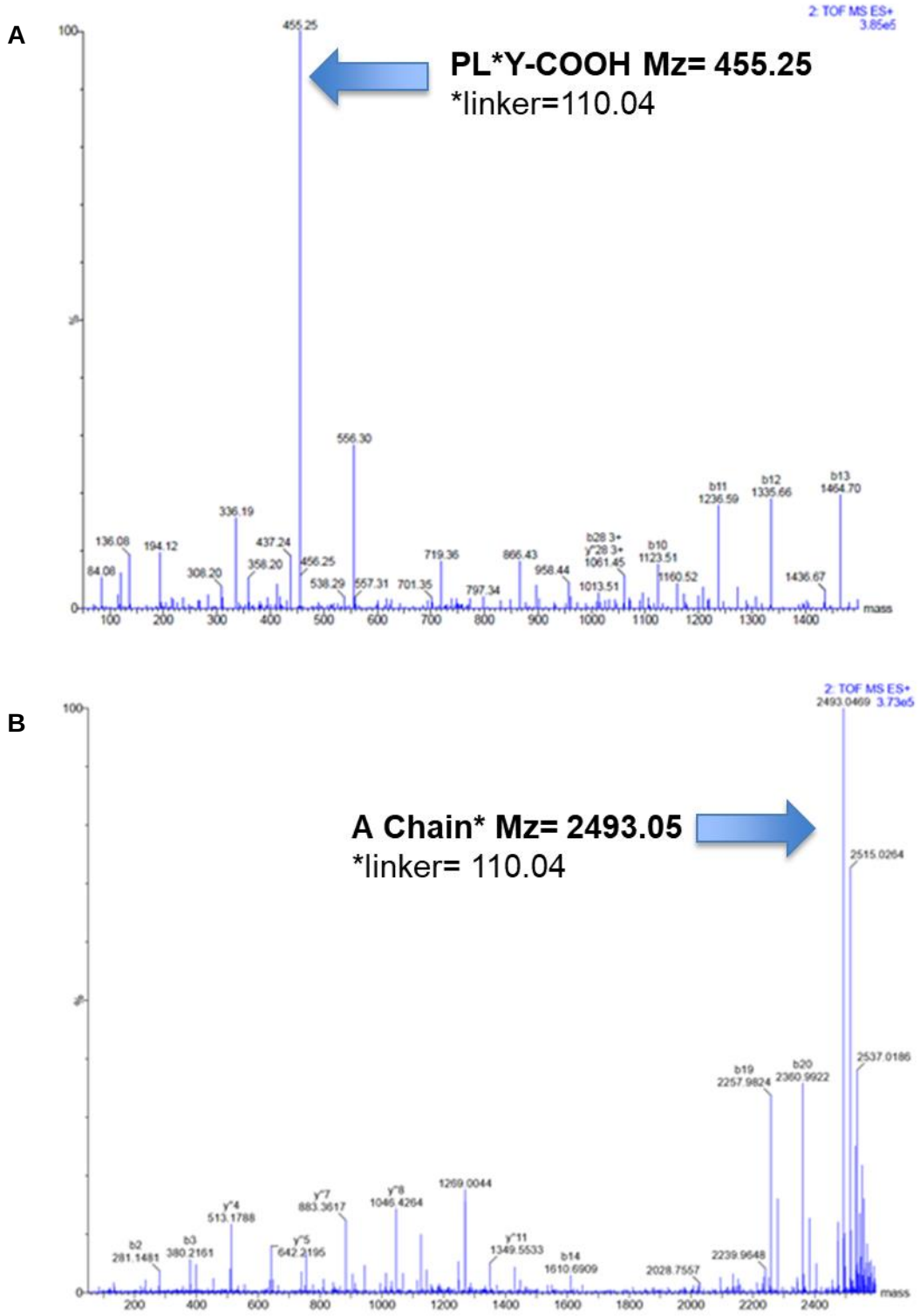

Figure 35 (A): Ins-Alk disulfide bonds were reduced via NH_4OAc and Dithiothreitol (DDT), run on an LC-MS revealed one Ins-Alk species to be modified on the B chain on the lysine residue; (B) shows the second Ins-Alk species modification was identified to be at the *N*-terminus of the A chain.

Initial CuAAC reaction conditions were used to conjugate Ins-Alk to HA-N_3 to produce $SAgA_{Ins}$ (2 Ins per HA). These SAgAs where characterized via RP-HPLC and sent off to our collaborators for preliminary biological studies. Upon further synthetic optimization of the CuAAC reaction, both medium valency $_{mv}SAgA_{Ins}$ (4 Ins per HA) and high valency $_{hv}SAgA_{Ins}$ (9 Ins per HA) were analyzed by RP-HPLC to determine the molecular weight and protein conjugation (Figure 36). The complete conjugation of Ins-Alk to HA-N_3 can be seen in both Figure 36A and Figure 36B. It should be noted, two aliquots from each reaction were taken before NaAsc was added. One aliquot was used to determine total Ins-Alk in solution and the second was analyzed in the same conditions as the reaction mixture without NaAsc to determine protein degradation over 24h (~1 Ins-Alk).

$^{1}H/^{13}C$ Heteronuclear Single Quantum Coherence (HSQC) NMR spectroscopy was used to qualitatively confirm the homopropargyl linker on the Ins-Alk (Figure 37A, 37C, green resonance; $\delta(^{1}H) \approx 2.9$ ppm, $\delta(^{13}C) \approx 70$ ppm). When both human insulin (red resonance) and Ins-Alk (green resonance) HSQC spectra were superimposed, some residue resonance signals pointed towards little to no structural change (Figure 37B, 37D; circled in purple), while distinct conformational differences can predominately be seen in the aromatic region for Ins-Alk (Figure 37B; circled in blue). These differences suggest the installation of the homopropargyl handle caused a buried aromatic amino acid (i.e. tryptophan) to surface, thus becoming detectable by NMR. Finally, HSQC analysis revealed the absence of the unique resonance signal for the homopropargyl linker on Ins-Alk ($\delta(^{1}H) \approx 2.9$ ppm, $\delta(^{13}C) \approx 70$ ppm) in both the $_{mv}SAgA_{Ins}$ and $_{hv}SAgA_{Ins}$ spectrum (Figure 37E and 37F), thus, confirming the final products contained only the conjugated protein.

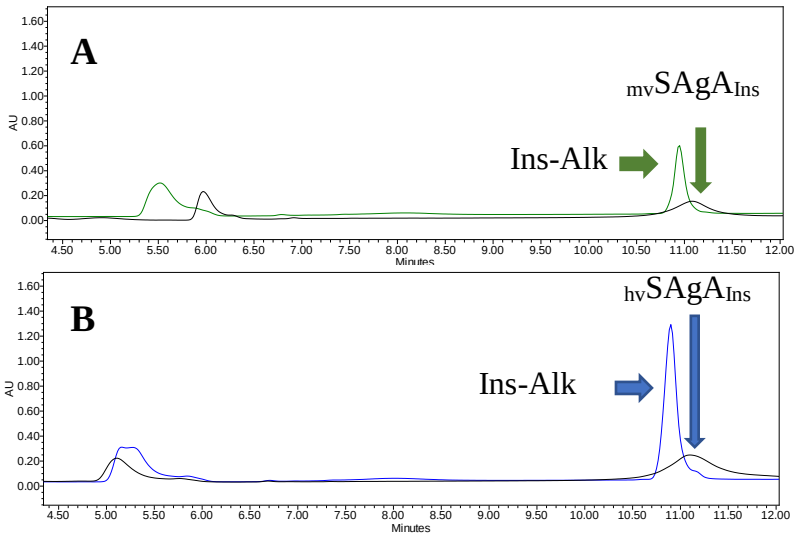

Figure 36: Reverse-phase analytical high-performance liquid chromatography (RP-HPLC) on an xBridge C4 5um (4.6 X 250mm) gradient 5:95 to 95:5 (Acetonitrile :Water) @ 214nM; (A) 24 h post-NaAsc $_{mv}SAgA_{Ins}$ (board black trace), overlaid pre-NaAsc (green trace); (B) 24 h post-NaAsc $_{hv}SAgA_{Ins}$ (board black trace), overlaid pre-NaAsc (blue trace).

Circular Dichroism analysis of human insulin was consistent with previously reported alpha helical secondary structure (Figure 38A-38D). $SAgA_{Ins}$ mostly retained alpha helical secondary structure in both neutral (pH 7.4) and acid media (pH 3.0), however, $_{hv}SAgA_{Ins}$ appeared to lose significant secondary structure in acidic conditions (Figure 38A-D). Further analysis of CD data revealed greater loss of alpha helical structure for $_{hv}SAgA_{Ins}$ when compared to $_{mv}SAgA_{Ins}$ in both acid and neutral solutions (Figure 38C, 38D). When directly studying the effect of pH on each SAgA, secondary structure in both cases are partial or completely lost at lower pH when compared to neutral pH. HSQC NMR analysis in combination with CD data may explain the loss of secondary structure of $SAgA_{Ins}$ when compared to native human insulin. Alkyne modification resulted in a physical change in protein structure that allowed for hydrophobic residues to be detected via HSQC NMR. These hydrophobic resides such as tryptophan may increasingly interfere with alpha helical structure. In addition, basic amino acids (i.e. arginine) becomes more protonated at lower pH, which may result in electrostatic repulsion that could alter the peptide secondary structure.

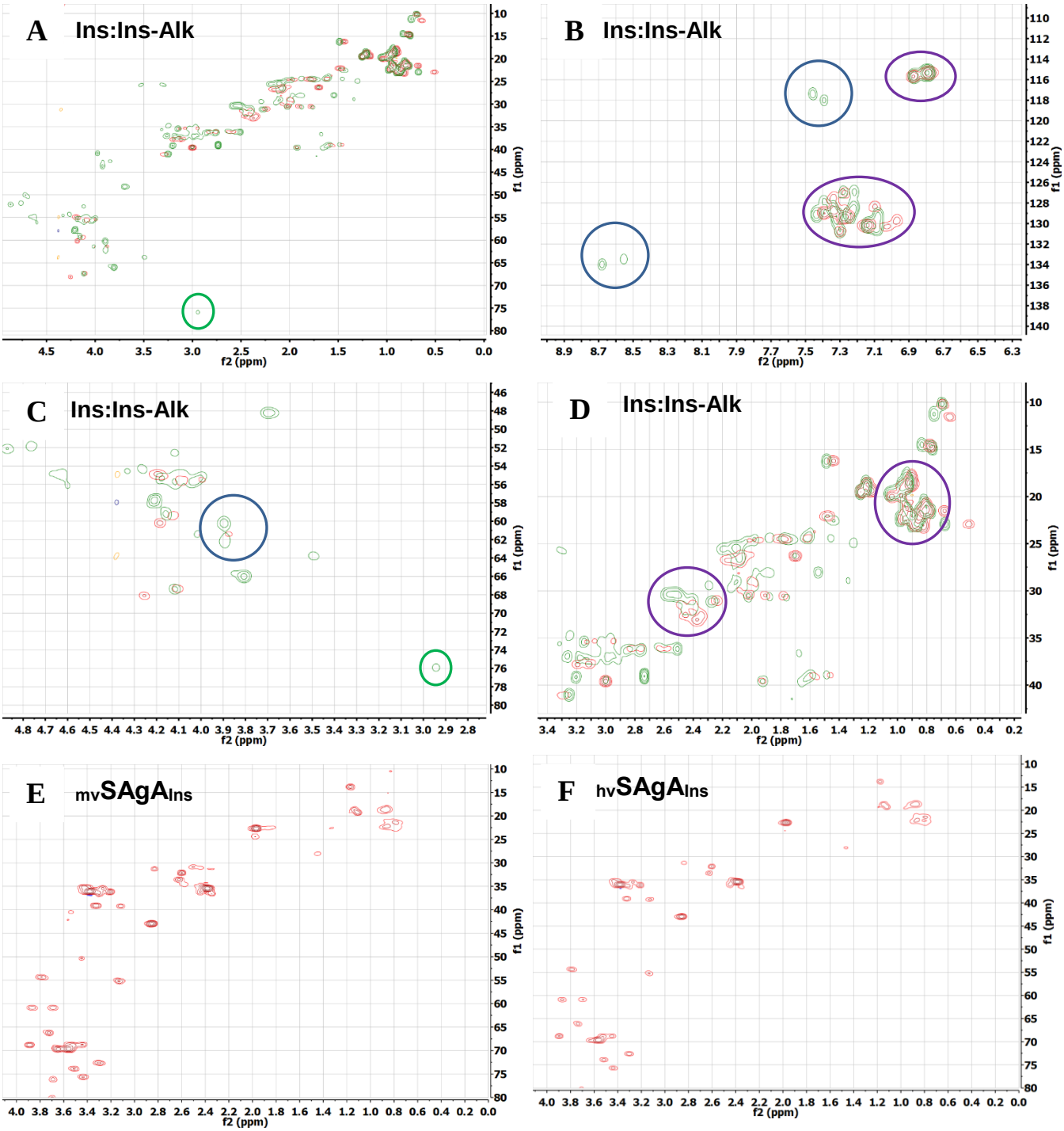

Figure 37: Overlapped HSQC NMR spectra of insulin (red) and Ins-Alk (green) (A-D). Multivalent SAgAs ($_{mv}$SAgA$_{Ins}$) (E) and ($_{hv}$SAgA$_{Ins}$) F show no resonances from the alkyne peak found only Ins-Alk present in either of the final compounds. The alkyne peak found only in Ins-Alk is not found in any of the products, which implies complete no residual unconjugated Ins-Alk. HSQC NMR of A focuses on highlighting in a green circle terminal alkyne proton in Ins-Alk. B shows more available aromatic residues in Ins-alk (green) when compared to insulin. C and D highlight Similarities (purple circles) and differences (blue circles) between insulin alkyne (green) and insulin (red).

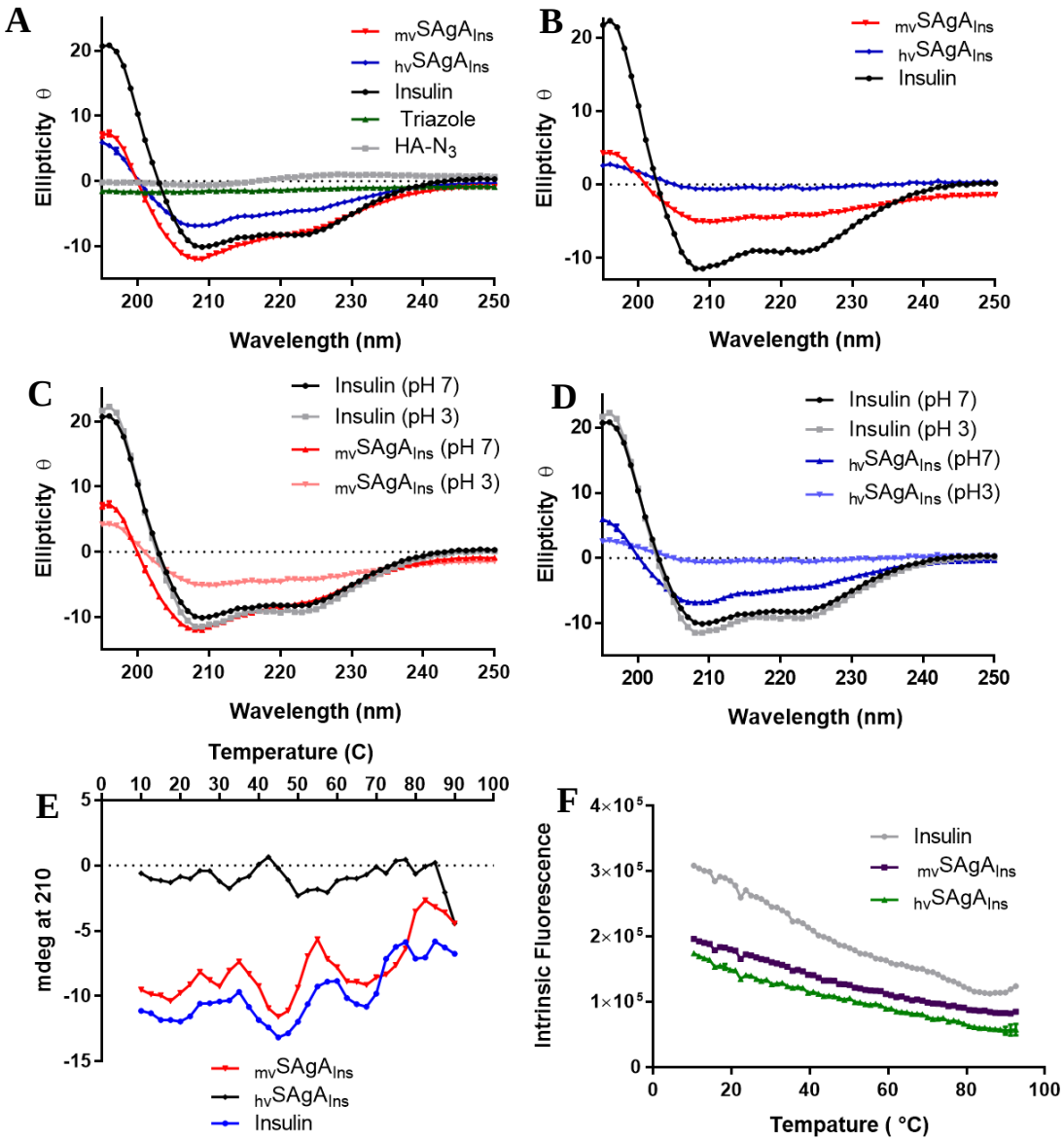

Figure 38: Far-UV Circular Dichroism of (A): medium and high valency SAgAs in phosphate buffer pH 7.4; (B): medium and high valency SAgAs in water pH 3.0; (C): medium valency SAgAs in phosphate buffer pH 7.4 and water pH 3.0;(D): high valency SAgAs in phosphate buffer pH 7.4 and water pH 3.0; (E): medium and high valency SAgAs water pH 3.0 temperature melt.; (F): Intrinsic fluorescent temperature melt of SAgAs.

A temperature melt plot based on intrinsic fluorescence (Figure 38F) showed an increase in nonradiative decay with temperature, which may suggest the absence of tertiary structure. This may be explained by the fact that insulin contains three disulfide bonds, which require significant amount of energy for a transition occur for an insulin monomer. Finally, dynamic light scattering

shows significant size increase for $_{hv}SAgA_{Ins}$, while $_{mv}SAgAIns$ show a predictable increase in size (Table 4). This large increase in size in $_{hv}SAgA_{Ins}$ may correlate with the partial loss in secondary alpha helical structure (Figure 38), where the insulin would now favor intermolecular interactions that may lead to aggregation rather than intramolecular interactions.

Table 4. Insulin molar conjugation, as determined by RP- HPLC[a] . Dynamic light scattering (DLS) of SAgAs and components.

Sample	Approx. MW (kDa)[b]	Insulin per Polymer[c]	DLS[d]	
			Radius (nm)	%Polydispersity
Insulin 	5.81	0	2.09 ± 0.02	0.08
HA-N_3 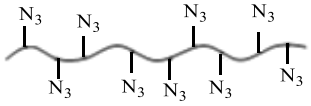	24.50	0	6.5 ± 0.03	24.50
$_{lv}SAgA_{Ins}$ 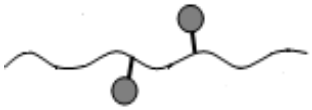	36.34	2	----------	----------
$_{mv}SAgA_{Ins}$ 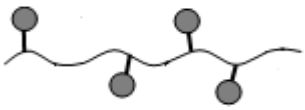	48.17	4	14.07 ± 0.63	26.55
$_{hv}SAgA_{Ins}$ 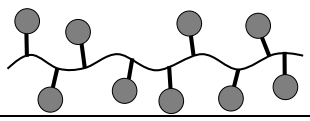	77.76	9	14.07 ± 0.15	24.52

[a] Results are an average of triplicate injections from a single batch preparation.
[b] Calculated from RP-HPLC data. MW, molecular weight.
[c] Insulin per HA, hyaluronic acid
[d] DLS data were collected in triplicate

4.3.2. $SAgA_{Ins}$ binding and effects on ex vivo IBCs

In order to address the biological relevance and potential therapeutic application of multimeric, insulin-polymer ($SAgA_{Ins}$) molecules, we first asked if $SAgA_{Ins}$ are capable of ligating B cell receptors (BCR) on the surface of IBCs. To this end, we utilized B cells from 125Tg mice in which, by virtue of heavy- and light-chain knock-in, harbor peripheral B cells with an insulin-fixed receptor repertoire. RBC-lysed, 125Tg splenocytes were first incubated with or without $SAgA_{Ins}$ (low or high avidity) or hyaluronic acid (HA) alone for 20 min, at 4°C, in complete medium containing 0.1 % NaN_3. Staining under these conditions prevents the internalization of ligated BCR. After being washed, cells were exposed to monomeric biotinylated insulin (ins-bt), washed, and subsequently stained with antibodies against B220 (B cells), CD79 (BCR) and, IgM (BCR) together with anti-biotin (Insulin). Depicted in Figure 39A, pre-treatment with $SAgA_{Ins}$, but not HA alone, blocked binding of ins-bt. Staining, in which ins-bt was omitted, serves as a positive control, and staining with no $SAgA_{Ins}$ pre-treatment serves as a negative control. In addition, neither $SAgA_{Ins}$ nor ins-bt bound to non- (B220-) B cells (data not shown). In anticipation for experiments in which we re-stimulate $SAgA_{Ins}$ tolerated IBCs, we wanted to ensure that $SAgA_{Ins}$ binding to the BCR does not obscure binding of BCR stimulating antibodies. In this case, cells previously exposed to the $SAgA_{Ins}$ where subsequently stained with anti-IgM [B76] and anti-CD79 [HM79]. No change in staining intensity was detected for anti-BCR antibodies in cells pre-treated with $SAgA_{Ins}$ (Figure 39B). Finally, in order to address $SAgA_{Ins}$ binding in a more physiologic setting, we utilized B cells (CD43-) purified from spleens of VH125.NOD mice in which ~1-3% of peripheral B cells bind insulin. To ensure specificity, MD4 B cells (HEL reactive) were mixed in at approximately the same frequency as IBCs. As before, cells were pre-treated with

$SAgA_{Ins}$ or HA alone before being stained with ins-bt/fab anti-bt-AF647 AND HEL-AF488. As displayed in Figure 39C, $SAgA_{Ins}$ only blocked binding of ins-bt but not HEL-AF488.

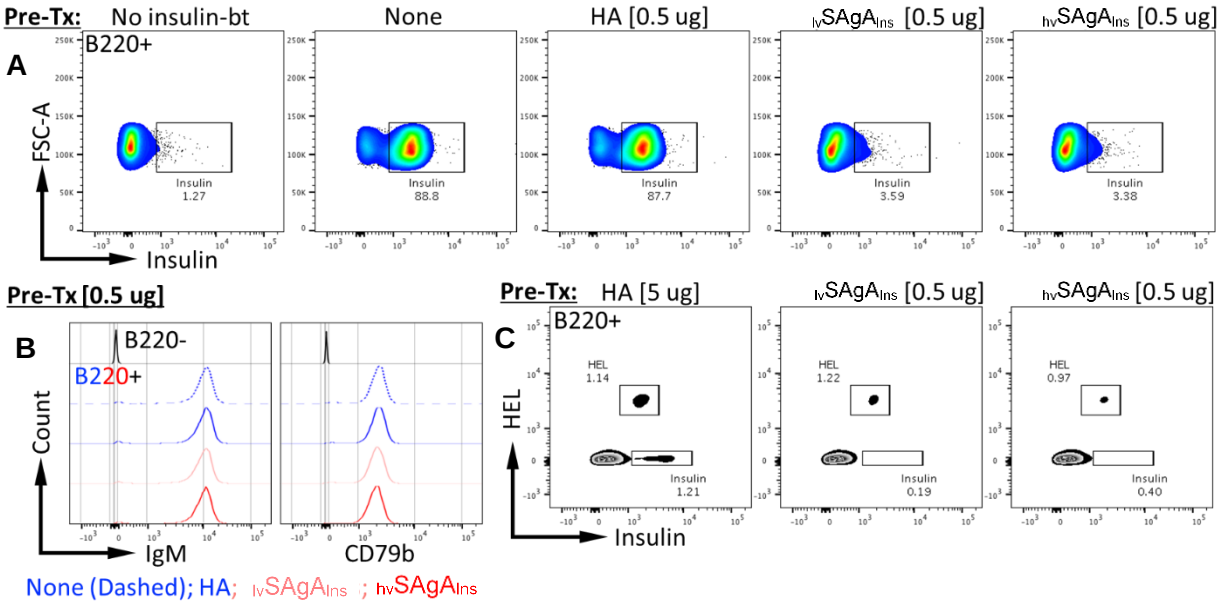

Figure 39: Specific binding of $SAgA_{Ins}$ to insulin binding cells (IBCs). Both $_{lv}SAgA_{Ins}$ and high-avidity ($_{hv}SAgA_{Ins}$) molecules, but not hyaluronic acid (HA) alone, block binding of monomeric biotinylated-insulin to insulin-specific (B220+;125Tg) B cells (A). Pretreatment of 125Tg B cells with either $SAgA_{Ins}$ or hyaluronic acid does not mask epitopes recognized by anti-IgM [B76] nor anti-CD79 [HM79] (B). $SAgA_{Ins}$ molecules block binding of insulin-bt to insulin specific B cells (CD43-, B220+;VH125.NOD) but not binding of hen egg lysozyme (HEL) to HEL specific B cells (CD43-, B220+;MD4) when both cell types are present at similar frequencies (C). Layout gate frequencies represent percent of B cells (B220+). Data are representative of at least 3 independent experiments.

4.3.3. *In vitro* incubation of IBCs with insulin-SAgA leads to decreased expression of BCR and desensitization of the BCR to additional stimulation.

The ultimate goal of designing $SAgA_{Ins}$ is to be used as a potential therapeutic agent for treating/preventing the development of T1D. B cells are required for the development of T1D in mice and have been strongly implicated in human disease, most likely as antigen presenting cells needed for T cell activation in the pancreas.[201] Depletion of B cells with an anti-CD20 antibody (rituximab) has been shown to delay the progression of disease in humans.[202] Similarly, tolerization of peripheral B cells via chronic BCR stimulation has been observed to delay disease onset in mice.[203] Following from this, we hypothesize that tolerizing antigen-(insulin) specific B cells may prove to be similarly efficacious in preventing T1D progression. Antigen specific

tolerization comes with the added benefit of allowing the rest of the B cell compartment to remain active for fighting infection and responding to vaccination. To ask if $SAgA_{Ins}$ is capable of tolerizing IBCs, we again utilized B cells from the 125Tg mouse. We first measured intracellular calcium mobilization in response to acute stimulation with $SAgA_{Ins}$ (Figure 40A). Anti-IgM and HA alone were used as positive and negative controls, respectively. $SAgA_{Ins}$ stimulated a similar calcium flux in comparison to stimulation with anti-IgM (note that 125Tg B cells exclusively express IgM). Next, we incubated 125Tg IBCs with or without $SAgA_{Ins}$ or HA alone for ~5 hours before measuring surface BCR expression and calcium mobilization (Figure 40B, 40C). Pre-incubation with $SAgA_{Ins}$ leads to decreased expression of surface BCR, as measured by CD79b, reminiscent of chronically stimulated, anergic B cells found in mice and humans (Figure 40B).[201] Pre-incubation with $SAgA_{Ins}$, but not HA, rendered IBC's refractory to re-stimulation through the

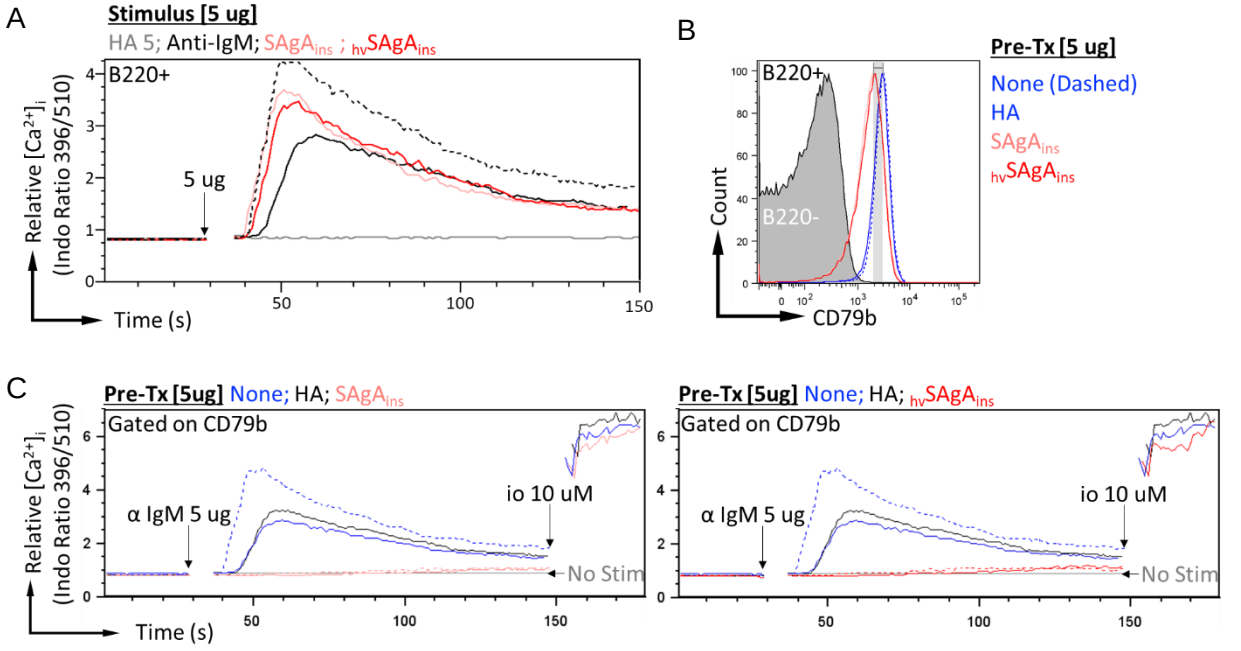

Figure 40: *$SAgA_{Ins}$* effects on ex-vivo, insulin-binding cells (IBCs). *$SAgA_{Ins}$* molecules, but not hyaluronic acid (HA) alone, are capable of aggregating B cell receptors (BCR) on insulin specific B cells (125Tg) and stimulating extracellular calcium influx (A). 5 hour pre-incubation of IBCs (125Tg) with *$SAgA_{Ins}$*, but not HA, leads to decreased expression of BCR on the surface of IBCs (B). Pre-incubation with *$SAgA_{Ins}$* renders IBCs refractory to re-stimulation through the BCR by anti-IgM [B76] but not to stimulation with the calcium ionophore, ionomycin (io) (C). This induced tolerance is independent of the surface expression of BCR (gating in B). Dashed calcium traces represent *$SAgA_{Ins}$* treated (C) or untreated (A) cells stimulated with a 5-fold excess [25 ug] of anti-IgM . Data are representative of at least 3 independent experiments.

BCR (Figure 40C). This inhibition was not due to masking of the epitope on the BCR recognized by B76 (Figure 40B) and was independent of the $SAgA_{Ins}$ induced decrease in surface BCR (gating in Figure 40B). In addition, $SAgA_{Ins}$ incubated cells remained refractory to a 5-fold excess of anti-IgM stimulation (Figure 13C dashed lines), which resulted in an increased calcium response in untreated or HA treated cells (Figure 40A, 40C). Finally, $SAgA_{Ins}$ induced desensitization of the BCR is independent of IP3 receptor-mediated release of intercellular calcium stores, as stimulation with the calcium ionophore, ionomycin, resulted in similar calcium influx in $SAgA_{Ins}$ treated, HA treated, and untreated cells. This suggests that $SAgA_{Ins}$ induced tolerance of IBCs may rely on mechanisms observed to be operative in anergic B cells found in mice and in humans.[204]

4.4. Conclusions

Both HA-N_3 and Ins-Alk were synthesized and verified via various analytical techniques. SAgAs were successfully synthesized by conjugating multiple modified autoantigen human insulin (Ins-Alk) molecules to a 16 kDa linear polymer hyaluronic acid (HA) to produce the following bioconjugates: low valency $SAgA_{Ins}$ (2 insulin per HA), medium valency $_{mv}SAgA_{Ins}$ (4 insulin per HA), high valency $_{hv}SAgA_{Ins}$ (9 insulin per HA). The $_{mv}SAgA_{Ins}$ and $_{hv}SAgA_{Ins}$ SAgAs were shown to maintain alpha helical structure at physiological pH. They were also successfully used to make $SAgA_{Ins}$ that silence *ex vivo* IBCs by inducing refractory B cell receptor signaling. $SAgA_{Ins}$ binds specifically to insulin-reactive B cells without masking epitopes recognized by antibodies against the BCR. Pre-incubation of IBCs (125Tg) with $SAgA_{Ins}$, but not HA, renders the BCR desensitized to re-stimulation. This effect is independent of $SAgA_{Ins}$ induced decrease in BCR expression and is also independent of IP3R-mediated intracellular calcium release. This activity is dependent on $SAgA_{Ins}$ binding to BCR on the surface of IBCs, and its ability to acutely

stimulate these cells. Finally, the biophysical difference between high and low valency $SAgA_{Ins}$ does not appear to modulate biologic activity, as both molecules produced similar levels of receptor blockade and BCR desensitization. In the future these $SAgA_{Ins}$ will be tested as therapeutic in VH125 NOD mice.

CHAPTER 5:
CONCLUSIONS AND FUTURE DIRECTIONS

CHAPTER 5: CONCLUSIONS AND FUTURE DIRECTIONS

5.1. Introduction

The need for novel antigen-specific immunotherapies (ASIT) for the treatment of autoimmunity is a pressing matter that must be addressed. Bioconjugation techniques such as copper-catalyzed azide-alkyne cycloaddition (CuAAC) allow for the facile construction of immunological probes to visualize or modulate autoimmunity. This dissertation highlighted in detail the two different ASIT approaches for the potential treatment of autoimmune via antigen-drug conjugates (AgDCs) and soluble antigen arrays (SAgAs) summarized in Section 5.2. The key findings in these chapters setup the future directions for these projects, which is discussed in Section 5.3.

5.2. Summary of dissertation chapters

In Chapter 1, an introduction into autoimmunity and current clinically available non-antigen-specific treatments were presented, along with an overview of the emergence of antigen-specific immunotherapies (ASIT) as an improved strategy for the treatment of autoimmune diseases. Furthermore, a detailed background into the chemistry utilized in this work to construct novel antigen-specific probes as potential therapies for autoimmune disorders was also presented. Autoimmune diseases afflict 5% of the world's population and are believed to be caused by the loss of tolerance to autoantigen.[1] All current treatments for autoimmunity are not antigen-specific and either treat symptoms or slow down the progression of the disease. Scientist may be able to induce tolerance to autoantigen in individuals afflicted by autoimmune diseases via ASIT. In order to construct antigen-specific bioconjugate probes as potential therapies to treat autoimmunity, a detailed background and literature review of copper-catalyzed azide-alkyne cycloaddition

(CuAAC) chemistry was presented. Key information on CuAAC reactions were discussed, such as approaches for installation of azide and alkyne handles into various bioactive molecules, as well as, insights into reported bioconjugates used as probes and their ability to modulate biological functions. Finally, CuAAC considerations and challenges were discussed to set the foundation for the design and optimization for the bioconjugate probes discussed in this work.

Chapter 2 presented the synthesis and development of chemical biology tools for probing antigen-specific immunotherapy. Specifically, the synthesis of a library of various azide or alkyne containing small molecules, modified-mimotopes, and synthetic epitopes, as building blocks for Antigen Drug Conjugates (AgDCs) and other immunologically active materials used later in this work. Similar to antibody drug conjugates (ADCs), AgDCs are a novel co-delivery ASIT designed to deliver a potent drug (cargo), which is chemically linked to an autoantigen (vehicle). Initial CuAAC reaction optimization utilizing the multiple sclerosis (MS) mimotope substrate propargylglycine-PLP (pPLP) to coumarin-azide (Comarin-N_3) was unsuccessful, and it was determined that the primary amine in the pPLP handle inhibited the reaction. A redesign of our mimotope alkyne handle eliminated the presence of the primary amine and thus homopropargyl-PLP (hpPLP) was synthesized, characterized, and successfully used in a CuAAC reaction. With the success of the new handle design, the *N*-terminus of a type 1 diabetes (T1D) mimotope p79 was modified via solid state peptide chemistry to contain a homopropargyl linker (hpP79). CuAAC reaction between hpP79 (vehicle) and the immunosuppressant dexamethasone-azide (Dex-N_3; cargo) was successfully optimized, purified, and ready for potential screening of the AgDC in future studies. Also, hpP79 was conjugated to the fluorophore Rhodamine B-azide (Rhod-N_3) for potential future visualization in the mechanism elucidation of p79 uptake into immune cells. The

future direction for the AgDC Dex-p79 was explained in Section 5.3.1. and the future direction of AgDCs for other disease indications was discussed in Section 5.3.4.

Chapter 3 was inspired by previous research in our group which utilized a novel antigen delivery strategy know as Soluble Antigen Arrays (SAgAs) for the potential treatment of MS. SAgAs are constructed by conjugating multiple repeating autoantigen to a hydrophilic linear polymer backbone hyaluronic acid (HA). The technology was repurposed as a potential therapeutic for T1D by using the T cell stimulatory mimotope p79 from chapter 2. Similar to previous work published in the Berkland group,[64, 154] two different linker chemistries were used to conjugate p79 to HA. Either a non-hydrolyzable 'click" CuAAC linker chemistry to furnish $cSAgA_{p79}$ or hydrolyzable aminooxy chemistry was used to produce $SAgA_{p79}$. Our ASIT technology was characterized via various analytical techniques: high-performance liquid chromatography (HPLC), nuclear magnetic resonance spectroscopy (NMR), circular dichroism (CD), dynamic light scattering (DLS), and fluorescence. The biophysical characterization revealed a similar secondary structure of peptides conjugated to SAgAs as their parent peptide hpP79 and aoP79. No definitive tertiary structure was detected for either $cSAgA_{p79}$ or $SAgA_{p79}$. The specificity and efficiency of T cell stimulation by these SAgAs was demonstrated by *in vitro* treatment of splenocytes from BDC2.5 versus NOD mice, and we identified conventional dendritic cells (cDCs) as the most efficient type of APCs responsible for uptake and presentation of SAgA-derived epitopes to T cells. We also observed that cSAgAp79 are more stimulatory than $SAgA_{p79}$, a property that appears to be more associated with the *N*-terminal peptide modification than their peptide release properties. Future work for p79 containing SAgAs was discussed in Section 5.3.2.

Chapter 4 focused on alternative T1D therapy SAgA constructed by conjugating full-length human insulin protein to HA. Unlike the p79-SAgA work, only CuAAC chemistry was used to

construct $SAgA_{Ins}$ and three different valences of autoantigen insulin (2, 4, 9) per HA were synthesized. Analysis of CD data reveled that both medium valency ($_{mv}SAgA_{Ins}$) and high valency ($_{hv}SAgA_{Ins}$) SAgAs were shown to maintain alpha helical structure at physiological pH and no higher order structure was detected by fluorescence for either $SAgA_{Ins}$. $SAgA_{Ins}$ *ex vivo* were able to ligate B cell receptor (BCR) on the surface of insulin-binding cells IBCs in B cells from both 125Tg (NOD) and VH125.NOD mice. The biophysical difference between $SAgA_{Ins}$ does not appear to modulate biologic activity, as both molecules produced similar levels of receptor blockade and BCR desensitization. The future direction of this work will be discussed in Section 5.3.3.

5.3. Future directions

5.3.1. Adjusting design of AgDCs to improve solubility Dex-p79

First, Dex-p79 AgDCs needs to be screened in order to determine if specificity of the peptide is retained *in vitro*. If successful, drug release and stability studies will be performed. Then, the AgDCs need to be studied to determine if they can induce an antigen-specific immune response. If specificity and immune tolerance is possible, Rhod-p79 can be used to determine the potential mechanism of action for Dex-p79. However, it should be highlighted that solubility of Dex-p79 was poor in aqueous solution. In order to improve solubility, either an alternative water-soluble drug should be used (ie. 5-Fluoro-5'-deoxycytidine; 5'-DFCR)[205] and/or a hydrophilic

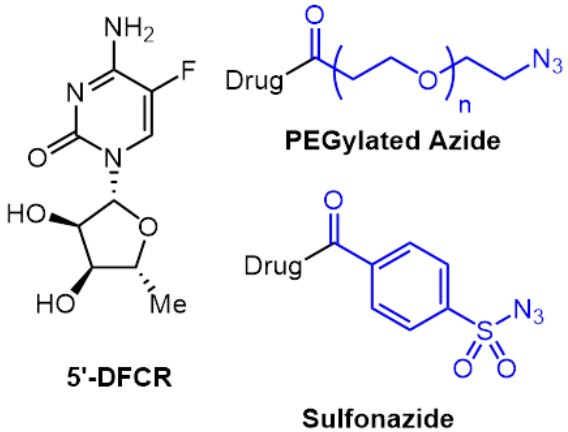

Figure 41: Hydrophilic drug 5-Fluoro-5'-deoxycytidine (5'-DFCR) and Pegylated/Sulfonated-

linker (i.e. PEGylated or Sulfonated) should be used (Figure 41). AgDCs for other disease indications are also possible with the use of other autoantigens (see Section 5.3.4).

5.3.2. Continued p79-SAgA development

The *in vitro* success of both $cSAgA_{p79}$ and $SAgA_{p79}$ in splenocytes from BDC2.5 mice has promoted future *in vivo* studies. Furthermore, stability studies can be performed to better understand the potential bioavailability of the p79-containing SAgAs *in vivo*. SAgAs can be redesigned by making structural changes. Dintzis and coworkers reported that a tolerogenic immune response could be induced by varying both the peptide valency and/or polymer backbone. Therefore, modification of p79-containing SAgAs's valency and polymer backbone in the future could potentially improve its efficacy.[206] Valency can be controlled by either changing the reactive azides available on the HA on $cSAgA_{p79,}$ or optimizing the reaction conjugation (i.e. time, temp, stoichiometry, etc.) to conjugate less p79 per HA for $SAgA_{p79}$ and $cSAgA_{p79}$. Finally, if lower valency maintains or increases potency, then different polymer backbone such as shorter HA or multi-arm-PEGylated polymers may be used to improve bioavailability and potency.[167] The multi-arm-PEGylated system may present different modulatory effects due to its ability to contour antigen-specific cell surfaces in a multidirectional manner, unlike the linear SAgAs used in this work.

5.3.3. Continued $SAgA_{Ins}$ development

The $SAgA_{Ins}$ have shown potential *in vitro,* but require further testing *in vivo* to determine if $SAgA_{Ins}$ are capable of improve the disease state of VH125.NOD mice. These studies would require a significant amount of human insulin, and therefore may require optimization to improve

synthesis and purification of Ins-Alk. HPLC analysis of crude Ins-Alk resulted in 60% yield of the desired product, however, upon isolation of Ins-Alk the final yield dropped to 32%. $SAgA_{Ins}$ was able to induce tolerance with only2 insulins per HA, thus, maybe simply tethering two insulin molecules via a bifunctional hydrophilic linker (e.g. PEGylated), similar potency may be observed. Such bioconjugation would significantly reduce the analytical characterization for future scientist in our group.

5.3.4. Alternative Autoantigens for Future deployment of AgDCs and SAgAs

This thesis presented the synthesis and characterization of chemical biology probes as potential therapeutics for T1D. Utilizing the same basic design of the AgDCs or SAgAs, it may be possible to design, synthesize, and characterize chemical biology probes for other autoimmune diseases. A few examples are listed in Table 5 below.

Table 5. A few examples of potential autoantigen for antigen-specific immunotherapies (ASIT) for both AgDCs and SAgAs

Autoimmune Disease	Antigen
Multiple Sclerosis	MBP, MOG
Type 1 Diabetes	IA-2, GAD-65
Rheumatoid Arthritis	Collagen, Aggrecan
Neuromyelitis Optica	AQP4, MOG
Celiacs Disease	TG2

Both peptides and full-length protein autoantigen can be utilized in our ASIT design, but a few considerations must be taken into account for the construction of future AgDCs or SAgAs for other autoimmune diseases. First, the best antigen for modification must be determined via epitope screening. Then for full length proteins, possible site for selective modification without losing efficacy must be determined. Furthermore, the solubility of the autoantigen selected must be taken into consideration to avoid inducing undesired pro-inflammatory responses as seen in vaccines. Finally, a well characterized animal model to test the efficacy of the antigen-specific chemical biological probes is needed.

5.4. Conclusions

In this dissertation, an azide/alkyne library of small molecules, modified peptides, and polymers were synthesized and used to construct various bioconjugates to visualize or modulate immunological systems. The use of CuAAC chemistry allowed for the rapid construction of bioconjugates, which were efficacious in their respective animal models. Finally, a significant amount of work is left for the future elucidation of the mechanism or the novel antigen-specific therapies as potential therapeutics for the treatment of T1D.

REFERENCES

1. Murphy, K. M., *Janeway's Immunobiology*. 8th ed.; Garland Science: 2012.
2. Rosenblum, M. D.; Remedios, K. A.; Abbas, A. K., Mechanisms of human autoimmunity. *J. Clin. Invest.* **2015,** *125* (6), 2228-2233.
3. Edwards, J.; Cambridge, G.; Abrahams, V., Do self-perpetuating B lymphocytes drive human autoimmune disease? *Immunology* **1999,** *97* (2), 188-196.
4. Stastny, P., Association of the B-cell alloantigen DRw4 with rheumatoid arthritis. *N. Engl. J. Med.* **1978,** *298* (16), 869-871.
5. Guo, Y.; Wu, Q.; Ni, B.; Mou, Z.; Jiang, Q.; Cao, Y.; Dong, H.; Wu, Y., Tryptase is a candidate autoantigen in rheumatoid arthritis. *Immunology* **2014,** *142* (1), 67-77.
6. Pianta, A.; Arvikar, S. L.; Strle, K.; Drouin, E. E.; Wang, Q.; Costello, C. E.; Steere, A. C., Two rheumatoid arthritis–specific autoantigens correlate microbial immunity with autoimmune responses in joints. *J. Clin. Invest.* **2017,** *127* (8), 2946-2956.
7. Compston, A.; Coles, A., Already Registered? Please Login. *Lancet* **2002,** *359* (9313), 1221-1231.
8. Müller-Ladner, U.; Pap, T.; Gay, R. E.; Neidhart, M.; Gay, S., Mechanisms of disease: the molecular and cellular basis of joint destruction in rheumatoid arthritis. *Nat Rev Rheumatol* **2005,** *1* (2), 102.
9. Podbielska, M.; Banik, N. L.; Kurowska, E.; Hogan, E. L., Myelin recovery in multiple sclerosis: the challenge of remyelination. *Brain Sci.* **2013,** *3* (3), 1282-1324.
10. Dyment, D. A.; Ebers, G. C.; Sadovnick, A. D., Genetics of multiple sclerosis. *Lancet Neurol* **2004,** *3* (2), 104-110.
11. Sundqvist, E.; Sundström, P.; Linden, M.; Hedström, A.; Aloisi, F.; Hillert, J.; Kockum, I.; Alfredsson, L.; Olsson, T., Epstein-Barr virus and multiple sclerosis: interaction with HLA. *Genes Immun.* **2012,** *13* (1), 14.
12. Termeer, C.; Averbeck, M.; Hara, H.; Eibel, H.; Herrlich, P.; Sleeman, J.; Simon, J. C., Targeting dendritic cells with CD44 monoclonal antibodies selectively inhibits the proliferation of naive CD4+ T-helper cells by induction of FAS-independent T-cell apoptosis. *Immunology* **2003,** *109* (1), 32-40.
13. Pociot, F.; Lernmark, Å., Genetic risk factors for type 1 diabetes. *Lancet* **2016,** *387* (10035), 2331-2339.
14. Knip, M.; Veijola, R.; Virtanen, S. M.; Hyöty, H.; Vaarala, O.; Åkerblom, H. K., Environmental triggers and determinants of type 1 diabetes. *Diabetes* **2005,** *54* (suppl 2), S125-S136.
15. Palmer, J. P.; Asplin, C. M.; Clemons, P.; Lyen, K.; Tatpati, O.; Raghu, P. K.; Paquette, T. L., Insulin antibodies in insulin-dependent diabetics before insulin treatment. *Science* **1983,** *222* (4630), 1337-1339.
16. Bottazzo, G.; Florin-Christensen, A.; Doniach, D., Islet-cell antibodies in diabetes mellitus with autoimmune polyendocrine deficiencies. *Lancet* **1974,** *304* (7892), 1279-1283.
17. Bonifacio, E.; Lampasona, V.; Bingley, P. J., IA-2 (islet cell antigen 512) is the primary target of humoral autoimmunity against type 1 diabetes-associated tyrosine phosphatase autoantigens. *J. Immunol.* **1998,** *161* (5), 2648-2654.
18. Baekkeskov, S.; Aanstoot, H.-J.; Christgai, S.; Reetz, A.; Solimena, M.; Cascalho, M.; Folli, F.; Richter-Olesen, H.; Camilli, P.-D., Identification of the 64K autoantigen in insulin-dependent diabetes as the GABA-synthesizing enzyme glutamic acid decarboxylase. *Nature* **1990,** *347* (6289), 151.
19. Rosenblum, M. D.; Gratz, I. K.; Paw, J. S.; Abbas, A. K., Treating human autoimmunity: current practice and future prospects. *Sci. Transl. Med.* **2012,** *4* (125), 125sr1.
20. Fletcher, S.; Lalor, S.; Sweeney, C.; Tubridy, N.; Mills, K., T cells in multiple sclerosis and experimental autoimmune encephalomyelitis. *Clin Exp Immunol.* **2010,** *162* (1), 1-11.
21. Chittasupho, C.; Siahaan, T. J.; Vines, C. M.; Berkland, C., Autoimmune therapies targeting costimulation and emerging trends in multivalent therapeutics. *Ther Deliv* **2011,** *2* (7), 873-889.

22. Steinman, L., Blocking adhesion molecules as therapy for multiple sclerosis: natalizumab. *Nat. Rev. Drug Discov.* **2005,** *4* (6), 510.
23. Podojil, J. R.; Turley, D. M.; Miller, S. D., Therapeutic blockade of T-cell antigen receptor signal transduction and costimulation in autoimmune disease. In *Multichain Immune Recognition Receptor Signaling*, Springer: 2008; pp 234-251.
24. Brezar, V.; Carel, J.-C.; Boitard, C.; Mallone, R., Beyond the hormone: insulin as an autoimmune target in type 1 diabetes. *Endocr. Rev.* **2011,** *32* (5), 623-669.
25. Cross, A.; Naismith, R., Established and novel disease-modifying treatments in multiple sclerosis. *J. Intern. Med.* **2014,** *275* (4), 350-363.
26. Her, M.; Kavanaugh, A., Advances in use of immunomodulatory agents—a rheumatology perspective. *Nat. Rev. Gastroenterol. Hepatol.* **2015,** *12* (6), 363.
27. Ruiz-Irastorza, G.; Danza, A.; Khamashta, M., Glucocorticoid use and abuse in SLE. *Rheumatology* **2012,** *51* (7), 1145-1153.
28. Miller, S. D.; Turley, D. M.; Podojil, J. R., Antigen-specific tolerance strategies for the prevention and treatment of autoimmune disease. *Nat. Rev. Immunol.* **2007,** *7* (9), 665.
29. Rudick, R.; Polman, C.; Clifford, D.; Miller, D.; Steinman, L., Natalizumab: bench to bedside and beyond. *JAMA Neurol* **2013,** *70* (2), 172-182.
30. Dörner, T.; Radbruch, A.; Burmester, G. R., B-cell-directed therapies for autoimmune disease. *Nat Rev Rheumatol* **2009,** *5* (8), 433.
31. Hauser, S. L.; Waubant, E.; Arnold, D. L.; Vollmer, T.; Antel, J.; Fox, R. J.; Bar-Or, A.; Panzara, M.; Sarkar, N.; Agarwal, S., B-cell depletion with rituximab in relapsing–remitting multiple sclerosis. *N. Engl. J. Med.* **2008,** *358* (7), 676-688.
32. Leandro, M. J.; Edwards, J. C.; Cambridge, G.; Ehrenstein, M. R.; Isenberg, D. A., An open study of B lymphocyte depletion in systemic lupus erythematosus. *Arthritis Rheumatol.* **2002,** *46* (10), 2673-2677.
33. Yao, S.; Zhu, Y.; Chen, L., Advances in targeting cell surface signalling molecules for immune modulation. *Nat. Rev. Drug Discov.* **2013,** *12* (2), 130.
34. Sharpe, A. H.; Freeman, G. J., The B7–CD28 superfamily. *Nat. Rev. Immunol.* **2002,** *2* (2), 116.
35. Sabatos-Peyton, C. A.; Verhagen, J.; Wraith, D. C., Antigen-specific immunotherapy of autoimmune and allergic diseases. *Curr. Opin. Immunol.* **2010,** *22* (5), 609-615.
36. Krishna, M.; Huissoon, A., Clinical immunology review series: an approach to desensitization. *Clin. Exp. Immunol.* **2011,** *163* (2), 131-146.
37. Badawi, A. H.; Siahaan, T. J., Immune modulating peptides for the treatment and suppression of multiple sclerosis. *Clin. Immunol.* **2012,** *144* (2), 127-138.
38. Feldmann, M.; Steinman, L., Design of effective immunotherapy for human autoimmunity. *Nature* **2005,** *435* (7042), 612.
39. Larche, M.; Wraith, D. C., Peptide-based therapeutic vaccines for allergic and autoimmune diseases. *Nat. Med.* **2005,** *11* (4s), S69.
40. Aharoni, R., The mechanism of action of glatiramer acetate in multiple sclerosis and beyond. *Autoimmun rev* **2013,** *12* (5), 543-553.
41. Kang, Y.; Xu, L.; Wang, B.; Chen, A.; Zheng, G., Cutting edge: immunosuppressant as adjuvant for tolerogenic immunization. *J. Immunol.* **2008,** *180* (8), 5172-5176.
42. Kang, Y.; Zhao, J.; Liu, Y.; Chen, A.; Zheng, G.; Yu, Y.; Mi, J.; Zou, Q.; Wang, B., FK506 as an adjuvant of tolerogenic DNA vaccination for the prevention of experimental autoimmune encephalomyelitis. *J Gene Med* **2009,** *11* (11), 1064-1070.
43. Garren, H.; Ruiz, P. J.; Watkins, T. A.; Fontoura, P.; Nguyen, L.-V. T.; Estline, E. R.; Hirschberg, D. L.; Steinman, L., Combination of gene delivery and DNA vaccination to protect from and reverse Th1 autoimmune disease via deviation to the Th2 pathway. *Immunity* **2001,** *15* (1), 15-22.
44. Lewis, J. S.; Dolgova, N. V.; Zhang, Y.; Xia, C. Q.; Wasserfall, C. H.; Atkinson, M. A.; Clare-Salzler, M. J.; Keselowsky, B. G., A combination dual-sized microparticle system modulates

dendritic cells and prevents type 1 diabetes in prediabetic NOD mice. *Clin. Immunol.* **2015,** *160* (1), 90-102.
45. Tisch, R.; Wang, B.; Weaver, D. J.; Liu, B.; Bui, T.; Arthos, J.; Serreze, D. V., Antigen-specific mediated suppression of β cell autoimmunity by plasmid DNA vaccination. *J. Immunol.* **2001,** *166* (3), 2122-2132.
46. Li, A. F.; Hough, J.; Henderson, D.; Escher, A., Co-delivery of pro-apoptotic BAX with a DNA vaccine recruits dendritic cells and promotes efficacy of autoimmune diabetes prevention in mice. *Vaccine* **2004,** *22* (13-14), 1751-1763.
47. Capini, C.; Jaturanpinyo, M.; Chang, H.-I.; Mutalik, S.; McNally, A.; Street, S.; Steptoe, R.; O'Sullivan, B.; Davies, N.; Thomas, R., Antigen-specific suppression of inflammatory arthritis using liposomes. *J. Immunol.* **2009,** *182* (6), 3556-3565.
48. Yeste, A.; Nadeau, M.; Burns, E. J.; Weiner, H. L.; Quintana, F. J., Nanoparticle-mediated codelivery of myelin antigen and a tolerogenic small molecule suppresses experimental autoimmune encephalomyelitis. *Proc. Natl. Acad. Sci. U.S.A.* **2012,** *109* (28), 11270-11275.
49. Peine, K. J.; Guerau-de-Arellano, M.; Lee, P.; Kanthamneni, N.; Severin, M.; Probst, G. D.; Peng, H.; Yang, Y.; Vangundy, Z.; Papenfuss, T. L., Treatment of experimental autoimmune encephalomyelitis by codelivery of disease associated peptide and dexamethasone in acetalated dextran microparticles. *Mol. Pharm.* **2014,** *11* (3), 828-835.
50. Kobayashi, N.; Kobayashi, H.; Gu, L.; Malefyt, T.; Siahaan, T. J., Antigen-specific suppression of experimental autoimmune encephalomyelitis by a novel bifunctional peptide inhibitor. *J. Pharmacol. Exp. Ther.* **2007,** *322* (2), 879-886.
51. Murray, J. S.; Oney, S.; Page, J. E.; Kratochvil-Stava, A.; Hu, Y.; Makagiansar, I. T.; Brown, J. C.; Kobayashi, N.; Siahaan, T. J., Suppression of type 1 diabetes in NOD mice by bifunctional peptide inhibitor: modulation of the immunological synapse formation. *Chem Biol Drug Des* **2007,** *70* (3), 227-236.
52. Kolb, H. C.; Finn, M. G.; Sharpless, K. B., Click Chemistry: Diverse Chemical Function from a Few Good Reactions. *Angew Chem Int Ed* . **2001,** *40* (11), 2004-2021.
53. Sletten, E. M.; Bertozzi, C. R., Bioorthogonal chemistry: fishing for selectivity in a sea of functionality. *Angew Chem Int Ed Engl.* **2009,** *48* (38), 6974-6998.
54. Empting, M.; Avrutina, O.; Meusinger, R.; Fabritz, S.; Reinwarth, M.; Biesalski, M.; Voigt, S.; Buntkowsky, G.; Kolmar, H., "Triazole bridge": Disulfide-bond Replacement by Ruthenium-catalyzed Formation of 1,5-Disubstituted 1,2,3-triazoles. *Angew Chem Int Ed* . **2011,** *50* (22), 5207-11.
55. van Maarseveen, J. H.; Horne, W. S.; Ghadiri, M. R., Efficient Route to C2 Symmetric Heterocyclic Backbone Modified Cyclic Peptides. *Org. Lett.* **2005,** *7* (20), 4503-4506.
56. Torres, O.; Yüksel, D.; Bernardina, M.; Kumar, K.; Bong, D., Peptide Tertiary Structure Nucleation by Side-Chain Crosslinking with Metal Complexation and Double “Click” Cycloaddition. *ChemBioChem* **2008,** *9* (11), 1701-1705.
57. Lim, S. I.; Mizuta, Y.; Takasu, A.; Hahn, Y. S.; Kim, Y. H.; Kwon, I., Site-specific Fatty Acid-conjugation to Prolong Protein Half-life In vivo. *J. Control. Release* **2013,** *170* (2), 219-25.
58. Zimmerman, E. S.; Heibeck, T. H.; Gill, A.; Li, X.; Murray, C. J.; Madlansacay, M. R.; Tran, C.; Uter, N. T.; Yin, G.; Rivers, P. J.; Yam, A. Y.; Wang, W. D.; Steiner, A. R.; Bajad, S. U.; Penta, K.; Yang, W.; Hallam, T. J.; Thanos, C. D.; Sato, A. K., Production of Site-Specific Antibody–Drug Conjugates Using Optimized Non-Natural Amino Acids in a Cell-Free Expression System. *Bioconjugate Chem.* **2014,** *25* (2), 351-361.
59. VanBrunt, M. P.; Shanebeck, K.; Caldwell, Z.; Johnson, J.; Thompson, P.; Martin, T.; Dong, H.; Li, G.; Xu, H.; D’Hooge, F.; Masterson, L.; Bariola, P.; Tiberghien, A.; Ezeadi, E.; Williams, D. G.; Hartley, J. A.; Howard, P. W.; Grabstein, K. H.; Bowen, M. A.; Marelli, M., Genetically Encoded Azide Containing Amino Acid in Mammalian Cells Enables Site-Specific Antibody–Drug Conjugates Using Click Cycloaddition Chemistry. *Bioconjugate Chem.* **2015,** *26* (11), 2249-2260.

60. Swiderska, K. W.; Szlachcic, A.; Czyrek, A.; Zakrzewska, M.; Otlewski, J., Site-specific Conjugation of Fibroblast Frowth Factor 2 (FGF2) Based on Incorporation of Alkyne-reactive Unnatural Amino Acid. *Bioorganic Med. Chem.* **2017,** *25* (14), 3685-3693.
61. Sola, L.; Damin, F.; Gagni, P.; Consonni, R.; Chiari, M., Synthesis of Clickable Coating Polymers by Postpolymerization Modification: Applications in Microarray Technology. *Langmuir* **2016,** *32* (40), 10284-10295.
62. Tornøe, C. C., C.; Meldal, M., Peptidotriazoles on Solid Phase: [1,2,3]-triazoles by Regiospecific Copper(I)-Catalyzed 1,3-Dipolar Cycloadditions of Terminal Alkynes to Azides. *J. Org. Chem.* **2002,** *67*, 3057-3064.
63. Gao, Y.; Shi, W.; Wang, W.; Leng, Y.; Zhao, Y., Inkjet Printing Patterns of Highly Conductive Pristine Graphene on Flexible Substrates. *Ind. Eng. Chem. Res.* **2014,** *53* (43), 16777-16784.
64. Hartwell, B. L.; Pickens, C. J.; Leon, M.; Berkland, C., Multivalent Soluble Antigen Arrays Exhibit High Avidity Binding and Modulation of B Cell Receptor-Mediated Signaling to Drive Efficacy against Experimental Autoimmune Encephalomyelitis. *Biomacromolecules* **2017,** *18* (6), 1893-1907.
65. Nuhn, L.; Hartmann, S.; Palitzsch, B.; Gerlitzki, B.; Schmitt, E.; Zentel, R.; Kunz, H., Water-Soluble Polymers Coupled with Glycopeptide Antigens and T-Cell Epitopes as Potential Antitumor Vaccines. *Angew Chem Int Ed Engl.* **2013,** *52* (40), 10652-10656.
66. Gori, A.; Sola, L.; Gagni, P.; Bruni, G.; Liprino, M.; Peri, C.; Colombo, G.; Cretich, M.; Chiari, M., Screening Complex Biological Samples with Peptide Microarrays: The Favorable Impact of Probe Orientation via Chemoselective Immobilization Strategies on Clickable Polymeric Coatings. *Bioconjugate Chem.* **2016,** *27* (11), 2669-2677.
67. Goswami, L. N.; Houston, Z. H.; Sarma, S. J.; Jalisatgi, S. S.; Hawthorne, M. F., Efficient Synthesis of Diverse Heterobifunctionalized Clickable Oligo(ethylene glycol) Linkers: Potential Applications in Bioconjugation and Targeted Drug Delivery. *Org. Biomol. Chem.* **2013,** *11* (7), 1116-1126.
68. Gong, H.; Holcomb, I.; Ooi, A.; Wang, X.; Majonis, D.; Unger, M. A.; Ramakrishnan, R., Simple Method To Prepare Oligonucleotide-Conjugated Antibodies and Its Application in Multiplex Protein Detection in Single Cells. *Bioconjugate Chem.* **2016,** *27* (1), 217-225.
69. van Geel, R.; Wijdeven, M. A.; Heesbeen, R.; Verkade, J. M.; Wasiel, A. A.; van Berkel, S. S.; van Delft, F. L., Chemoenzymatic Conjugation of Toxic Payloads to the Globally Conserved N-Glycan of Native mAbs Provides Homogeneous and Highly Efficacious Antibody-Drug Conjugates. *Bioconjugate Chem.* **2015,** *26* (11), 2233-42.
70. Nair, D. P.; Podgórski, M.; Chatani, S.; Gong, T.; Xi, W.; Fenoli, C. R.; Bowman, C. N., The Thiol-Michael Addition Click Reaction: A Powerful and Widely Used Tool in Materials Chemistry. *Chem. Mater.* **2014,** *26* (1), 724-744.
71. Anami, Y.; Xiong, W.; Gui, X.; Deng, M.; Zhang, C. C.; Zhang, N.; An, Z.; Tsuchikama, K., Enzymatic Conjugation Using Branched Linkers for Constructing Homogeneous Antibody-drug Conjugates with High Potency. *Org. Biomol. Chem.* **2017,** *15* (26), 5635-5642.
72. Wang, H.; Wang, R.; Cai, K.; He, H.; Liu, Y.; Yen, J.; Wang, Z.; Xu, M.; Sun, Y.; Zhou, X.; Yin, Q.; Tang, L.; Dobrucki, I. T.; Dobrucki, L. W.; Chaney, E. J.; Boppart, S. A.; Fan, T. M.; Lezmi, S.; Chen, X.; Yin, L.; Cheng, J., Selective In vivo Metabolic Cell-Labeling-mediated Cancer Targeting. *Nat. Chem. Biol.* **2017,** *13* (4), 415-424.
73. Yoon, H. I.; Yhee, J. Y.; Na, J. H.; Lee, S.; Lee, H.; Kang, S.-W.; Chang, H.; Ryu, J. H.; Lee, S.; Kwon, I. C.; Cho, Y. W.; Kim, K., Bioorthogonal Copper Free Click Chemistry for Labeling and Tracking of Chondrocytes In Vivo. *Bioconjugate Chem.* **2016,** *27* (4), 927-936.
74. Besanceney-Webler, C.; Jiang, H.; Wang, W.; Baughn, A. D.; Wu, P., Metabolic Labeling of Fucosylated Glycoproteins in Bacteroidales species. *Bioorganic Med. Chem. Lett.* **2011,** *21* (17), 4989-4992.

75. Dehnert, K. W.; Beahm, B. J.; Huynh, T. T.; Baskin, J. M.; Laughlin, S. T.; Wang, W.; Wu, P.; Amacher, S. L.; Bertozzi, C. R., Metabolic Labeling of Fucosylated Glycans in Developing Zebrafish. *ACS Chem. Biol.* **2011,** *6* (6), 547-552.
76. Hart, C.; Chase, L. G.; Hajivandi, M.; Agnew, B., Metabolic Labeling and Click Chemistry Detection of Glycoprotein Markers of Mesenchymal Stem Cell Differentiation. *Methods Mol. Biol.* **2011,** *698*, 459-84.
77. Zaro, B. W.; Yang, Y. Y.; Hang, H. C.; Pratt, M. R., Chemical Reporters for Fluorescent Detection and Identification of O-GlcNAc-modified Proteins Reveal Glycosylation of the Ubiquitin Ligase NEDD4-1. *Proc. Natl. Acad. Sci. U.S.A.* **2011,** *108* (20), 8146-51.
78. Rangan, K. J.; Yang, Y.-Y.; Charron, G.; Hang, H. C., Rapid Visualization and Large-Scale Profiling of Bacterial Lipoproteins with Chemical Reporters. *J. Am. Chem. Soc.* **2010,** *132* (31), 10628-10629.
79. Martin, B. R.; Cravatt, B. F., Large-scale Profiling of Protein Palmitoylation in Mammalian Cells. *Nat. Methods* **2009,** *6* (2), 135-138.
80. Wilson, J. P.; Raghavan, A. S.; Yang, Y. Y.; Charron, G.; Hang, H. C., Proteomic Analysis of Fatty-acylated Proteins in Mammalian Cells with Chemical Reporters Reveals S-Acylation of Histone H3 Variants. *Molecular & cellular proteomics : MCP* **2011,** *10* (3), M110.001198.
81. Kho, Y.; Kim, S. C.; Jiang, C.; Barma, D.; Kwon, S. W.; Cheng, J.; Jaunbergs, J.; Weinbaum, C.; Tamanoi, F.; Falck, J.; Zhao, Y., A Tagging-via-Substrate Technology for Detection and Proteomics of Farnesylated Proteins. *Proc. Natl. Acad. Sci. U.S.A.* **2004,** *101* (34), 12479-84.
82. Yount, J. S.; Moltedo, B.; Yang, Y. Y.; Charron, G.; Moran, T. M.; Lopez, C. B.; Hang, H. C., Palmitoylome Profiling Reveals S-palmitoylation-dependent Antiviral Activity of IFITM3. *Nat. Chem. Biol.* **2010,** *6* (8), 610-4.
83. Martin, B. R.; Wang, C.; Adibekian, A.; Tully, S. E.; Cravatt, B. F., Global Profiling of Dynamic Protein Palmitoylation. *Nat. Methods* **2012,** *9* (1), 84-89.
84. Palsuledesai, C. C.; Ochocki, J. D.; Kuhns, M. M.; Wang, Y. C.; Warmka, J. K.; Chernick, D. S.; Wattenberg, E. V.; Li, L.; Arriaga, E. A.; Distefano, M. D., Metabolic Labeling with an Alkyne-modified Isoprenoid Analog Facilitates Imaging and Quantification of the Prenylome in Cells. *ACS Chem. Biol.* **2016,** *11* (10), 2820-2828.
85. DeGraw, A. J.; Palsuledesai, C.; Ochocki, J. D.; Dozier, J. K.; Lenevich, S.; Rashidian, M.; Distefano, M. D., Evaluation of Alkyne-modified Isoprenoids as Chemical Reporters of Protein Prenylation. *Chem Biol Drug Des* **2010,** *76* (6), 460-71.
86. Charron, G.; Tsou, L. K.; Maguire, W.; Yount, J. S.; Hang, H. C., Alkynyl-farnesol Reporters for Detection of Protein S-Prenylation in Cells. *Mol. BioSyst.* **2011,** *7* (1), 67-73.
87. Neef, A. B.; Samain, F.; Luedtke, N. W., Metabolic Labeling of DNA by Purine Analogues in Vivo. *ChemBioChem* **2012,** *13* (12), 1750-1753.
88. Marks, I. S.; Kang, J. S.; Jones, B. T.; Landmark, K. J.; Cleland, A. J.; Taton, T. A., Strain-Promoted "Click" Chemistry for Terminal Labeling of DNA. *Bioconjugate Chem.* **2011,** *22* (7), 1259-1263.
89. Winz, M.-L.; Linder, E. C.; André, T.; Becker, J.; Jäschke, A., Nucleotidyl Transferase Assisted DNA Labeling with Different Click Chemistries. *Nucleic Acids Res.* **2015,** *43* (17), e110.
90. Sawant, A. A.; Tanpure, A. A.; Mukherjee, P. P.; Athavale, S.; Kelkar, A.; Galande, S.; Srivatsan, S. G., A Versatile Toolbox for Posttranscriptional Chemical Labeling and Imaging of RNA. *Nucleic Acids Res.* **2016,** *44* (2), e16.
91. Jao, C. Y.; Roth, M.; Welti, R.; Salic, A., Metabolic Labeling and Direct Imaging of Choline Phospholipids In vivo. *Proc. Natl. Acad. Sci. U.S.A.* **2009,** *106* (36), 15332-15337.
92. Taskova, M.; Madsen, C. S.; Jensen, K. J.; Hansen, L. H.; Vester, B.; Astakhova, K., Antisense Oligonucleotides Internally Labeled with Peptides Show Improved Target Recognition and Stability to Enzymatic Degradation. *Bioconjugate Chem.* **2017,** *28* (3), 768-774.

93. Mulder, G. E.; Kruijtzer, J. A. W.; Liskamp, R. M. J., A Combinatorial Approach Toward Smart Libraries of Discontinuous Epitopes of HIV GP120 on a TAC Synthetic Scaffold. *Chem Commun* **2012,** *48* (80), 10007-10009.
94. Das, S.; Nag, A.; Liang, J.; Bunck, D. N.; Umeda, A.; Farrow, B.; Coppock, M. B.; Sarkes, D. A.; Finch, A. S.; Agnew, H. D.; Pitram, S.; Lai, B.; Yu, M. B.; Museth, A. K.; Deyle, K. M.; Lepe, B.; Rodriguez-Rivera, F. P.; McCarthy, A.; Alvarez-Villalonga, B.; Chen, A.; Heath, J.; Stratis-Cullum, D. N.; Heath, J. R., A General Synthetic Approach for Designing Epitope Targeted Macrocyclic Peptide Ligands. *Angew Chem Int Ed* . **2015,** *54* (45), 13219-24.
95. Kim, S.; Ko, W.; Sung, B. H.; Kim, S. C.; Lee, H. S., Direct Protein–protein Conjugation by Genetically Introducing Bioorthogonal Functional Groups into Proteins. *Bioorganic Med. Chem.* **2016,** *24* (22), 5816-5822.
96. Kirshenbaum, K.; Carrico, I. S.; Tirrell, D. A., Biosynthesis of Proteins Incorporating a Versatile Set of Phenylalanine Analogues. *ChemBioChem* **2002,** *3* (2-3), 235-237.
97. Sivakumar, K.; Xie, F.; Cash, B. M.; Long, S.; Barnhill, H. N.; Wang, Q., A fluorogenic 1, 3-dipolar cycloaddition reaction of 3-azidocoumarins and acetylenes. *Org. Lett.* **2004,** *6* (24), 4603-4606.
98. Chen, Q.; Millar, H. J.; McCabe, F. L.; Manning, C. D.; Steeves, R.; Lai, K.; Kellogg, B.; Lutz, R. J.; Trikha, M.; Nakada, M. T., αv integrin-targeted immunoconjugates regress established human tumors in xenograft models. *Clin. Cancer Res.* **2007,** *13* (12), 3689-3695.
99. Ikeda, H.; Hideshima, T.; Fulciniti, M.; Lutz, R. J.; Yasui, H.; Okawa, Y.; Kiziltepe, T.; Vallet, S.; Pozzi, S.; Santo, L., The monoclonal antibody nBT062 conjugated to cytotoxic Maytansinoids has selective cytotoxicity against CD138-positive multiple myeloma cells in vitro and in vivo. *Clin. Cancer Res.* **2009,** *15* (12), 4028-4037.
100. Besanceney-Webler, C.; Jiang, H.; Zheng, T.; Feng, L.; Soriano del Amo, D.; Wang, W.; Klivansky, L. M.; Marlow, F. L.; Liu, Y.; Wu, P., Increasing the Efficacy of Bioorthogonal Click Reactions for Bioconjugation: A Comparative Study. *Angew Chem Int Ed Engl.* **2011,** *50* (35), 8051-8056.
101. Erickson, H. K.; Phillips, G. D. L.; Leipold, D. D.; Provenzano, C. A.; Mai, E.; Johnson, H. A.; Gunter, B.; Audette, C. A.; Gupta, M.; Pinkas, J., The effect of different linkers on target cell catabolism and pharmacokinetics/pharmacodynamics of trastuzumab maytansinoid conjugates. *Mol. Cancer Ther.* **2012,** *11* (5), 1133-1142.
102. Leonard, G. F., T.; Bates, S., The Role of ABC Transporters in Clinical Practice. *Oncologist* **2003,** *8*, 411-424.
103. Beck, A.; Goetsch, L.; Dumontet, C.; Corvaia, N., Strategies and Challenges for the Next Generation of Antibody-drug Conjugates. *Nat Rev Drug Discov* **2017,** *16* (5), 315-337.
104. Lyon, R. P.; Meyer, D. L.; Setter, J. R.; Senter, P. D., Conjugation of Anticancer Drugs Through Endogenous Monoclonal Antibody Cysteine Residues. *Meth. Enzymol.* **2012,** *502*, 123-138.
105. Li, X.; Fang, T.; Boons, G. J., Preparation of Well-defined Antibody-drug Conjugates through Glycan Remodeling and Strain-promoted azide-alkyne Cycloadditions. *Angew Chem Int Ed* . **2014,** *53* (28), 7179-82.
106. Zeglis, B. M.; Davis, C. B.; Aggeler, R.; Kang, H. C.; Chen, A.; Agnew, B. J.; Lewis, J. S., Enzyme-Mediated Methodology for the Site-Specific Radiolabeling of Antibodies Based on Catalyst-Free Click Chemistry. *Bioconjugate Chem.* **2013,** *24* (6), 1057-1067.
107. Meyer, J. P.; Adumeau, P.; Lewis, J. S.; Zeglis, B. M., Click Chemistry and Radiochemistry: The First 10 Years. *Bioconjugate Chem.* **2016,** *27* (12), 2791-2807.
108. Akkapeddi, P.; Azizi, S.-A.; Freedy, A. M.; Cal, P. M. S. D.; Gois, P. M. P.; Bernardes, G. J. L., Construction of Homogeneous Antibody-drug Conjugates Using Site-Selective Protein Chemistry. *Chem Sci.* **2016,** *7* (5), 2954-2963.
109. Hong, V.; Presolski, S. I.; Ma, C.; Finn, M. G., Analysis and Optimization of Copper-catalyzed azide-alkyne Cycloaddition for Bioconjugation. *Angew Chem Int Ed* . **2009,** *48* (52), 9879-83.

110. Lim, S. I.; Mizuta, Y.; Takasu, A.; Kim, Y. H.; Kwon, I., Site-specific Bioconjugation of a Murine Dihydrofolate Reductase Enzyme by Copper(I)-catalyzed azide-alkyne Cycloaddition with Retained Activity. *PLoS One* **2014,** *9* (6), e98403.
111. Li, S.; Cai, H.; He, J.; Chen, H.; Lam, S.; Cai, T.; Zhu, Z.; Bark, S. J.; Cai, C., Extent of the oxidative side reactions to peptides and proteins during the cuaac reaction. *Bioconjugate Chem.* **2016,** *27* (10), 2315-2322.
112. Fisher, S. A.; Baker, A. E.; Shoichet, M. S., Designing Peptide and Protein Modified Hydrogels: Selecting the Optimal Conjugation Strategy. *J. Am. Chem. Soc.* **2017,** *139* (22), 7416-7427.
113. Takahashi, A.; Suzuki, Y.; Suhara, T.; Omichi, K.; Shimizu, A.; Hasegawa, K.; Kokudo, N.; Ohta, S.; Ito, T., In situ cross-linkable hydrogel of hyaluronan produced via copper-free click chemistry. *Biomacromolecules* **2013,** *14* (10), 3581-3588.
114. Huerta-Angeles, G.; Němcová, M.; Příkopová, E.; Šmejkalová, D.; Pravda, M.; Kučera, L.; Velebný, V., Reductive alkylation of hyaluronic acid for the synthesis of biocompatible hydrogels by click chemistry. *Carbohydr. Polym.* **2012,** *90* (4), 1704-1711.
115. Hu, X.; Li, D.; Zhou, F.; Gao, C., Biological hydrogel synthesized from hyaluronic acid, gelatin and chondroitin sulfate by click chemistry. *Acta Biomater.* **2011,** *7* (4), 1618-1626.
116. Barrett, T. W., Solution Properties of Hyaluronic Acid. **1981,** *150*, 229-250.
117. Fakhari, A.; Berkland, C., Applications and Emerging Trends of Hyaluronic Acid in Tissue Engineering, as a Dermal Filler and in Osteoarthritis Treatment. *Acta Biomater.* **2013,** *9* (7), 7081-92.
118. Erickson, H. K.; Park, P. U.; Widdison, W. C.; Kovtun, Y. V.; Garrett, L. M.; Hoffman, K.; Lutz, R. J.; Goldmacher, V. S.; Blattler, W. A., Antibody-maytansinoid Conjugates are Activated in Targeted Cancer Cells by Lysosomal Degradation and Linker-dependent Intracellular Processing. *Cancer Res.* **2006,** *66* (8), 4426-33.
119. Oflazoglu, E.; Stone, I. J.; Gordon, K.; Wood, C. G.; Repasky, E. A.; Grewal, I. S.; Law, C. L.; Gerber, H. P., Potent Anticarcinoma Activity of the Humanized Anti-CD70 Antibody h1F6 Conjugated to the Tubulin Inhibitor Auristatin via an Uncleavable Linker. *Clin. Cancer Res.* **2008,** *14* (19), 6171-80.
120. Phillips, G. D. L.; Li, G.; Dugger, D. L.; Crocker, L. M.; Parsons, K. L.; Mai, E.; Blättler, W. A.; Lambert, J. M.; Chari, R. V.; Lutz, R. J., Targeting HER2-Positive Breast Cancer with Trastuzumab-DM1, an Antibody–Cytotoxic Drug Conjugate. *Cancer Res.* **2008,** *68* (22), 9280-9290.
121. Dubowchik, G. M.; Firestone, R. A.; Padilla, L.; Willner, D.; Hofstead, S. J.; Mosure, K.; Knipe, J. O.; Lasch, S. J.; Trail, P. A., Cathepsin B-labile Dipeptide Linkers for Lysosomal Release of Doxorubicin from Internalizing Immunoconjugates: Model Studies of Enzymatic Drug Release and Antigen-Specific In vitro Anticancer Activity. *Bioconj. Chem.* **2002,** *13* (4), 855-69.
122. Ritchie, M.; Tchistiakova, L.; Scott, N., Implications of Receptor-mediated Endocytosis and Intracellular Trafficking Dynamics in the Development of Antibody Drug Conjugates. *mAbs* **2013,** *5* (1), 13-21.
123. Strop, P.; Liu, S. H.; Dorywalska, M.; Delaria, K.; Dushin, R. G.; Tran, T. T.; Ho, W. H.; Farias, S.; Casas, M. G.; Abdiche, Y.; Zhou, D.; Chandrasekaran, R.; Samain, C.; Loo, C.; Rossi, A.; Rickert, M.; Krimm, S.; Wong, T.; Chin, S. M.; Yu, J.; Dilley, J.; Chaparro-Riggers, J.; Filzen, G. F.; O'Donnell, C. J.; Wang, F.; Myers, J. S.; Pons, J.; Shelton, D. L.; Rajpal, A., Location Natters: Site of Conjugation Modulates Stability and Pharmacokinetics of Antibody Drug Conjugates. *Chem Biol.* **2013,** *20* (2), 161-7.
124. Elgersma, R. C.; Coumans, R. G.; Huijbregts, T.; Menge, W. M.; Joosten, J. A.; Spijker, H. J.; de Groot, F. M.; van der Lee, M. M.; Ubink, R.; van den Dobbelsteen, D. J.; Egging, D. F.; Dokter, W. H.; Verheijden, G. F.; Lemmens, J. M.; Timmers, C. M.; Beusker, P. H., Design, Synthesis, and Evaluation of Linker-Duocarmycin Payloads: Toward Selection of HER2-Targeting Antibody-Drug Conjugate SYD985. *Mol. Pharmaceutics* **2015,** *12* (6), 1813-35.

125. van der Lee, M. M.; Groothuis, P. G.; Ubink, R.; van der Vleuten, M. A.; van Achterberg, T. A.; Loosveld, E. M.; Damming, D.; Jacobs, D. C.; Rouwette, M.; Egging, D. F.; van den Dobbelsteen, D.; Beusker, P. H.; Goedings, P.; Verheijden, G. F.; Lemmens, J. M.; Timmers, M.; Dokter, W. H., The Preclinical Profile of the Duocarmycin-Based HER2-Targeting ADC SYD985 Predicts for Clinical Benefit in Low HER2-Expressing Breast Cancers. *Mol. Cancer Ther.* **2015,** *14* (3), 692-703.
126. Jain, N.; Smith, S. W.; Ghone, S.; Tomczuk, B., Current ADC Linker Chemistry. *Pharm. Res.* **2015,** *32* (11), 3526-40.
127. Joubert, M. K.; Hokom, M.; Eakin, C.; Zhou, L.; Deshpande, M.; Baker, M. P.; Goletz, T. J.; Kerwin, B. A.; Chirmule, N.; Narhi, L. O.; Jawa, V., Highly Aggregated Antibody Therapeutics Can Enhance the In vitro Innate and Late-stage T-cell Immune Responses. *J. Biol. Chem.* **2012,** *287* (30), 25266-79.
128. Phillips, G. D. L.; de Haas, S.; Girish, S.; Guardino, E., ADCs Approved for Use: Trastuzumab Emtansine (Kadcyla®, T-DM1) in Patients with Previously Treated HER2-Positive Metastatic Breast Cancer. *Antibody-Drug Conjugates: Fundamentals, Drug Development, and Clinical Outcomes to Target Cancer* **2016**, 345.
129. Al-Katib, A. M.; Aboukameel, A.; Mohammad, R.; Bissery, M.-C.; Zuany-Amorim, C., Superior antitumor activity of SAR3419 to rituximab in xenograft models for non-Hodgkin's lymphoma. *Clin. Cancer Res.* **2009,** *15* (12), 4038-4045.
130. Kovtun, Y. V.; Audette, C. A.; Mayo, M. F.; Jones, G. E.; Doherty, H.; Maloney, E. K.; Erickson, H. K.; Sun, X.; Wilhelm, S.; Ab, O.; Lai, K. C.; Widdison, W. C.; Kellogg, B.; Johnson, H.; Pinkas, J.; Lutz, R. J.; Singh, R.; Goldmacher, V. S.; Chari, R. V., Antibody-maytansinoid Conjugates Designed to Bypass Multidrug Resistance. *Cancer Res.* **2010,** *70* (6), 2528-37.
131. Hamblett, K. J.; Senter, P. D.; Chace, D. F.; Sun, M. M.; Lenox, J.; Cerveny, C. G.; Kissler, K. M.; Bernhardt, S. X.; Kopcha, A. K.; Zabinski, R. F., Effects of Drug Loading on the Antitumor Activity of a Monoclonal Antibody Drug Conjugate. *Clin. Cancer. Res.* **2004,** *10* (20), 7063-7070.
132. Wang, L.; Amphlett, G.; Blättler, W. A.; Lambert, J. M.; Zhang, W., Structural Characterization of the Maytansinoid–MonoclonalAntibody Immunoconjugate, huN901–DM1, by Mass Spectrometry. *Protein Sci.* **2005,** *14* (9), 2436-2446.
133. Lyon, R. P.; Bovee, T. D.; Doronina, S. O.; Burke, P. J.; Hunter, J. H.; Neff-LaFord, H. D.; Jonas, M.; Anderson, M. E.; Setter, J. R.; Senter, P. D., Reducing Hydrophobicity of Homogeneous Antibody-drug Conjugates Improves Pharmacokinetics and Therapeutic Index. *Nat. Biotechnol.* **2015,** *33* (7), 733-735.
134. Wang, W.; Singh, S. K.; Li, N.; Toler, M. R.; King, K. R.; Nema, S., Immunogenicity of Protein Aggregates--Concerns and Realities. *Int. J. Pharm.* **2012,** *431* (1-2), 1-11.
135. Ahn, Y. H.; Kang, H. G.; Lee, J. M.; Choi, H. J.; Ha, I. S.; Cheong, H. I., Development of Antirituximab Antibodies in Children with Nephrotic Syndrome. *Pediatr. Nephrol.* **2014,** *29* (8), 1461-4.
136. Mazilu, D.; Opris, D.; Gainaru, C.; Iliuta, M.; Apetrei, N.; Luca, G.; Borangiu, A.; Gudu, T.; Peltea, A.; Groseanu, L.; Constantinescu, C.; Saulescu, I.; Bojinca, V.; Balanescu, A.; Predeteanu, D.; Ionescu, R., Monitoring drug and Antidrug Levels: a Rational Approach in Rheumatoid Arthritis Patients Treated with Biologic Agents Who Experience Inadequate Response While Being on a Stable Biologic Treatment. *BioMed Res. Int.* **2014,** *2014*, 702701.
137. Roederer, M.; Quaye, L.; Mangino, M.; Beddall, M. H.; Mahnke, Y.; Chattopadhyay, P.; Tosi, I.; Napolitano, L.; Barberio, M. T.; Menni, C., The genetic architecture of the human immune system: a bioresource for autoimmunity and disease pathogenesis. *Cell* **2015,** *161* (2), 387-403.
138. Northrup, L.; Christopher, M. A.; Sullivan, B. P.; Berkland, C., Combining antigen and immunomodulators: Emerging trends in antigen-specific immunotherapy for autoimmunity. *Adv. Drug Deliv. Rev.* **2016,** *98*, 86-98.
139. Atkinson, M. A.; Eisenbarth, G. S.; Michels, A. W., Type 1 diabetes. *Lancet* **2014,** *383* (9911), 69-82.

140. Meng, Q.; Yu, M.; Zhang, H.; Ren, J.; Huang, D., Synthesis and application of N-hydroxysuccinimidyl rhodamine B ester as an amine-reactive fluorescent probe. *Dyes Pigm.* **2007,** *73* (2), 254-260.
141. Flygare, J. A.; Pillow, T. H.; Aristoff, P., Antibody-drug conjugates for the treatment of cancer. *Chem Biol Drug Des* **2013,** *81* (1), 113-121.
142. Hein, J. E.; Fokin, V. V., Copper-catalyzed azide-alkyne Cycloaddition (CuAAC) and Beyond: New Reactivity of Copper(I) Acetylides. *Chem. Soc. Rev.* **2010,** *39* (4), 1302-15.
143. Hong, V.; Presolski, S. I.; Ma, C.; Finn, M., Analysis and Optimization of Copper-Catalyzed Azide–Alkyne Cycloaddition for Bioconjugation. *Angew Chem Int Ed Engl.* **2009,** *48* (52), 9879-9883.
144. Presolski, S. I.; Hong, V. P.; Finn, M., Copper-Catalyzed Azide–Alkyne Click Chemistry for Bioconjugation. *Curr Protoc Chem Biol* **2011**, 153-162.
145. Tang, W.; Becker, M. L., "Click" Reactions: a Versatile Toolbox for the Synthesis of Peptide-conjugates. *Chem. Soc. Rev.* **2014,** *43* (20), 7013-7039.
146. Dirksen, A.; Madsen, M.; Dello Iacono, G.; Matin, M. J.; Bacica, M.; Stanković, N.; Callans, S.; Bhat, A., Parallel Synthesis and Screening of Peptide Conjugates. *Bioconjugate Chem.* **2014,** *25* (6), 1052-1060.
147. Kotagiri, N.; Li, Z.; Xu, X.; Mondal, S.; Nehorai, A.; Achilefu, S., Antibody Quantum Dot Conjugates Developed via Copper-Free Click Chemistry for Rapid Analysis of Biological Samples Using a Microfluidic Microsphere Array System. *Bioconjugate Chem.* **2014,** *25* (7), 1272-1281.
148. Merten, H.; Brandl, F.; Plückthun, A.; Zangemeister-Wittke, U., Antibody–Drug Conjugates for Tumor Targeting—Novel Conjugation Chemistries and the Promise of non-IgG Binding Proteins. *Bioconjugate Chem.* **2015,** *26* (11), 2176-2185.
149. Pickens, C. J.; Johnson, S. N.; Pressnall, M. M.; Leon, M. A.; Berkland, C. J., Practical Considerations, Challenges, and Limitations of Bioconjugation via Azide–Alkyne Cycloaddition. *Bioconjugate Chem.* **2017,** *29* (3), 686-701.
150. Rossi, C.; Chrétien, M.-L.; Casasnovas, R.-O., Antibody–Drug Conjugates for the Treatment of Hematological Malignancies: A Comprehensive Review. *Targeted oncology* **2018**, 1-22.
151. Wållberg, M.; Cooke, A., Immune mechanisms in type 1 diabetes. *Trends Immunol.* **2013,** *34* (12), 583-591.
152. Akdis, M.; Akdis, C. A., Mechanisms of allergen-specific immunotherapy. *J. Allergy Clin. Immunol.* **2007,** *119* (4), 780-789.
153. von Moos, S.; Kündig, T. M.; Senti, G., Novel administration routes for allergen-specific immunotherapy: a review of intralymphatic and epicutaneous allergen-specific immunotherapy. *Immunol Allergy Clin North Am* **2011,** *31* (2), 391-406.
154. Hartwell, B. L.; Pickens, C. J.; Leon, M.; Northrup, L.; Christopher, M. A.; Griffin, J. D.; Martinez-Becerra, F.; Berkland, C., Soluble antigen arrays disarm antigen-specific B cells to promote lasting immune tolerance in experimental autoimmune encephalomyelitis. *J. Autoimmun.* **2018**.
155. Jones, D. S., Multivalent compounds for antigen-specific B cell tolerance and treatment of autoimmune diseases. *Curr. Med. Chem.* **2005,** *12* (16), 1887-1904.
156. Puffer, E. B.; Pontrello, J. K.; Hollenbeck, J. J.; Kink, J. A.; Kiessling, L. L., Activating B cell signaling with defined multivalent ligands. *ACS Chem. Biol.* **2007,** *2* (4), 252-262.
157. Cairo, C. W.; Gestwicki, J. E.; Kanai, M.; Kiessling, L. L., Control of multivalent interactions by binding epitope density. *J. Am. Chem. Soc.* **2002,** *124* (8), 1615-1619.
158. Gestwicki, J. E.; Cairo, C. W.; Strong, L. E.; Oetjen, K. A.; Kiessling, L. L., Influencing receptor−ligand binding mechanisms with multivalent ligand architecture. *J. Am. Chem. Soc.* **2002,** *124* (50), 14922-14933.
159. Kiessling, L. L.; Gestwicki, J. E.; Strong, L. E., Synthetic multivalent ligands in the exploration of cell-surface interactions. *Curr. Opin. Chem. Biol.* **2000,** *4* (6), 696-703.

160. Hartwell, B. L.; Antunez, L.; Sullivan, B. P.; Thati, S.; Sestak, J. O.; Berkland, C., Multivalent nanomaterials: learning from vaccines and progressing to antigen-specific immunotherapies. *J. Pharm. Sci.* **2015,** *104* (2), 346-361.
161. Krishnamurthy, V. M.; Estroff, L. A.; Whitesides, G. M., *Multivalency in ligand design*. 2006; Vol. 34, p 11-53.
162. Dintzis, H.; Dintzis, R.; Vogelstein, B., Molecular determinants of immunogenicity: the immunon model of immune response. *Proc. Natl. Acad. Sci. U.S.A.* **1976,** *73* (10), 3671-3675.
163. Hartwell, B. L.; Martinez-Becerra, F. J.; Chen, J.; Shinogle, H.; Sarnowski, M.; Moore, D. S.; Berkland, C., Antigen-Specific Binding of Multivalent Soluble Antigen Arrays Induces Receptor Clustering and Impedes B Cell Receptor Mediated Signaling. *Biomacromolecules* **2016,** *17* (3), 710-722.
164. Hartwell, B. L.; Smalter Hall, A.; Swafford, D.; Sullivan, B. P.; Garza, A.; Sestak, J. O.; Northrup, L.; Berkland, C., Molecular Dynamics of Multivalent Soluble Antigen Arrays Support a Two-Signal Co-delivery Mechanism in the Treatment of Experimental Autoimmune Encephalomyelitis. *Mol. Pharm.* **2016,** *13* (2), 330-343.
165. Northrup, L.; Sestak, J. O.; Sullivan, B. P.; Thati, S.; Hartwell, B. L.; Siahaan, T. J.; Vines, C. M.; Berkland, C., Co-delivery of autoantigen and b7 pathway modulators suppresses experimental autoimmune encephalomyelitis. *AAPS J.* **2014,** *16* (6), 1204-1213.
166. Sestak, J.; Mullins, M.; Northrup, L.; Thati, S.; Forrest, M. L.; Siahaan, T. J.; Berkland, C., Single-step grafting of aminooxy-peptides to hyaluronan: a simple approach to multifunctional therapeutics for experimental autoimmune encephalomyelitis. *J. Control. Release* **2013,** *168* (3), 334-340.
167. Sestak, J. O.; Fakhari, A.; Badawi, A. H.; Siahaan, T. J.; Berkland, C., Structure, size, and solubility of antigen arrays determines efficacy in experimental autoimmune encephalomyelitis. *AAPS J.* **2014,** *16* (6), 1185-1193.
168. Sestak, J. O.; Sullivan, B. P.; Thati, S.; Northrup, L.; Hartwell, B.; Antunez, L.; Forrest, M. L.; Vines, C. M.; Siahaan, T. J.; Berkland, C., Codelivery of antigen and an immune cell adhesion inhibitor is necessary for efficacy of soluble antigen arrays in experimental autoimmune encephalomyelitis. *Mol Ther Methods Clin Dev* **2014,** *1*.
169. Thati, S.; Kuehl, C.; Hartwell, B.; Sestak, J.; Siahaan, T.; Forrest, M. L.; Berkland, C., Routes of administration and dose optimization of soluble antigen arrays in mice with experimental autoimmune encephalomyelitis. *J. Pharm. Sci.* **2015,** *104* (2), 714-721.
170. Judkowski, V.; Pinilla, C.; Schroder, K.; Tucker, L.; Sarvetnick, N.; Wilson, D. B., Identification of MHC class II-restricted peptide ligands, including a glutamic acid decarboxylase 65 sequence, that stimulate diabetogenic T cells from transgenic BDC2. 5 nonobese diabetic mice. *J. Immunol.* **2001,** *166* (2), 908-917.
171. Haskins, K.; Portas, M.; Bergman, B.; Lafferty, K.; Bradley, B., Pancreatic islet-specific T-cell clones from nonobese diabetic mice. *Proc. Natl. Acad. Sci. U.S.A.* **1989,** *86* (20), 8000-8004.
172. Delong, T.; Baker, R. L.; He, J.; Barbour, G.; Bradley, B.; Haskins, K., Diabetogenic T-cell clones recognize an altered peptide of chromogranin A. *Diabetes* **2012**, DB_120112.
173. Delong, T.; Wiles, T. A.; Baker, R. L.; Bradley, B.; Barbour, G.; Reisdorph, R.; Armstrong, M.; Powell, R. L.; Reisdorph, N.; Kumar, N., Pathogenic CD4 T cells in type 1 diabetes recognize epitopes formed by peptide fusion. *Science* **2016,** *351* (6274), 711-714.
174. Fife, B. T.; Guleria, I.; Bupp, M. G.; Eagar, T. N.; Tang, Q.; Bour-Jordan, H.; Yagita, H.; Azuma, M.; Sayegh, M. H.; Bluestone, J. A., Insulin-induced remission in new-onset NOD mice is maintained by the PD-1–PD-L1 pathway. *J. Exp. Med.* **2006,** *203* (12), 2737-2747.
175. Berry, G.; Waldner, H., Accelerated type 1 diabetes induction in mice by adoptive transfer of diabetogenic CD4+ T cells. *J. Vis. Exp.* **2013,** (75).
176. Wei, Y.; Larson, N. R.; Angalakurthi, S. K.; Russell Middaugh, C., Improved Fluorescence Methods for High-Throughput Protein Formulation Screening. *SLAS Technol.* **2018**, 2472630318780620.

177. Wei, Y.; Wahome, N.; Kumar, P.; Whitaker, N.; Picking, W. L.; Middaugh, C. R., Effect of Phosphate Ion on the Structure of Lumazine Synthase, an Antigen Presentation System From Bacillus anthracis. *J. Pharm. Sci.* **2018,** *107* (3), 814-823.
178. Clemente-Casares, X.; Blanco, J.; Ambalavanan, P.; Yamanouchi, J.; Singha, S.; Fandos, C.; Tsai, S.; Wang, J.; Garabatos, N.; Izquierdo, C.; Agrawal, S.; Keough, M. B.; Yong, V. W.; James, E.; Moore, A.; Yang, Y.; Stratmann, T.; Serra, P.; Santamaria, P., Expanding antigen-specific regulatory networks to treat autoimmunity. *Nature* **2016,** *530* (7591), 434-40.
179. Dintzis, R.; Middleton, M.; Dintzis, H., Studies on the immunogenicity and tolerogenicity of T-independent antigens. *J. Immunol.* **1983,** *131* (5), 2196-2203.
180. Dintzis, R.; Vogelstein, B.; Dintzis, H., Specific cellular stimulation in the primary immune response: experimental test of a quantized model. *Proc. Natl. Acad. Sci. U.S.A.* **1982,** *79* (3), 884-888.
181. You, S.; Chen, C.; Lee, W.-H.; Wu, C.-H.; Judkowski, V.; Pinilla, C.; Wilson, D. B.; Liu, C.-P., Detection and characterization of T cells specific for BDC2. 5 T cell-stimulating peptides. *J. Immunol.* **2003,** *170* (8), 4011-4020.
182. Chan, A.; Schutte, A. J., Interview: Experiences targeting B cells for the treatment of multiple sclerosis. *Immunotherapy* **2014,** *6* (2), 127-130.
183. Lehmann-Horn, K.; Kronsbein, H. C.; Weber, M. S., Targeting B cells in the treatment of multiple sclerosis: recent advances and remaining challenges. *Ther Adv Neurol Disord* **2013**, 1756285612474333.
184. Wong, F. S.; Wen, L.; Tang, M.; Ramanathan, M.; Visintin, I.; Daugherty, J.; Hannum, L. G.; Janeway, C. A.; Shlomchik, M. J., Investigation of the role of B-cells in type 1 diabetes in the NOD mouse. *Diabetes* **2004,** *53* (10), 2581-2587.
185. Serreze, D. V.; Fleming, S. A.; Chapman, H. D.; Richard, S. D.; Leiter, E. H.; Tisch, R. M., B lymphocytes are critical antigen-presenting cells for the initiation of T cell-mediated autoimmune diabetes in nonobese diabetic mice. *J. Immunol.* **1998,** *161* (8), 3912-3918.
186. Silveira, P. A.; Johnson, E.; Chapman, H. D.; Bui, T.; Tisch, R. M.; Serreze, D. V., The preferential ability of B lymphocytes to act as diabetogenic APC in NOD mice depends on expression of self-antigen-specific immunoglobulin receptors. *Eur. J. Immunol.* **2002,** *32* (12), 3657-3666.
187. Greeley, S. A. W.; Moore, D. J.; Noorchashm, H.; Noto, L. E.; Rostami, S. Y.; Schlachterman, A.; Song, H. K.; Koeberlein, B.; Barker, C. F.; Naji, A., Impaired activation of islet-reactive CD4 T cells in pancreatic lymph nodes of B cell-deficient nonobese diabetic mice. *J. Immunol.* **2001,** *167* (8), 4351-4357.
188. Vehik, K.; Beam, C. A.; Mahon, J. L.; Schatz, D. A.; Haller, M. J.; Sosenko, J. M.; Skyler, J. S.; Krischer, J. P.; Group, T. N. H. S., Development of autoantibodies in the TrialNet natural history study. *Diabetes Care* **2011,** *34* (9), 1897-1901.
189. Bennett, J.; O'Connor, K.; Bar-Or, A.; Zamvil, S.; Hemmer, B.; Tedder, T.; von Büdingen, H.; Stuve, O.; Yeaman, M.; Smith, T., B lymphocytes in neuromyelitis optica. Neurol Neuroimmunol Neuroinflamm 2: e104. 2015.
190. Quan, C.; ZhangBao, J.; Lu, J.; Zhao, C.; Cai, T.; Wang, B.; Yu, H.; Qiao, J.; Lu, C., The immune balance between memory and regulatory B cells in NMO and the changes of the balance after methylprednisolone or rituximab therapy. *J. Neuroimmunol.* **2015,** *282*, 45-53.
191. Fernandez-Nebro, A.; de la Fuente, J. M.; Carreno, L.; Izquierdo, M. G.; Tomero, E.; Rúa-Figueroa, I.; Hernández-Cruz, B.; Narváez, J.; Ucar, E.; Olivé, A., Multicenter longitudinal study of B-lymphocyte depletion in refractory systemic lupus erythematosus: the LESIMAB study. *Lupus* **2012,** *21* (10), 1063-1076.
192. Vital, E. M.; Dass, S.; Buch, M. H.; Henshaw, K.; Pease, C. T.; Martin, M. F.; Ponchel, F.; Rawstron, A. C.; Emery, P., B cell biomarkers of rituximab responses in systemic lupus erythematosus. *Arthritis Rheumatol.* **2011,** *63* (10), 3038-3047.
193. Boster, A.; Ankeny, D. P.; Racke, M. K., The potential role of B cell-targeted therapies in multiple sclerosis. *Drugs* **2010,** *70* (18), 2343-2356.

194. Oh, S.; Cudrici, C.; Ito, T.; Rus, H., B-cells and humoral immunity in multiple sclerosis. Implications for therapy. *Immunol Res* **2008,** *40* (3), 224-234.
195. Bates, D., Treatment effects of immunomodulatory therapies at different stages of multiple sclerosis in short-term trials. *Neurology* **2011,** *76* (1 Supplement 1), S14-S25.
196. Brunswick, M.; Finkelman, F.; Highet, P.; Inman, J.; Dintzis, H. M.; Mond, J., Picogram quantities of anti-Ig antibodies coupled to dextran induce B cell proliferation. *J. Immunol.* **1988,** *140* (10), 3364-3372.
197. Dintzis, R. Z.; Okajima, M.; Middleton, M. H.; Dintzis, H. M., Inhibition of antibody formation by receptor cross-linking: the molecular characteristics of inhibitory haptenated polymers. *Eur. J. Immunol.* **1990,** *20* (1), 229-232.
198. Reim, J. W.; Symer, D. E.; Watson, D. C.; Dintzis, R. Z.; Dintzis, H. M., Low molecular weight antigen arrays delete high affinity memory B cells without affecting specific T-cell help. *Mol. Immunol.* **1996,** *33* (17-18), 1377-1388.
199. Roozendaal, R.; Mebius, R. E.; Kraal, G., The conduit system of the lymph node. *Int. Immunol.* **2008,** *20* (12), 1483-1487.
200. Rantakari, P.; Auvinen, K.; Jäppinen, N.; Kapraali, M.; Valtonen, J.; Karikoski, M.; Gerke, H.; Iftakhar-E-Khuda, I.; Keuschnigg, J.; Umemoto, E., The endothelial protein PLVAP in lymphatics controls the entry of lymphocytes and antigens into lymph nodes. *Nat. Immunol.* **2015,** *16* (4), 386.
201. Pescovitz, M. D.; Greenbaum, C. J.; Bundy, B.; Becker, D. J.; Gitelman, S. E.; Goland, R.; Gottlieb, P. A.; Marks, J. B.; Moran, A.; Raskin, P., B-lymphocyte depletion with rituximab and beta-cell function: two-year results. *Diabetes Care* **2013**, DC_130626.
202. Pescovitz, M. D.; Greenbaum, C. J.; Krause-Steinrauf, H.; Becker, D. J.; Gitelman, S. E.; Goland, R.; Gottlieb, P. A.; Marks, J. B.; McGee, P. F.; Moran, A. M., Rituximab, B-lymphocyte depletion, and preservation of beta-cell function. *N. Engl. J. Med.* **2009,** *361* (22), 2143-2152.
203. Hardy, I. R.; Anceriz, N.; Rousseau, F.; Seefeldt, M. B.; Hatterer, E.; Irla, M.; Buatois, V.; Chatel, L. E.; Getahun, A.; Fletcher, A., Anti-CD79 antibody induces B cell anergy that protects against autoimmunity. *J. Immunol.* **2014**, 1302672.
204. Cambier, J. C.; Gauld, S. B.; Merrell, K. T.; Vilen, B. J., B-cell anergy: from transgenic models to naturally occurring anergic B cells? *Nat. Rev. Immunol.* **2007,** *7* (8), 633.
205. Pentheroudakis, G.; Twelves, C., The rational development of capecitabine from the laboratory to the clinic. *Anticancer Res.* **2002,** *22* (6B), 3589-3596.
206. Siliciano, R.; Colello, R.; Keegan, A.; Dintzis, R.; Dintzis, H.; Shin, H., Antigen valence determines the binding of nominal antigen to cytolytic T cell clones. *J. Exp. Med.* **1985,** *162* (2), 768-773.